การดัดแปลงตัวรองรับไทเทเนียมไดออกไซด์สำหรับปฏิกิริยาออกซิเดชัน
ของคาร์บอนมอนนอกไซด์

นางณัฐญา คุ้มทรัพย์

MODIFICATION OF TITANIUM DIOXIDE SUPPORT
FOR CARBON MONOXIDE OXIDATION

Mrs. Nattaya Comsup

A Dissertation Submitted in Partial Fulfillment of the Requirements

for the Degree of Doctor of Engineering Program in Chemical Engineering

Department of Chemical Engineering

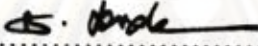Faculty of Engineering

Chulalongkorn University
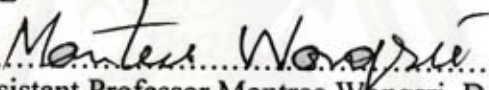
Academic Year 2009

Thesis Title   MODIFICATION OF TITANIUM DIOXIDE SUPPORT
                    FOR CARBON MONOXIDE OXIDATION
By   Mrs. Nattaya Comsup
Field of Study   Chemical Engineering
Thesis Advisor   Professor Piyasan Praserthdam, Dr.Ing.
Thesis Co-Advisor   Assistant Professor Joongjai Panpranot, Ph.D.
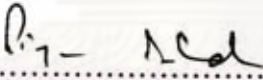

Accepted by the Faculty of Engineering, Chulalongkorn University in
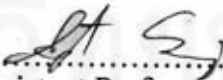Partial Fulfillment of the Requirements for the Doctoral Degree

.... Dean of the Faculty of Engineering
(Associate Professor Boonsom Lerdhirunwong, Dr.Ing.)

THESIS COMMITTEE

.... Chairman
(Assistant Professor Montree Wongsri, D.Sc.)

.... Thesis Advisor
(Professor Piyasan Praserthdam, Dr.Ing.)

.... Thesis Co-Advisor
(Assistant Professor Joongjai Panpranot, Ph.D.)

.... Examiner
(Assistant Professor Anongnat Somwangthanaroj, Ph.D.)

.... Examiner
(Akawat Sirisuk, Ph.D.)

.... External Examiner
(Assistant Professor Okorn Mekasuwandumrong, Dr.Eng.)

ฉัฐญา คุ้มทรัพย์: การดัดแปลงตัวรองรับไทเทเนียมไดออกไซด์สำหรับปฏิกิริยา ออกซิเดชันของคาร์บอนมอนนอกไซด์ (MODIFICATION OF TITANIUM DIOXIDE SUPPORT FOR CARBON MONOXIDE OXIDATION) อ. ที่ปรึกษา วิทยานิพนธ์หลัก: ศาสตราจารย์ ดร. ปิยะสาร ประเสริฐธรรม, อ. ที่ปรึกษาวิทยานิพนธ์ ร่วม: ผู้ช่วยศาสตราจารย์ ดร. จูงใจ ปั้นประณต, 106 หน้า.

งานวิจัยนี้ศึกษาผลของการดัดแปลงพื้นผิวของตัวรองรับไทเทเนียมไดออกไซด์ที่มีต่อ ความว่องไวในปฏิกิริยาออกซิเดชันของคาร์บอนมอนนอกไซด์ โดยใช้สองวิธีในการดัดแปลง ตัวรองรับไทเทเนียมไดออกไซด์ ได้แก่ การสร้างตำแหน่งที่บกพร่องบนพื้นผิวของไทเทเนียม ไดออกไซด์ และการดัดแปลงพื้นผิวด้วยธาตุในปริมาณเล็กน้อย จากผลการทดลองพบว่า ผลึก ของไทเทเนียมไดออกไซด์ที่มีขนาดใหญ่กว่าจะมีปริมาณ Ti^{3+} มากกว่า ซึ่งการมีปริมาณของ Ti^{3+} บนผลึกไทเทเนียมไดออกไซด์ขนาดใหญ่จะช่วยให้อนุภาคโลหะคงสภาพขนาดเล็กได้ใน ระหว่างการเคลือบฝัง การเผา และระหว่างขั้นตอนการรีดักชัน อันเป็นผลมาจากการเกิดอันตร กิริยาที่แข็งแรงระหว่างโลหะกับตัวรองรับ ส่งผลให้ความว่องไวในปฏิกิริยาออกซิเดชันของ คาร์บอนมอนนอกไซด์สูงขึ้น นอกจากนี้ วิธีการดัดแปลงตัวรองรับไทเทเนียมไดออกไซด์ด้วย ธาตุในปริมาณเล็กน้อย สามารถปรับปรุงความว่องไวในปฏิกิริยาออกซิเดชันของคาร์บอนมอน นอกไซด์ได้ ในจำนวนธาตุทั้งหมดที่ใช้ในการดัดแปลงนั้น (ซึ่งได้แก่ อลูมิเนียม ซิลิกอน และ ฟอสฟอรัส) ไทเทเนียมไดออกไซด์ที่ถูกดัดแปลงด้วยซิลิกอนให้ประสิทธิภาพสูงสุดในการเร่ง ปฏิกิริยาของตัวเร่งปฏิกิริยาเงิน อย่างไรก็ตาม อัตราส่วนโดยโมลที่เหมาะสมของซิลิกอนต่อไท เทเนียมที่ส่งผลต่อการปรับปรุงความว่องไวในปฏิกิริยาออกซิเดชันของคาร์บอนมอนนอกไซด์ ได้ควรอยู่ระหว่าง 0.05 ถึง 0.1 หากปริมาณของซิลิกอนต่อไทเทเนียมเพิ่มขึ้นเป็น 0.3 จะไม่ส่งผล ให้ความว่องไวของตัวเร่งปฏิกิริยาเงินในปฏิกิริยาออกซิเดชันของคาร์บอนมอนนอกไซด์เพิ่มขึ้น เนื่องจากเกิดซิลิกาที่มีโครงสร้างแบบอสัณฐานแทนที่การเกิดพันธะแบบ Ti-O-Si การดัดแปลง ไทเทเนียมไดออกไซด์ด้วยฟอสฟอรัส เพื่อใช้เป็นตัวรองรับสำหรับตัวเร่งปฏิกิริยาเงิน โดยใช้ สารตั้งต้นฟอสฟอรัสที่อยู่ในรูปออกไซด์นั้น จะช่วยให้เกิดการดูดซับออกซิเจนแบบไม่แข็งแรง และส่งผลให้ความว่องไวในปฏิกิริยาออกซิเดชันของคาร์บอนมอนนอกไซด์สูงขึ้น

ภาควิชา..วิศวกรรมเคมี... ลายมือชื่อนิสิต...

สาขาวิชา..วิศวกรรมเคมี....ลายมือชื่อ อ.ที่ปรึกษาวิทยานิพนธ์หลัก...........................

ปีการศึกษา........2552......ลายมือชื่อ อ.ที่ปรึกษาวิทยานิพนธ์ร่วม..........................

5071808921: MAJOR CHEMICAL ENGINEERING

KEYWORDS : SUPPORT MODIFICATION / CO OXIDATION/ TITANIUM DIOXIDE / SURFACE DEFECT / SOLVOTHERMAL

NATTAYA COMSUP : MODIFICATION OF TITANIUM DIOXIDE SUPPORT FOR CARBON MONOXIDE OXIDATION. THESIS ADVISOR: PROFESSOR PIYASAN PRASERTHDAM, Dr. Ing., THESIS CO-ADVISOR: ASSISTANT PROFESSOR JOONGJAI PANPRANOT, Ph.D., 106 pp.

This research is to study the effect of surface modification of TiO_2 support on the catalytic activity in CO oxidation. Two methods were employed for surface modification of TiO_2 support: the creation of defective sites on TiO_2 surface and the modification with trace element. The results found that the presence of higher amount of Ti^{3+} on the larger crystallite size TiO_2 stabilizes small metal particles during impregnation, calcination, and reduction steps via stronger metal-support interaction; hence higher CO oxidation activities. In addition, the modification of TiO_2 support with trace element can improve the CO oxidation activity. All of element dopants (i.e., Al, Si and P), the Si-modified TiO_2 showed the highest catalytic performance of Ag/TiO_2 catalyst. However, there existed an optimum content of Si/Ti molar ratio at ca. 0.05-0.1 which resulted in an improved catalytic activity of Ag/TiO_2 in CO oxidation. There was no improvement in CO oxidation activity of the Ag/TiO_2 catalyst when the Si/Ti was further increased to 0.3 due probably to the formation of amorphous SiO_2 instead of the Ti-O-Si bond. The P-modified TiO_2 supported Ag catalysts using phosphorus precursor in the form of oxide promoted the weak adsorbed oxygen species and resulted in catalytic activity improvement in CO oxidation.

Department: Chemical Engineering   Student's Signature Nattaya Comsup

Field of Study: Chemical Engineering   Advisor's Signature

Academic Year: 2009   Co-Advisor's Signature

ACKNOWLEDGEMENTS

CONTENTS

LIST OF TABLES

LIST OF FIGURES

CHAPTER I

INTRODUCTION

Titanium dioxide (TiO_2) is the most widely used material in many technological applications. Nowadays, as concerns with global environmental issues increase, the application of TiO_2 to treatment of polluted air and wastewater has received great attention because of its easy to access, chemical stability, non-toxic and low cost [1-5]. TiO_2 is used both as a catalyst and catalyst support in heterogeneous catalytic reaction including photocatalytic reaction, hydrogenation, and oxidation reaction. It is well known that TiO_2 is reducible metal oxide that stronger interacts with group VIII noble metals than other metal oxides such as SiO_2, Al_2O_3, and MgO [6-10]. For this reason, TiO_2 has attracted much attention for the application as noble metal catalyst support in many reactions.

The Carbon monoxide (CO) oxidation reaction is of practical importance for the control of the environmental pollution that results from combustion process. The most active catalyst in CO oxidation is noble metal group. Among of these metals, gold catalysts exhibit high catalytic activity for CO oxidation at a temperature as low as 200K [11], followed by Cu and Ag [12]. Low temperature CO oxidation catalysts are used in residential and automotive air cleaning technologies, gas masks for mining applications, CO detectors, and selective oxidation of CO in reformer gas for fuel cell applications. However, because of their relatively high cost, many researchers have attempted to improve performance of the other catalysts in order to replace the gold catalysts. In general, CO oxidation is classified as a structure insensitive in which the activity depends mainly on the amount of active site. Thus, the improvement of metal catalysts dispersion is a crucial factor affecting catalytic activity in CO oxidation. The surface properties of support materials are important in determining the catalytic activities of metals dispersed on them [13]. Support modification usually brings about changes in surface properties of the support such as surface area, surface defect, surface acidity or basicity of the support, and etc., which are a crucial factor affecting dispersion of the metal catalyst. This implies that the surface modification of supports would effectively provide supported metal catalysts with improved or controlled

activities. The modification of the support by varying the chemical environment or amount of the interacting component [14] has the possibility to control the properties of the supported metals.

The modification of support with trace element has been investigated widely by many researchers. This method can result in changes in surface chemistry, crystal structure, crystal defects and size of support. Many researchers reported that the incorporation of trace element increased surface area and thermal stability of support. CO oxidation is one of the reactions that have been frequently investigated using TiO_2 as the support. Nevertheless, only a few studies have reported about the modification of TiO_2 with trace elements in order to use as support in CO oxidation reaction. The Type and amount of doping elements have influence on the physical and chemical properties of TiO_2 such as crystallite size, morphology, and crystalline phase [15]. These parameters also have significant influence on the dispersion and dimension of metal species on TiO_2 supports especially when the TiO_2 particles were in nanometer-size [16-19]. Knowledge of the effects of impurities on surface properties of TiO_2 is essential in order to be able to utilize them effectively.

The main objective of this research is to investigate the surface modification of TiO_2 for using as support in CO oxidation reaction. The solvothermal method has been employed to synthesize TiO_2 nanoparticles. The method for modification of TiO_2 support that has been used in this research consists of two methods: (1) the method of changing the synthesis condition of the solvothermal preparation and (2) the method of trace element doping in TiO_2 support. For the first method, the effects of amount of surface defect on TiO_2 support on catalytic activity in CO oxidation have been investigated. In the second method, the effects of type, amount and precursor type of doping element on catalytic activity in CO oxidation have been studied. The physical and chemical properties of unmodified and modified TiO_2 nanoparticles were characterized in order to compare their properties with unmodified TiO_2.

The scope of the research presented is given below,

1. TiO_2 nanoparticles were synthesized by solvothermal method and employed as the supports for metal catalysts in CO oxidation reaction.

2. TiO_2 support was modified to obtain a different amount of surface defects by changing the synthesis condition of the solvothermal method.

3. The different transition metals catalysts (Ag, Pt, Ni, and Co) were supported on TiO_2 support with different amount of surface defects for both low and high metal loadings (1 and 25%at., respectively). The CO oxidation activity of these catalysts was compared.

4. TiO_2 support was modified by doping with different elements (Al, Si and P) with constant molar ratio of element/Ti at 0.03. The Ag catalyst was supported on modified TiO_2 to compare the CO oxidation activity.

5. TiO_2 support was modified by doping with at least one element selected from the group of element in (4) with the molar ratios of element/Ti varied in the range of 0.01 to 0.3. The Ag catalyst was supported on modified TiO_2 to compare the CO oxidation activity.

6. TiO_2 support was modified by doping with various precursor of doping element selected from the group of element in (4) with constant molar ratio of element/Ti at 0.03. The Ag catalyst was supported on modified TiO_2 to compare the CO oxidation activity.

7. The physicochemical properties of the catalysts were characterized by X-ray diffraction (XRD), X-ray photoelectron spectroscopy (XPS), BET surface area, transmission electron microscope (TEM), electron spin resonance (ESR), Fourier Transform Infrared (FTIR) Spectroscopy and O_2-Temperature programmed desorption (O_2-TPD).

8. The amount of active sites of the catalysts was characterized by pulse chemisorption techniques.

CHAPTER II

BACKGROUND

The purpose of this chapter provides the fundamental concepts and literature underlying the work presented in this thesis. The first section of the chapter describes the fundamental information about the general properties of TiO_2, its applications and surface modification. The fundamental theory of the CO oxidation reaction and using the TiO_2 as a support for metal catalysts in CO oxidation was provided in the next section. In the last section give the description about the modification of TiO_2 for CO oxidation reaction.

2.1 Titanium dioxide

Titanium dioxide (TiO_2), also known as titania, is the naturally occurring oxide of titanium. Titanium dioxide was first industrially introduced to replace toxic lead oxides as a white paint pigment in 1900's. Nowadays, the annual world consumption of TiO_2 exceeds 4.4 million tons [20]. TiO_2 has received a great amount of applications due to its strong oxidizing power of the photogenerated holes, chemical inertness, non-toxicity, low cost, high refractive index and other advantageous surface properties. For this reasons, TiO_2 has been steadily gaining importance for use as catalyst or catalyst support. TiO_2 has a wide range of applications in heterogeneous catalytic reactions including photocatalysis, air purification, water treatment, self-cleaning, antifogging, and so on. TiO_2 is successfully used as gas sensor (due to the dependence of the electric conductivity on the ambient gas composition [21]) and is utilized in the determination of oxygen and CO concentrations at high temperatures (>600 °C) [22], and simultaneously determining CO/O_2 and CO/CH_4 concentrations [23]. Due to its hemocompatibility with the human body, TiO_2 is used as a biomaterial. TiO_2 is also used in catalytic reactions acting as a promoter, a carrier for metals and metal oxides, an additive, or as a catalyst [24]. Reactions carried out with TiO_2 catalysts include selective reduction of NOx to N_2 [25], effective decomposition of VOCs [26], hydrogen production by

gas shift production [27], Fischer–Tropsch synthesis [28], CO oxidation by O_2 [29], H_2S oxidation to S, reduction of SO_2 to S by CO [30], and NO_2 storage [31].

2.1.1 Crystal structure and properties

Titanium dioxide exists in the three crystal forms: anatase (tetragonal), rutile (tetragonal) and brookite (rhombohedral), the structure of anatase, rutile and brookite are illustrated in **Figure 2.1**. The rutile structure is the most common form and the most stable form. Anatase and brookite both convert to rutile upon heating. While anatase and rutile TiO_2 have been extensively studied and used in many aspects, brookite TiO_2 is scarce and difficult to purify.

Titanium dioxide surface is a complex and extremely sensitive to thermo chemical history such as temperature, pressure, cooling rate, impurity. Principally the surface contains several atoms, ions and molecules via ionic, covalent or coordinated bonding such as basic terminal and acidic bridged-hydroxyl groups; labile Ti-O-Ti bonds; water molecules adsorbed at Lewis acid sites or bound to surface hydroxyl groups; adsorbed anions such as sulfate or chloride process residues; potential electron donor and acceptor sites; possibly adsorbed oxidants such as hydroxyl or hydroperoxyl radicals; or activated oxygen species generated by photocatalytic processes [32]. There are also many surface defects on TiO_2 that include step edges, oxygen vacancies, line deficiencies, foreign cations, crystallographic shear planes. In addition, TiO_2 involve several surface planes. The surface of rutile is formed from three crystal planes including the (1 1 0), (0 0 1) and (1 0 0), with (1 1 0) being the most stable one. For anatase, the (1 0 1), (1 0 0) and (0 1 0) surface planes are found in powders, together with some (0 0 1). Such complex TiO_2 surface plays a vital role in all the aforementioned wide range of applications. Some of the most important bulk properties of TiO_2 are presented in **Table 2.1**.
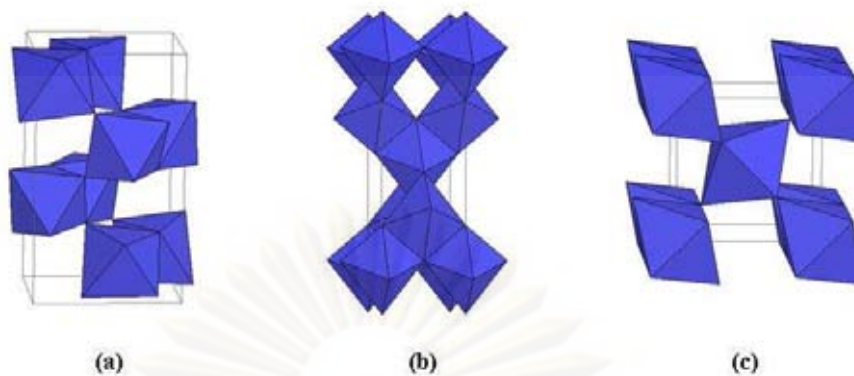
Figure 2.1 Crystal structures of anatase (a), rutile (b), and brookite (c) [33]

Table 2.1 Some bulk properties of the three main polymorphs of TiO_2
(anatase, rutile, and brookite) [33].

Crystal structure	System	Density (kg/m^3)	Lattice parameters (nm)				Band gap (eV)	Refractive index	
			a	b	c	c/a		n_g	n_p
Rutile	Tetragonal	4240	0.4584	-	0.2953	0.644	3.05	2.9467	2.6506
Anatase	Tetragonal	3830	0.3733	-	0.937	2.51	3.26	2.5688	2.6584
Brookite	Rhombohedral	4170	0.5436	0.9166	-	0.944	-	2.809	2.677

It is now recognized that oxygen vacancy defects on the surface of TiO_2, as shown in **Figure 2.2**, play an essential part in governing the adsorption of O_2, where O_2 molecules seek the vacancy defect sites for non-dissociative adsorption, producing the superoxide species, O_2^-. This takes place by O_2 interaction with surface Ti^{3+} sites which are produced by thermal reduction of the surface by removal of surface O_2^- anions. Defects on the $TiO_2(110)$ surface are easily created by electron bombardment, sputtering, or simply by thermal annealing the surface to high temperatures. Thermally created defects have been recognized extensively in the literature as point
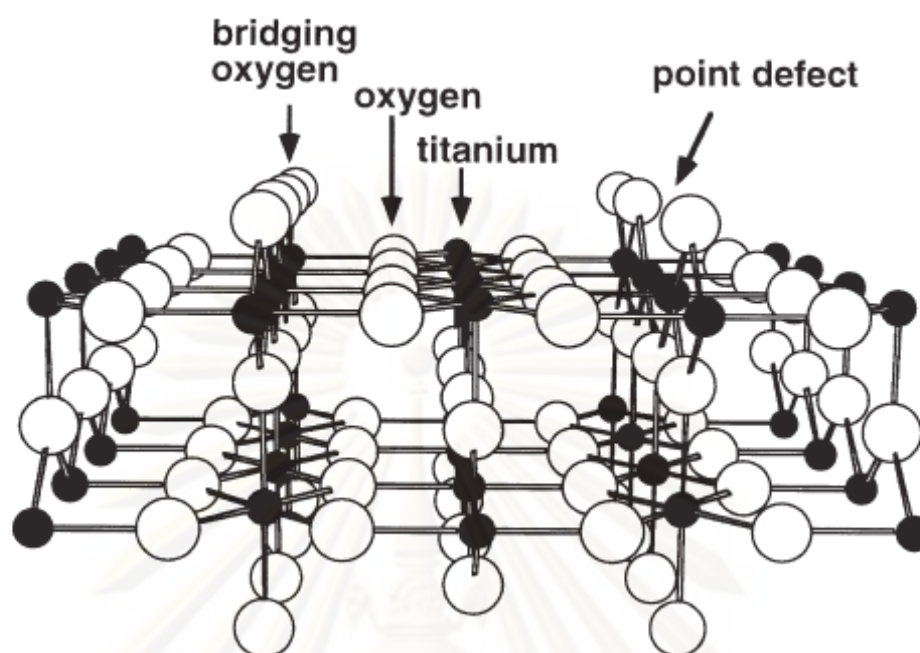
Figure 2.2 Ball-and-stick model of a point defect (missing oxygen atom in the bridging oxygen rows) on the rutile TiO_2 surface [34].

defects that exist as oxygen vacancy sites located within the bridging oxygen rows of the $TiO_2(110)$-(1 x 1) surface [35]. The creation of these defects has a profound effect on the electronic properties of the surface. Macroscopically, the presence of oxygen vacancies creates an overall reduced state of the TiO_2 crystal, both in the bulk and in the surface. Upon the annealing, the creation of defects within the bulk is associated with the creation of color centers and Ti^{3+} interstitial ions [36], and an overall reduced stoichiometry as a result of the loss of oxygen atoms. This effect occurs on the surface as well, where the presence of an oxygen vacancy site leaves an exposed Ti^{+3} ion which may be visualized as a Ti^{4+} ion associated with a somewhat localized electron. It has been shown by many authors that this site is an active adsorption site for adsorbates, and that interesting chemistry may occur at this Ti^{3+} site.

The stoichiometric state of the surface can be regained by annealing the crystal in a flux of oxygen to high temperature [7]. This treatment has been studied by scanning tunneling microscopy (STM) and shown to completely reoxidize exposed Ti^{+3} atoms as well as interstitial titanium ions that diffuse from the bulk to the surface

during annealing [37-39]. This treatment causes the incorporation of oxygen into the surface layers of the TiO_2 resulting in the addition of layers of TiO_2 to the surface [40]. The lack of surface defects as a result, leaves the surface relatively inactive chemically. The process of reduction and oxidation of the surface layers is reversible, although extensive annealing of the crystal leads to high concentrations of Ti^{3+} interstitials, extensive bulk oxygen loss and the formation of crystallographic shear planes [41]. While annealing in O_2 oxidizes surface vacancies, the high concentration of thermally created defects remaining within the bulk may lead to eventual inactivity as a photocatalyst and to irreversible changes to the electronic structure of TiO_2 (110).

2.1.2 Applications of TiO_2

The consumption of TiO_2 increased in the last few years in a number of minor end-use sectors such as a photocatalyst, as a catalyst support or promoter, as gas sensor, as in electric and electrochromic devices, and so on.

- **Pigment**

Titanium dioxide is the most widely used white pigment because of its brightness and very high refractive index ($n = 2.7$), in which it is surpassed only by a few other materials. Approximately 4 million tons of pigmentary TiO_2 are consumed annually worldwide. When deposited as a thin film, its refractive index and colour make it an excellent reflective optical coating for dielectric mirrors. TiO_2 is also an effective opacifier in powder form, where it is employed as a pigment to provide whiteness and opacity to products such as paints, coatings, plastics, papers, inks, foods, medicines (i.e. pills and tablets) as well as most toothpastes. Opacity is improved by optimal sizing of the titanium dioxide particles.

Titanium dioxide used as a white food colouring, It is often used to whiten skimmed milk; this has been shown statistically to increase skimmed milk's palatability [42]. In cosmetic and skin care products, titanium dioxide is used both as a pigment and a thickener. It is also used as a tattoo pigment and in styptic pencils. This pigment is used extensively in plastics and other applications for its UV resistant

properties where it acts as a UV absorber, efficiently transforming destructive UV light energy into heat.

In ceramic glazes titanium dioxide acts as an opacifier and seeds crystal formation. Titanium dioxide is found in almost every sunscreen with a physical blocker because of its high refractive index, its strong UV light absorbing capabilities and its resistance to discoloration under ultraviolet light. This advantage enhances its stability and ability to protect the skin from ultraviolet light. Sunscreens designed for infants or people with sensitive skin are often based on titanium dioxide and/or zinc oxide, as these mineral UV blockers are believed to cause less skin irritation than chemical UV absorber ingredients. The titanium dioxide particles used in sunscreens have to be coated with silica or alumina, because titanium dioxide creates radicals in the photocatalytic reaction. These radicals are carcinogenic, and could damage the skin.

- **Photocatalysis**

Titanium dioxide, particularly in the anatase form, is a photocatalyst under ultraviolet light. Recently it has been found that TiO_2, when spiked with nitrogen ions or doped with metal oxide like tungsten trioxide, is also a photocatalyst under visible and UV light. The strong oxidative potential of the positive holes oxidizes water to create hydroxyl radicals. It can also oxidize oxygen or organic materials directly. TiO_2 is thus added to paints, cements, windows, tiles, or other products for its sterilizing, deodorizing and anti-fouling properties and is used as a hydrolysis catalyst. It is also used in the Graetzel cell, a type of chemical solar cell. The photocatalytic properties of titanium dioxide were discovered by Akira Fujishima in 1967 and published in 1972 [43, 44]. TiO_2 has potential for use in energy production: as a photocatalyst,

(1) TiO_2 can carry out hydrolysis; i.e., break water into hydrogen and oxygen. Were the hydrogen collected, it could be used as a fuel. The efficiency of this process can be greatly improved by doping the oxide with carbon.

(2) TiO_2 can also produce electricity when in nanoparticle form. Research suggests that by using these nanoparticles to form the pixels of a screen, they generate electricity when transparent and under the influence of light. If subjected to electricity

on the other hand, the nanoparticles blacken, forming the basic characteristics of a LCD screen.

In 1995 Fujishima and his group discovered the superhydrophilicity phenomenon for titanium dioxide coated glass exposed to sun light [44]. This resulted in the development of self-cleaning glass and anti-fogging coatings. TiO_2 incorporated into outdoor building materials, such as paving stones in noxer blocks or paints, can substantially reduce concentrations of airborne pollutants such as volatile organic compounds and nitrogen oxides. TiO_2 offers great potential as an industrial technology for detoxification or remediation of wastewater due to several factors:

(1) The process occurs under ambient conditions very slowly; direct UV light exposure increases the rate of reaction.

(2) The formation of photocyclized intermediate products, unlike direct photolysis techniques, is avoided.

(3) Oxidation of the substrates to CO_2 is complete.

(4) The photocatalyst is inexpensive and has a high turnover.

(5) TiO_2 can be supported on suitable reactor substrates.

The photocatalytic activity of TiO_2 is greatly influenced by its crystal structure, particle size, surface area and porosity. When the size of TiO_2 particle is decreased to the nanometer scale, the catalytic activity is enhanced because the optical band gap is widened due to the quantum size effect, combined with the increased surface area [45, 46]. Furthermore, since the photocatalytic reaction occurs on the surface, the specific surface area of the powder needs to be large for the more effective photocatalytic activity. Hence, it is of great importance to improve the preparation method of nanocrystalline TiO_2.

- **Gas Sensor**

Another successfully existing utilization of TiO_2 is as gas sensor because it may change its electrical conductivity upon gas adsorption like SnO_2 and ZnO semiconductors. So far, TiO_2 is commonly used as gas sensor at high temperatures for the detection of H_2, O_2, CH_4 and CO [22, 47], e.g. to evaluate the

combustion process of fuel in car engines for controlling fuel consumption and environmental pollution [48]. Although adsorption of molecules on metal oxide surfaces generally takes place by means of electrostatic interactions [49, 50], in some cases an electron transfer occurs to or from the surface, involving a change in the substrate electric resistance. This phenomenon is used to monitor the presence of the molecule and is the basis of gas-sensing. A detailed knowledge of the gas/surface interaction is then necessary to understand the mechanism, which rules out such processes. Kirner et al. [51] studied that TiO_2-based oxygen sensors had different detection principles when operating in two different temperature regimes. At high temperatures, TiO_2 devices acted as thermodynamically controlled bulk defect sensors, providing oxygen partial pressure measurements over a very large range. The intrinsic behavior of the defects responsible for the sensing mechanism could be controlled by doping with tri and pentavalent ions. However, at low temperatures, they found that the Pt/TiO_2 Schottky-diodes as oxygen sensors showed reversible current-voltage shift characteristics and changed sensitively upon changes in the oxygen partial pressures [51].

- **Catalyst Support or Promoter**

The anatase phase, although thermodynamically less stable than rutile, has received in the last years much attention because of its higher (photo) catalytic activity [52]. Anatase is used both as active phase and as support in many commercial catalytic reactions such as the selective catalytic reduction of NO [53].

2.1.3 Preparation of TiO_2 nanoparticle

The final properties of TiO_2 nanoparticle depend to size, morphology and crystalline phase of the prepared TiO_2 nanopowder. In order to prepare of TiO_2 nanostructured material with significant properties several processes have been developed over the last decade and can be classified as liquid process (sol–gel [54-56], solvothermal [57, 58], hydrothermal [59, 60]), solid state processing routes (mechanical alloying/milling [61], mechanochemical [62, 63]), RF thermal plasma [64] and other routes such as laser ablation. From the above methods, the sol–gel method is normally used for preparation nanometer TiO_2 powder. Experimental

results have shown that the prepared powders by uncontrolled sol–gel method generally lack the properties of uniform size, shape, and unagglomerated state and providing the titanium oxide with favor properties need to control process conditions. There are several parameters for controlling sol–gel process to prepare TiO_2 nanopowder with significant properties. It has been demonstrated that the precursor's concentration of titanium alkoxide greatly affects the crystallization behavior and characteristics of the final powder [65]. In addition, the size, stability, and morphology of the produced sol from alkoxides is strongly affected by the water titanium molar ratio ($r = [H_2O]/[Ti]$) [66, 67]. The formation of colloidal TiO_2 at high r ratio is of great interest, because the small size of particles is formed under this condition. The sol–gel method is widely used to prepare nanometer TiO_2. But as the precipitates derived by sol–gel are amorphous in nature, in order to obtain crystalline products, further heat treatment at high temperature is compulsory. This calcination process will inevitably cause the grain growth and reduction in specific surface area of particles and even induce phase transformation.

Hydrothermal synthesis, in which chemical reactions can occur in aqueous or organic media under the self-produced pressure at low temperature, (usually lower than 250°C) can solve those problems encountered during sol–gel process. This automatically raises the effective boiling point of the solvent, which can also solve the problems due to the limitations of their rather low boiling points. This technique is also called solvothermal by the many researchers [68-71], while in the special case of the solvent being water, often called hydrothermal. The solvothermal treatment could be useful to control grain size, particle morphology, crystalline phase and surface chemistry by regulating sol composition, reaction temperature, pressure, property of solvent, additives, and aging time. Thus, it demonstrates that the different surface properties of TiO_2 depend on the preparation methods and the condition of preparation.

2.2 CO oxidation reaction

Carbon monoxide (CO) is a colorless, odorless, poisonous gas which is a major product of the incomplete combustion of carbon and carbon-containing

compounds. It is a byproduct of vehicle exhausts, which contributes a very large amount of CO emissions in cities, particularly in areas with heavy traffic congestion. Other sources of CO emissions include industrial processes, tobacco smoke and fuel combustion in sources such as boilers and incinerators. It is also present in the atmosphere naturally, chiefly as a product of volcanic activity and natural gases (in coal mines) and forest fires. Carbon monoxide from automobile and industrial emissions is a dangerous pollutant that may contribute to the greenhouse effect and global warming. Carbon monoxide is dangerous and life-threatening to humans and other forms of air-breathing life, as inhaling even relatively small amounts of it can lead to hypoxic injury, neurological damage, and possibly death.

When it enters the body, it combines with hemoglobin to form carboxyhemoglobin, reducing the oxygen-carrying ability of the blood if the level of CO atmosphere is around 100 ppm. Long term exposure to low levels of carbon monoxide may result in heart disease and damage to the nervous system. Exposure of pregnant women to carbon monoxide may cause low birthrates and nervous system damage to the offspring. The concentration of carbon monoxide in the atmosphere varies from one region to another but the levels normally present are unlikely to cause ill effect. The concentration may reach harmful levels in poorly ventilated rooms during operation of unflued gas heaters, or defective non-electric heating appliances, or in the passenger compartment of vehicles with defective exhaust systems. The fatal damage can be prevented by an oxidation of CO pollutant in the atmosphere into CO_2,

$$CO + \frac{1}{2}O_2 \longrightarrow CO_2, \quad \Delta G_{298K} = -257.1 \, kJ \bullet mol^{-1} \quad (2.1)$$

There are three possible mechanisms by which CO can be oxidized on a surface:

2.2.1 Langmuir–Hinshelwood mechanism

It was generally believed that CO oxidation on transition metals followed a Langmuir–Hinshelwood mechanism. The oxygen molecules can readily dissociate on all transition metals at room temperatures. The mechanism involves an external

source of O_2 or a pre-oxidizing treatment, and is frequently proposed to take place at metal-dispersed catalysts. Three elementary steps have been proposed during the CO oxidation [72]:

(i)   CO is adsorbed on surfaces of metal catalyst;

$$CO(g) \Leftrightarrow CO(a) \tag{2.2}$$

(ii)   Oxygen is dissociatively adsorbed on surfaces of metal catalyst to form oxygen adatoms;

$$O_2(g) \Leftrightarrow O(a) + O(a) \tag{2.3}$$

(iii)   Adsorbed CO molecule reacted with adsorbed oxygen to form CO_2 and desorbed from the surface of metal catalyst;

$$CO(a) + O(a) \rightarrow CO_2(a) \tag{2.4}$$

$$CO_2(a) \rightarrow CO_2(g) \tag{2.5}$$

It was note that at low temperatures CO blocks the surface and the reaction is slow according to Equation (2.4). With increasing temperature, above ~373 K, CO is partially desorbed, and O_2 is chemisorbed on the surface. The reaction rate passes through a maximum around 473 K, after which it falls again. The reaction is structure-insensitive in case of noble metal catalysts [73]. However, when the reaction conditions vary, the mechanism may be changed.

2.2.2 Eley-Rideal (ER) mechanism

In a case of competitive adsorption [73] if the supported noble metal oxides catalyst is first exposed to O_2, then atomic adsorption of oxygen on the surface occurs. CO is then introduced at room temperature and the reaction proceeds rapidly by the Eley-Rideal mechanism according to Equation (2.6):

$$CO(g) + O(a) \rightarrow CO_2(g) \quad \textbf{(fast)} \tag{2.6}$$
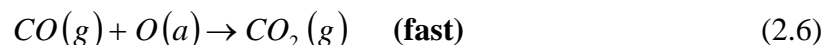
If CO is first adsorbed and then oxygen is introduced then no reaction occurs according to Equation (2.7).

$$CO(a) + \frac{1}{2}O_2(g) \nrightarrow CO_2(g) \tag{2.7}$$

2.2.3 Mars-van-Krevelen mechanism

The direct participation of lattice O atoms in this oxidation reaction is known as a Mars-van-Krevelen mechanism and has been proposed to explain the CO_2 and CO_3^{2-} formation upon metal oxide exposure to CO [74]. In this case, such lattice oxygen atoms should be sufficiently basic sites to attack CO. In other words, the oxygen atoms on the surface must be reactive enough to allow the adsorption of CO at these sites. Such sites do not exist on perfect stoichiometric surfaces and require some corrugation. Once CO has approached the activated O atom, an electron transfer takes place from the molecule to the surface and the cationic sites are reduced. As a result, CO binds to one surface O forming CO_2, or to two surface O forming carbonates CO_3^{2-}, at the same time that titanium cations are reduced.

Konova et al. [75] proposed the model of the reaction mechanism of Au/TiO_2 catalyst as shown in the equation below. The first step (2.8) of the proposed oxidation

$$\text{Au...O-Ti-O + CO}_{(g)} \rightarrow \text{Au...O-Ti-O} \tag{2.8}$$

$$\text{Au...O-Ti-O} \rightarrow \left[\text{Au...O-Ti-O} \right] \rightarrow \text{Au...-Ti-O + CO}_{2\,(g)} \tag{2.9}$$

$$\rightarrow \text{Au...O-Ti-O} \tag{2.10}$$
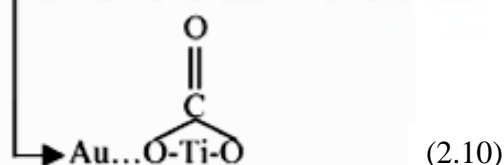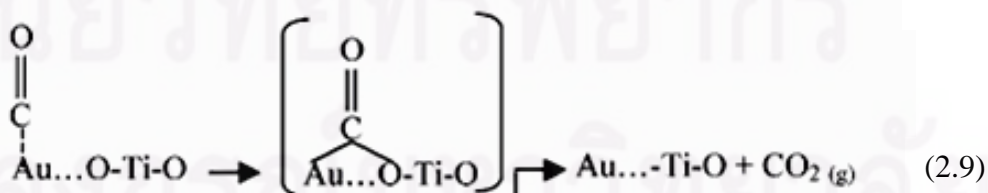
mechanism includes CO adsorption on the gold particle. During the second step (2.9), CO adsorbed on a gold particle as surface carbonyl, transform into an intermediate complex, which decomposes following two alternative parallel pathways. If the intermediate complex decomposes evolving the reaction product and liberating the active site, the second step can take place. The other possibility (2.10) for the intermediate complex is the change into surface carbonates deposited on the oxide support. This carbonatisation process leads to deactivation of the catalyst. They believe that reaction (2.10) has a much lower rate as compared to reaction (2.9). As a result of reaction (2.10), the amount of lattice oxygen of the metal-support border gradually decreases because of covering of the support surface area with carbonates. The oxygen coming from the gas phase is adsorbed on the oxygen vacancies of the metal oxide surface, passing through several oxidation forms and filling up the stores of surface oxygen (2.11). During the last step (2.12), the missing oxygen on the active site is restored and can again take part in the oxidation process.

$$O_2(g) \rightarrow \left(O_2^-\right)_{ad.} \rightarrow \left(2O^-\right)_{ad.} \rightarrow \left(2O^{2-}\right)_{ad.} \tag{2.11}$$

$$Au...Ti-O+\left(O^{2-}\right) \rightarrow Au...O-Ti-O \tag{2.12}$$
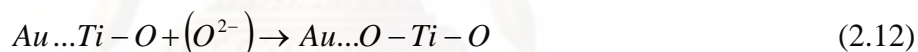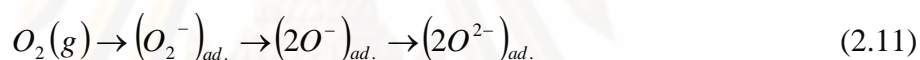
The mechanism for both Langmuir–Hinshelwood and Mars-van-Krevelen may act independently, as suggested for Cu supported on titania and ZnO [76]: whereas a direct oxidation of CO takes place at the surface of the metallic particles, an induced oxidation with the surface lattice oxygen species of the supports is also responsible for the formation of CO_2 and carbonate species.

CO usually binds weakly to the cation of the metal oxide surfaces and serves to test Lewis acidity [74, 77, 78]. At small coverage, CO is adsorbed C-down on top of the metallic center and its orientation is due to donation to the cationic site. Lin et al. [79] predict a stronger interaction for CO adsorption on anatase than on rutile despite their identical chemical composition. It is found that CO_2 is the main oxidation product obtained when exposing the pure anatase surface to CO although other oxidation products like carbonates or carboxylates have also been detected [22, 80-82]. Mguig et al. [83]proposed that the oxidation of CO on pure anatase can occur

without oxidizing conditions. Naturally, a preoxidizing treatment or the presence of oxygen in the reaction media will enhance it [81]. The presence of metals (Pd, Au, Na) or other metal oxides (Fe_2O_3, La_2O_3, CuO) dispersed on the anatase phase also contributes to increase the rate of CO oxidation.

The CO oxidation is usually considered as a typical example of a structure insensitive reaction. For example, the catalytic activity is almost equal over Pt/Al_2O_3 catalysts with widely varying particle size at high CO concentration. However, the reaction became structure sensitive in excess oxygen. CO oxidation has been mostly studied on the late 4d and 5d transition metals, such as Ru, Rh, Pt and Pd. Among them, Pt is known to be one of the most active catalysts, while Ru is the poorest one at low pressures of O_2 and CO, being only active at high O_2 partial pressures [84]. Recent STM experiments [85] further suggest that on other transition metals, such as Pt and Pd, the formation of oxide may largely improve the catalytic ability. Neither 3d transition metals, such as Fe, Co, Ni, nor the early transition metals, such as W, Zr are good catalysts for CO oxidation, presumably because these metals bond O atoms too strongly and they are not stable enough in the oxidative conditions. For recent years another new class of catalysts for CO oxidation, namely, oxide supported Au catalysts has attracted much attention [86]. Au-based catalysts have a superior high catalytic ability at low temperatures (e.g., below 300 K) compared to transition metal catalysts.

2.2.4   Application of TiO_2 for CO oxidation

The importance of TiO_2 in heterogeneous catalysis is also profound and the performances of many metals or metal oxides on high-surface-area TiO_2 support have been studied. These metal oxide/TiO_2 systems often serve as a model for other metal/oxide surfaces. It is well known that the role of TiO_2 on catalytic activity is more complex than simple to increase catalyst surface area and interactions between the catalyst and TiO_2 may occur that lead to changes in reactivity and selectivity [87]. Although TiO_2 is not suitable as a structural support material for metals compared with Al_2O_3 and SiO_2, small additions of TiO_2 can modify metal-based catalysts to a significant extent.

CO oxidation is one of the reactions that have been frequently investigated using TiO_2 as the support due to strong interaction with group VIII noble metals. TiO_2 can provide high dispersion of noble metal catalyst. It is well known that supported noble metal catalysts such as Au/TiO_2, Ir/TiO_2, and Ag/TiO_2 are effective in CO oxidation [12, 88, 89], of which Au/TiO_2 used for CO oxidation at low temperature was the most excited discovery [76]. Despite the inertness of gold metal compared to other transition metals, highly dispersed gold particles on reducible metal oxides can exhibit surprisingly high catalytic reactivity for many reactions. Several factors, such as size and shape of the cluster, metal-support interaction between Au clusters and the surface, have been suggested as the reason for the enhanced reactivity of small gold clusters. However, because of their relatively high cost, many researchers have attempted to study catalytic activity of other transition metals in order to replace the gold catalysts. Much attention has been given to non-noble metal catalysts, such as cobalt and copper [90-95].

2.3 Modification of TiO_2 nanopaticles

Properties of nanoparticles are different to those of matter of the same chemical composition on a larger scale. Therefore, research on nanoparticles is increasing rapidly, and numerous applications are anticipated. Although some nanomaterials have excellent physical and chemical bulk properties, they do not possess suitable surface properties for specific applications. Consequently, it may be necessary to modify the surface of such materials. Recently, there are many publications that studied heterogeneous catalytic reactions using the nanomaterials as support. The support was usually considered as an inert material before the concept of a strong metal–support interaction was proposed [6, 96]. This concept emphasized the importance of the support characteristics on the catalytic activities. Also, the concept of an interfacial metal–support interaction (IMSI) was proposed [97]; specifically, metal oxide species supported on oxygen ion conducting materials show a remarkable effect on the activity enhancement for CO oxidation [98]. With these concepts, support modifications have attracted much research interest and are considered an important factor in improving catalytic activity [99, 100].

2.3.1 Modification with defective surface creation

The nature of the support material, the preparation method, and the activation procedure are expected to influence the structure and reactivity of the supported metal species. TiO_2 has been studied extensively in the field of surface science due to the wide range of its applications and the expectation that insight into surface properties on the fundamental level that will help to improve its properties. The surface defect is one of the important topics in this field because the properties of the TiO_2 nanocrystal are often dependent on a nature and density of the surface defect sites. In case of a nature of surface defect, the dominant defect on the TiO_2 surface is oxygen vacancies site (Ti^{3+}) [101]. To control a density of this defect, some common methods such as UV radiation, annealing under vacuum, ion sputtering, plasma-treating have been used for creating the defect on the TiO_2 [102-104].

Perfect surfaces of TiO_2 are usually poorly reactive and it is generally assumed that the strongest adsorption occurs at defective sites. So, the presence of such defect on oxide surfaces plays an important role in the reactivity of these surfaces. Ether the ability of these surfaces to undergo adsorption of gases or the growth mode of thin metal deposits on the surfaces can be drastically influenced by the stoichiometery of the surface [105, 106] , that is to say by the presence of oxygen vacancies. In the same way, surface defects induced by ion can modify the distribution of nucleation sites on the surface and, therefore, the type of growth of a metal on the oxide surface [107].

The solvothermal method has been used to successfully synthesize TiO_2 in anatase polymorph with surface defect by controlling reaction condition. Wachiraphan Payakgul et al. [108] investigated the effect of organic solvent to the characteristic of the nanocrystalline TiO_2. They found that TiO_2 nanoparticles obtained in 1,4-butaindiol have higher thermal stability than the ones obtained in toluene. They suggested that the difference in thermal stability of the products results from different amount of defect structures or crystallinity obtained by different synthesis routes. Akawat Sirisuk et al. [109] studied the effects of reaction medium and crystallite size on Ti^{3+} surface defect in titanium dioxide nanoparticles prepared by solvothermal method. They found that the amount of surface defect increased with increasing the crystallite size of TiO_2 and the larger size of TiO_2 exhibited higher

photocatalytic activity. The dispersion of metal on defective TiO_2 was studied by Wallace et al. [110] and Kongkiat Suriye et al. [111] who reported that surface defect (Ti^{3+}) plays a significant role enhancing the dispersion and stability of supported metal such as gold cluster and cobalt via the strong interaction (SMSI) between the defect site and metal cluster. Thus, it demonstrates that the creation of surface defect (Ti^{3+}) on anatase is necessary for improving its properties for many applications.

2.3.2 Modification with trace element

In heterogeneous catalytic reactions, the support was usually considered as an inert material before the concept of a strong metal–support interaction was proposed [6, 96]. This concept emphasized the importance of the support characteristics on the catalytic activities. Also, the concept of an interfacial metal–support interaction (IMSI) was proposed [112]; specifically, metal oxide species supported on oxygen ion conducting materials show a remarkable effect on the activity enhancement for CO oxidation [98]. With these concepts, support modifications have attracted much research interest and are considered an important factor in improving catalytic activity [99, 100].

Although some nanomaterials have excellent physical and chemical bulk properties, they do not possess suitable surface properties for specific applications. Consequently, it may be necessary to modify the surface of such materials [113]. The factors that influence the activity of supported metal catalysts are the nature of the support. The most common way to modify the support material is the modification with trace element. Many research reported that the surface modification can stabilize nanoparticles against agglomeration and retard the phase transformation [114, 115].

Pestryakov et al. [116] modified γ-Al_2O_3 by addition of 5 wt% of Zr, Ce, La, and Cs oxides before gold impregnation and found that the modifying additions of rare and rare-earth metal oxides notoriously changed the electronic state of gold. These effects were reported to be caused not only by differences in the gold particle dispersivity, but also by interaction of gold atoms and ions with Lewis acid sites on the modified support.

Tai et al. [117] prepared titania aerogel and titania-coated silica aerogel incorporating Au nanoparticles. The size of the Au particles in the titania areogel increased with increasing the calcination temperature while the titania-coated silica aerogel were almost unchanged. They concluded that the size of the Au nanoparticles and the loading amount of Au can be independently controlled by using the titania-coated silica gel support. The modification of TiO_2 aerogel support with silica-coating improved the catalytic activity of Au/TiO_2 compared to that on pure TiO_2 support.

Yu et al. [118] reported that doping of La in TiO_2 support during the sol-gel synthesis also enhanced the catalytic activity of Au/TiO_2 in CO oxidation. They found that the presence of La in TiO_2 not only increased its surface area and restrained the growth of TiO_2 crystallites, but could also enhance the microstrain of TiO_2. The O_2-TPD results showed a new adsorbed species O^- on the surface of La-doped TiO_2. The high activity of Au/La_2O_3-TiO_2 was attributed to the presence of La promoting the reactivity of CO adsorbed on the Au site and the formation of the second active site on the surface of TiO_2.

CHAPTER III
EXPERIMENTAL

This chapter presents an overview of the research methodology that was used in this work. There are four main sections in this chapter that consist of the following: material and chemicals, TiO_2 support and the catalysts preparation, catalyst characterization, and reaction study in CO oxidation reaction. The first section depicted all materials and chemicals used for this research. The second illustrated the preparation of TiO_2 and modified TiO_2 support including metal catalyst. The third section described the characterization method of the support and the catalyst such as XRD, XPS, BET surface area, FT-IR, ESR, Pulse chemisorption technique and Temperature programmed desorption of oxygen (O_2-TPD). The reaction procedure for CO oxidation was explained in detail in the last section.

3.1 Material and chemicals

The details of chemicals used in this experiment are shown in Table 3.1.

Table 3.1 Chemicals used in the preparation of catalysts.

Chemical	Supplier
Titanium (IV) *n*-butoxide (TNB) 97%	Aldrich
1,4 butaindiol	Aldrich
Methanol	Merck
Silver nitrate ($AgNO_3$)	Aldrich
Nickel nitrate ($Ni(NO_3)_2.6H_2O$)	Aldrich
Cobalt nitrate ($Co(NO_3)_2.6H_2O$)	Merck
Chloroplatinic Acid Hexahydrate ($H_2PtCl_6.6H_2O$)	Aldrich
Tetraethylorthosilicate ($SiO_4(C_2H_5)_4$)	Aldrich
Aluminum triethoxide ($AlO_3(C_2H_5)_3$)	Aldrich
Triethyl phosphate ($PO_4 (C_2H_5)_3$)	Aldrich

Table 3.1 Chemicals used in the preparation of catalysts (Cont.).

Chemical	Supplier
Phosphoric acid (H_3PO_4)	Aldrich
Di-ammonium hydrogen phosphate ($(NH_4)_2HPO_4$)	Aldrich
Phosphorus pentoxide (P_2O_5)	Merck

3.2 Preparation of TiO$_2$ support and the catalysts

The detail of preparation of TiO$_2$ support and the catalysts were presented as follows:

3.2.1 Preparation of TiO$_2$ support

TiO$_2$ nanocrystals were prepared by solvothermal method according to a procedure reported by Wachiraphan Payakgul et al. [108] using titanium (IV) n-butoxide (TNB) as starting material. About 15 and 25 g of titanium (IV) n-butoxide (TNB) 97% from Aldrich was suspended in 100 cm^3 of 1,4-butanediol in a test tube and placed in an autoclave as shown in Figure 3.1. The gap between the test tube and the autoclave wall was contained with 30 cm^3 of the same solvent used in the test tube. The autoclave reactor was completely purged with nitrogen. The reactor was heated to a desired temperature (300°C or 320°C) at a rate of 2.5°C/min and held constant at that temperature for 0.5 h and 4 h for preparing TiO$_2$ supports with average crystallite size 7 and 15 nm, respectively. After the reactor was cooled to room temperature, the TiO$_2$ powders obtained in the test tube were repeatedly washed with methanol and dried in ambient air.

3.2.2 Preparation of modified-TiO$_2$ support

The modified-TiO$_2$ was prepared by solvothermal method as described above with the preparation condition: 25 g of TNB, holding time for 4 h and holding temperature at 320°C. In this study, TiO$_2$ was modified with trace element such as Si, Al, and P in order to investigate the effect of element type on the catalytic activities in

CO oxidation. The element precursors used were tetraethylorthosilicate $(SiO_4(C_2H_5)_4)$, aluminum triethoxide $(AlO_3(C_2H_5)_3)$, and triethyl phosphate $(PO_4(C_2H_5)_3)$ for preparation of modified TiO_2 with Si, Al, and P, respectively. In case of the study of phosphorus precursor effect, four types of the precursor used in this investigation were phosphoric acid (H_3PO_4), di-ammonium hydrogen phosphate $(NH_4)_2HPO_4$, triethyl phosphate $(PO_4(C_2H_5)_3)$, and phosphorus pentoxide (P_2O_5). A certain amount of modifier precursor (calculation as shown in Appendix A) was added into the mixed solution of TNB and 1,4-butanediol before setting up in the autoclave. After cooling naturally to room temperature, the products were repeatedly washed with methanol and dried in air.
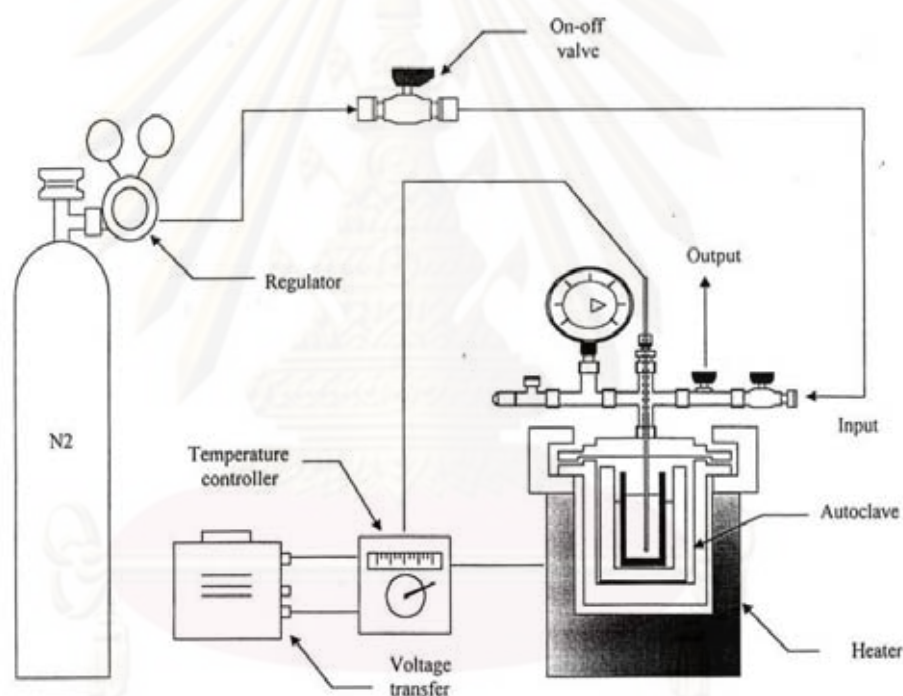
Figure 3.1 Diagram of the reaction equipment for the synthesis of titanium dioxide.

3.2.3   Preparation of the catalyst

The incipient wetness impregnation method was used to prepare supported metal catalysts. The aqueous solution of the metal precursor was dropped slowly onto TiO_2 or modified TiO_2 support to obtain the desired atomic percent of the catalyst

(calculation as shown in Appendix A). After impregnation, the catalyst were dried at room temperature for 6 h and then at 110°C overnight in an oven. The obtained samples were calcined in air at 450°C for 3 h. The metal precursors used in this investigation were $AgNO_3$, $Ni(NO_3)_2.6H_2O$, $Co(NO_3)_2.6H_2O$, and $H_2PtCl_6.6H_2O$ for preparation of Ag/TiO_2, Ni/TiO_2, Co/TiO_2, and Pt/TiO_2 catalysts, respectively.

3.3 Catalyst characterization technique

The various characterization techniques were used to gain more understanding about the catalyst structure and texture properties resulting in their catalytic properties.

3.3.1   X-ray Diffraction (XRD)

XRD were performed to determine the bulk crystalline phases of catalyst. It was conducted using a SIEMENS D-5000 X-ray diffractometer connected with a computer with Diffract ZT version 3.3 program for fully control of the XRD analyzer. The experiments were carried out by using CuK_α (λ = 1.54439 Å) radiation with Ni filter in the range $2\theta = 20$-80° resolution 0.04.

3.3.2 N_2 physisorption (BET surface area)

Surface area measurements were carried out by low temperature nitrogen adsorption in a Micromeritic ChemiSorb 2750 system. Calculations were performed on the basis of the BET isotherm. 0.2 grams of sample was loaded into u-shape cell made from Pyrex and heated in helium to 200^oC for 1 h in order to eliminate trace amount of water adsorbed on surface, then cooled down to room temperature. The analysis gas consist of $30\%N_2$ in helium was introduced to Pyrex cell. Sample adsorbed nitrogen at low temperature by dipped cell into liquid nitrogen dewar until it's surface was satuated with nitrogen and desorbed nitrogen at room temperature by moved away the dewar. The nitrogen that was desorbed from sample was measured by TCD detector.

3.3.3   Fourier Transform Infrared Spectroscopy (FT-IR)

FT-IR analysis of modified TiO_2 support was carried out in a Nicolet model 6700 of the IR spectrometer using the wavenumber ranging from 400–4000 cm^{-1} with a resolution of 4 cm^{-1}. A small amount of sample was thoroughly mixed with ground KBr in an agate mortar and pressed as pellets.

3.3.4   Electron Spin Resonance Spectroscopy (ESR)

A JEOL, JESRE2X model electron spin resonance spectroscopy (ESR) was used to measure the surface defect (Ti^{3+}) on the surface of TiO_2 support and modified TiO_2 support. Before measurement, the sample was dried at $110^{o}C$ overnight. About 0.1 g of sample was placed in a sample tube, which was sealed at atmospheric pressure and room temperature.

3.3.5   Transmission electron microscopy (TEM)

The morphology and size of the metal catalysts were determined using a transmission electron microscopy (TEM) with a Philips CM100 microscope.

3.3.6   Thermal Gravimetric Analysis (TGA)

TGA was performed to prove the interaction between the [Al]MAO and various supports. It was conducted using TA Instrument SDT Q600 analyzer. The samples of 10–20 mg and temperature ramping from room temperature to 800 ^{o}C at $10^{o}C$ /min were used in the operation. The carrier gas was air zero.

3.3.7   X-ray photoelectron spectroscopy (XPS)

XPS was used to examine the binding energy and the surface composition of the catalysts by using an Amicus photoelectron spectrometer with Mg K_{α} X-ray source at current of 20 mA and 10 keV, resolution of 0.1 ev/step, and pass energy of 75 kV. The binding energy was calibrated by the C 1s peak at 285.0 eV. The computer controlled by using the AMICUS "VISION2" software.

3.3.8 CO-Pulse Chemisorption

The active sites of Platinum catalyst was determined by CO-pulse chemisorption technique using Micromeritics ChemiSorb 2750 (pulse chemisorption system) and ASAP 2101C V.3.00 software. Approximately 100–200 mg of the catalyst was reduced in-situ in flowing hydrogen (50 cm^3/min) at 400°C for 1 h. After that, the sample was cooled to room temperature in N_2 flow and CO pulses were injected until the quantity of the exit CO pulse reached a steady value.

3.3.9 H$_2$-Pulse Chemisorption

The active sites of Nickel and Cobalt catalyst was determined by H$_2$-pulse chemisorption technique using Micromeritics ChemiSorb 2750 (pulse chemisorption system) and ASAP 2101C V.3.00 software. Approximately 100–200 mg of the catalyst was reduced in-situ in flowing hydrogen (50 cm^3/min) at 400°C for 1 h. After that, the sample was cooled to room temperature in N_2 flow and CO pulses were injected until the quantity of the exit CO pulse reached a steady value.

3.3.10 N$_2$O-Pulse Chemisorption

The amount of active site of Ag/TiO$_2$ catalyst was determined using the N$_2$O pulse method according to a method adapted from Evans et al. [119]. Before the measurement, about 100 mg of the catalyst sample was reduced at 400°C for 1 h. Then, the sample was cooled to 150°C in He stream and a certain amount of N$_2$O was injected. A TCD detector was used to analyze the gas leaving the He carrier sample. When N$_2$O was contacted with silver metal on TiO$_2$ support, the nitrous oxide was decomposed and producing N_2, shown in the following reaction:

$$N_2O\,(g)\ +\ 2\,Ag\,(s)\ \Leftrightarrow\ N_2\,(g)\ +\ (Ag-O-Ag)(s) \qquad (3.1)$$

3.3.11 O$_2$-Temperature programmed desorption

The O$_2$-TPD experiment was performed in order to study the characteristics of oxygen adsorption and desorption on the catalyst surface. Approximately, 0.1 g of the catalyst was reduced in hydrogen flow (50 cm^3/min) for 1 h. The temperature was then cooled down to 30°C in He stream (30 cm^3/min) and held at that temperature for 1 h to adsorb oxygen with a flow of 30 cm^3/min. The physically adsorbed oxygen on the catalyst surface was swept out with He stream and then the temperature was ramped with a heating rate of 10°C/min to 600°C.

3.4 Reaction study in CO oxidation reaction

Catalytic activity of the catalyst samples in CO oxidation were performed in a 5 mm i.d. glass tube fixed bed microreactor. The reactant and product composition were analyzed on-line with a Shimadzu GC-8ATP gas chromatograph equipped with a thermal conductivity detector (TCD) and a Porapak Q column with He as the carrier gas. An operating conditions used in this experiment are given in table D.1 (Appendix D). A Flow diagram of the system for testing the catalytic activity is shown in Figure 3.2. The reaction gas mixture contained 1% CO and 2% O$_2$ by volume with He balanced was passed through the catalyst bed at total gas flow rate of 100 cm^3/min (GHSV$\approx$ 30,600 h^{-1} or WHSV $\approx$ 60,000 cm^3 h^{-1} g^{-1}). The composition of the inlet gas was controlled by mass flow meters. The procedures of the catalytic testing as shown below;

(1) Approximately 100 mg of the catalyst powder was placed into the reactor and the catalyst bed was held by quartz wool at both ends.

(2) The glass reactor was placed inside a temperature-controlled tubular oven.

(3) A thermocouple was inserted into the tube with one end touching the catalyst zone in order to measure the bed temperature.

(4) Before a start of run, the catalyst was first reduced in-situ at 400°C for 1 h in flowing H$_2$ with a flow rate of 50 cm^3/min and cooled down to room temperature.

(5) Then the gas flow was switched to a reaction gas mixture. The temperature of the oven was increased from room temperature to the desired temperature and maintained at that temperature for 20 min.

(6) The composition of reactant and product were analyzed by Shimadzu GC-8ATP gas chromatograph.

Catalyst performance was evaluated in terms of the light-off temperature, defined as the temperature at which 50% conversion was obtained. The calculation of CO conversion was based on CO consumption. The conversion of CO was determined by using the following equation:

$$\% \, CO \, Conversion \; = \; \frac{(CO_{in} - CO_{out})}{CO_{in}} \times 100 \qquad\qquad (3.2)$$

Figure 3.2 Flow diagram of the system for testing the catalytic activity**.**
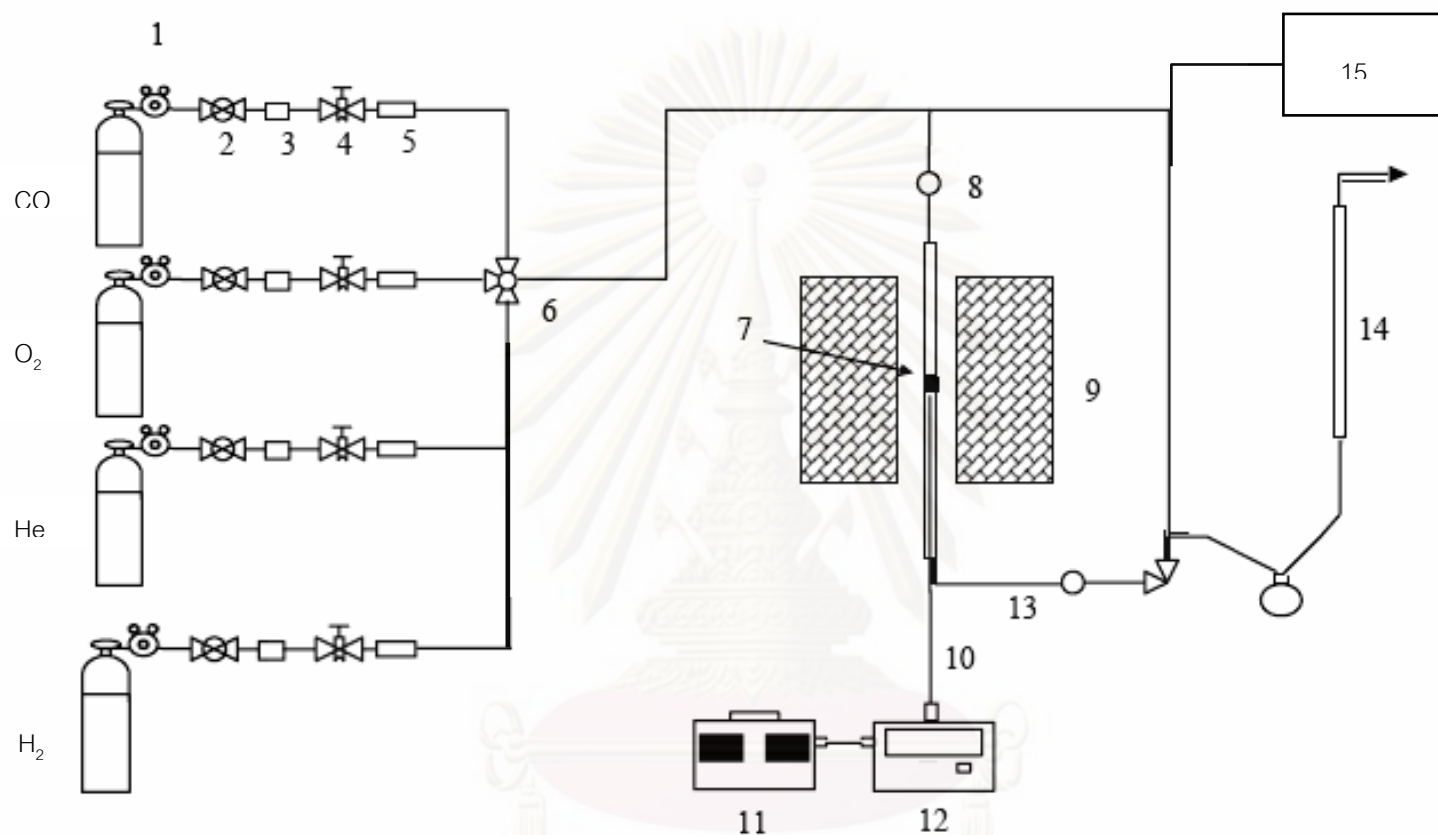
1. Pressure Regulator   2. On-Off Value   3. Gas Filter   4. Metering Valve
5. Back Pressure   6. 3-way Valve   7.Catalyst Bed   8. Sampling point
9. Furnace   10. Thermocouple   11. Variable Voltage Transformer   12. Temperature Controller
13. Heating Line   14. Bubble Flow Meter   15. TCD

CHAPTER IV
RESULTS AND DISCUSSION

The experimental studies described in this thesis are focused mainly on the surface modification of TiO_2 nanoparticles in order to have a potential for using as a support for metal catalysts in CO oxidation reaction. The study of modification of TiO_2 support was divided into two methods. Firstly, the TiO_2 nanoparticles were modified to obtain a different amount of surface defects by changing the synthesis condition of the solvothermal method. Lastly, the TiO_2 nanoparticles were modified by doping with trace element. The metal catalysts were loaded onto TiO_2 and modified TiO_2. The CO oxidation activity of the metal catalyst supported on modified TiO_2 was compared to the ones supported on TiO_2.

The results and discussion in this chapter are divided into four sections to study the effect of various parameters. The effect of amount of defect on a TiO_2 surface and its properties using support in CO oxidation was described in Section 4.1. The parameters of TiO_2 surface modification with trace element were investigated. The effect of the different dopant elements (Al, Si and P), the content of dopant element (Si), and the different phosphorus precursor were illustrated in Section 4.2-4.4, respectively. The catalytic activity of metal catalyst supported on modified TiO_2 was compared with the ones supported on TiO_2.

4.1 Effect of different amount of TiO_2 surface defect on the activity of CO oxidation

In this section, nanocrystalline TiO_2 with different crystallite sizes were synthesized by the solvothermal method using titanium *n*-butoxide and 1,4-butanediol as titanium precursor and solvent, respectively. Under inert organic solvent condition, thermal decomposition of TNB in toluene was occurred, yielding a $\equiv$Ti-O$^-$ anion. The nucleophilic attack of the titanate ion on another ion and crystallization was taken place, finally yielding the anatase titania. The mechanism of TNB in 1,4-butaindiol can be depicted as shown in **Figure 4.1**.
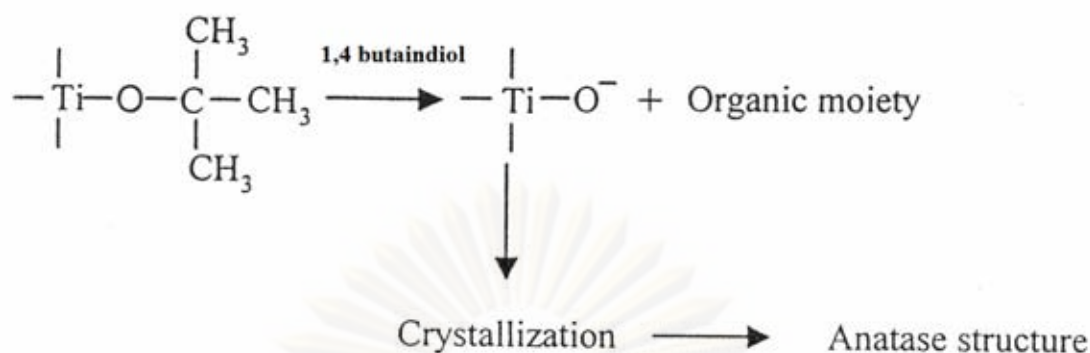
Figure 4.1 Mechanism of nanosized anatase TiO$_2$ synthesis in 1,4-butaindiol by solvothermal method.

     Figure 4.2 shows X-ray diffractograms of the TiO$_2$ supports were obtained by the solvothermal method. The diffraction peaks at 25° (major), 38°, 48°, 54°, 55°, 63°, 71°, and 75° 2θ, indicated that the TiO$_2$ supports contained only anatase phase TiO$_2$. The average TiO$_2$ crystallite sizes calculated from the full-width at half-maximum of the XRD peak at 2θ = 25° using the Scherrer equation were determined to be 7 and 15 nm. The TiO$_2$ supports with average crystallite size 7 and 15 nm are referred to as TiO$_2$-7nm and TiO$_2$-15nm, respectively. The average crystallite size of TiO$_2$ was increased by increasing amount of TNB precursor, synthesis temperature, and holding time [120]. The corresponding BET surface areas of the TiO$_2$ nanoparticles with average crystallite sizes 7 nm and 15 nm were 161 m^2/g and 77 m^2/g, respectively, as shown in **Table 4.1**.
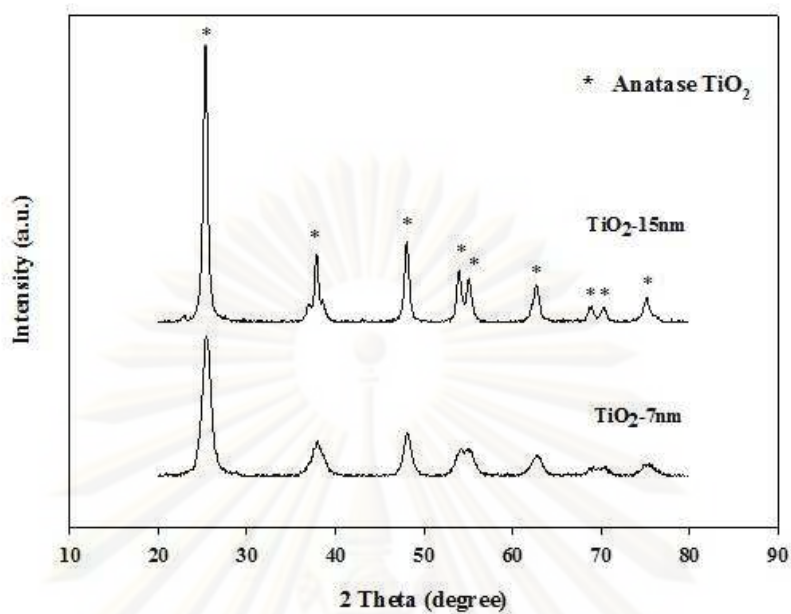
Figure 4.2 X-ray diffraction patterns of TiO_2-7nm and TiO_2-15nm supports prepared by solvothermal method.

Table 4.1 Physical properties of nanocrystalline TiO_2 supports prepared by olvothermal method.

Sample	Synthesis conditions				Average crystallite size	BET surface area (m^2/g)
	TNB amount (g)	1,4 butainediol (cm^3)	Synthesis temperature (°C)	Holding time (h)	(nm)	
TiO_2-7nm	15	100	300	0.5	7	161
TiO_2-15nm	25	100	320	4	15	77

The number of defective sites of TiO_2 was determined using electron spin resonance spectroscopy (ESR) technique and the results are shown in **Figure 4.3**. The ESR peak with a g value of 1.997 was assigned to Ti^{3+} defective sites on the TiO_2 surface [121-125]. It is clearly seen that the Ti^{3+} signal increased with increasing TiO_2 crystallite size. In other words, the larger crystallite size of nanocrystalline TiO_2 prepared via solvothermal synthesis contained higher amount of Ti^{3+} surface defects.

The TiO_2 powders with different amount of surface defects (TiO_2-7nm and TiO_2-15nm), were then employed as supports for dispersion of four different transition metals namely, Ag, Co, Ni, and Pt. The selected metals were classified into two groups; precious metals (Ag and Pt) and transition metals (Co and Ni). Each of the catalysts was loaded with two different atomic percent metal loadings (1 at.% and 25 at.%) by incipient wetness impregnation method.
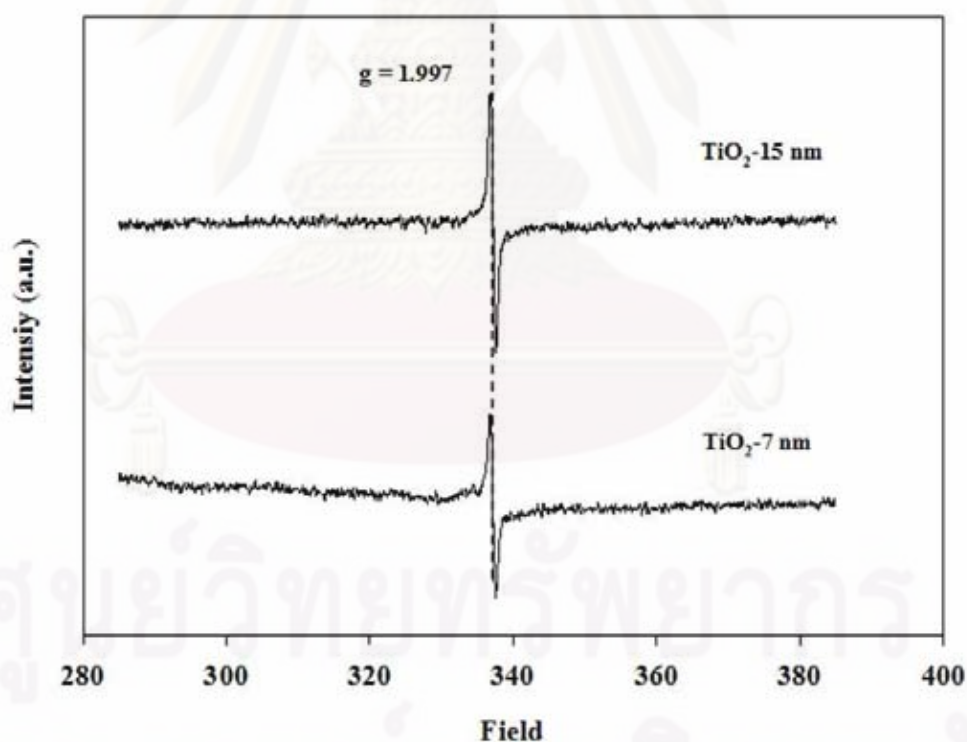
Figure 4.3 ESR spectra at atmospheric condition of TiO_2-7nm and TiO_2-15nm support prepared by solvothermal method.

Figure 4.4 shows TEM images of the TiO_2 supports before and after Ag metal loading. The crystal morphology of TiO_2-7nm was roughly spherical crystals while TiO_2-15nm was mostly cube crystal shapes. The average particle sizes determined from TEM were 6.8 nm and 15.1 nm for TiO_2-7nm and TiO_2-15nm, respectively, which were in good agreement with those calculated from XRD results. It is also confirmed that the crystallite size of TiO_2 supports were not altered after metal loading. Based on the Ag/TiO_2 catalysts with medium Ag loading (15 at.%), the Ag particles appeared to be homogeneously dispersed on both TiO_2 supports. There was no significant difference in terms of particle size distribution of the Ag metals.

Figure 4.5 shows TGA curves of TiO_2-15nm and 25%Ag/TiO_2-15nm catalyst. TGA thermogram exhibits two stages of weight loss for TiO_2-15nm. The first loss (1%) appears in the range 100-250°C and the second one (3.5%) appears in the range of 250-400°C. The first step of weight loss can be attributed to the removal of the structural water. The second step of weight loss can be ascribed to the combustion of organic moieties, originating from the organic solvents and certain new compounds formed in the solvothermal process. The TGA thermogram of 25%Ag/TiO_2-15nm catalyst indicates that the organic moieties cannot be removed by calcination [126]. However, the residual nitrate ions from silver nitrate precursor can be decomposed into nitrogen dioxide and oxygen at temperature below 300°C [127].

Table 4.2 shows a comparison of the amounts of metal active sites on Ag/TiO_2, Co/TiO_2, Ni/TiO_2, and Pt/TiO_2 catalysts for both sizes of the TiO_2 supports at 1 and 25 atomic% loadings. For any metal type, the catalysts supported on larger crystallite size TiO_2 possessed higher amount of metal active sites than those supported on smaller crystallite size one. It is noticed that the BET surface area of TiO_2-15nm was only half of that of the TiO_2-7nm. The higher amount of active metal dispersed on the larger crystallite size TiO_2 can be correlated with the higher number of Ti^{3+} sites on the larger crystallite size TiO_2 support. In the light of our previous studies for Co/TiO_2 Fischer-Tropsh, it is suggested that the presence of Ti^{3+} sites on the TiO_2 surface can inhibit agglomeration of metal particles during impregnation,
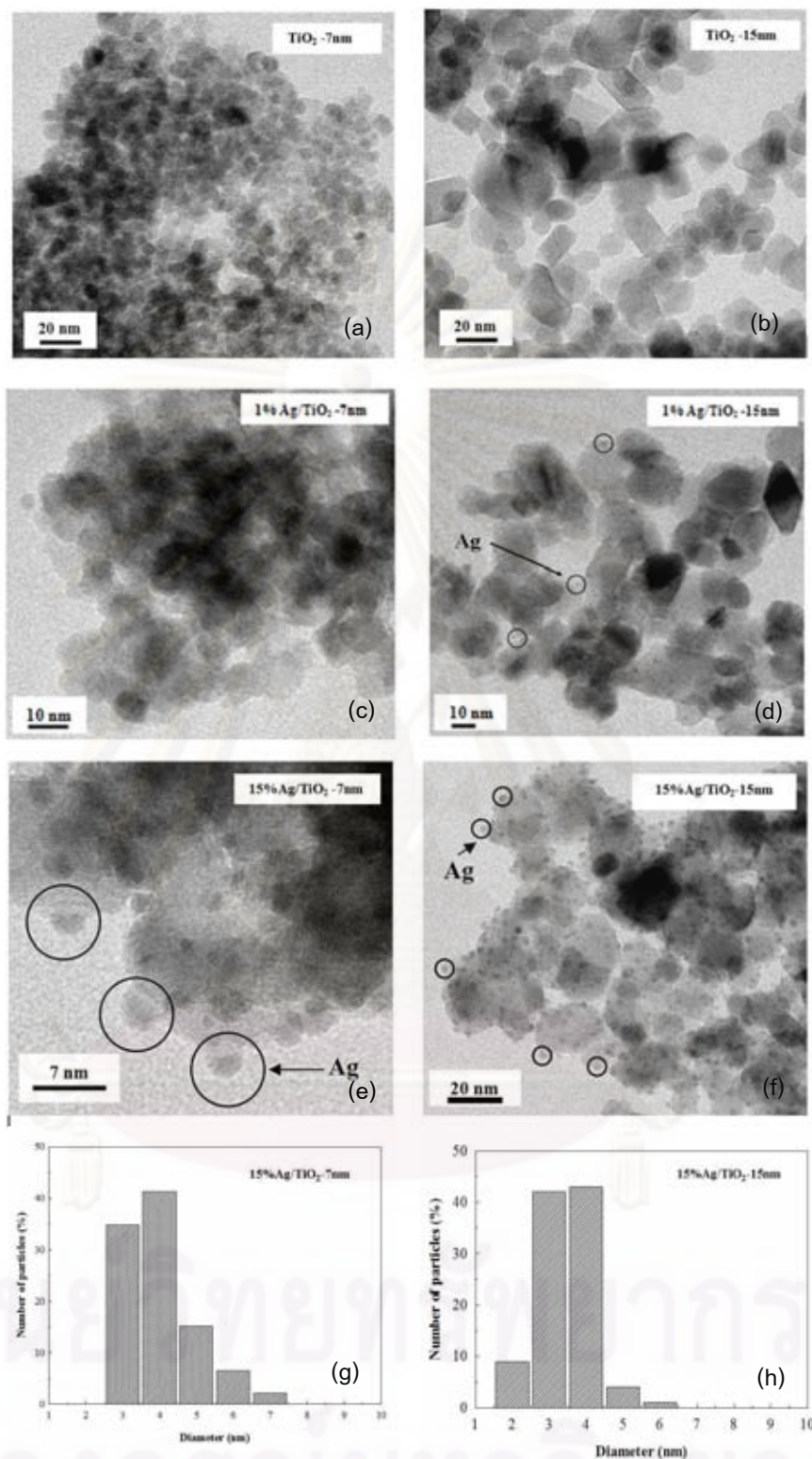
Figure 4.4 TEM images of TiO$_2$ support before and after Ag metal loading (a, b, c, d, e, f) and size distribution of Ag particles deposited on TiO$_2$ (g, h): (a) TiO$_2$-7nm; (b) TiO$_2$-15nm; (c) 1%Ag/TiO$_2$-7nm; (d) 1%Ag/TiO$_2$-15nm; (e, g) 15%Ag/TiO$_2$-7nm and (f, h) 15%Ag/TiO$_2$-15nm.
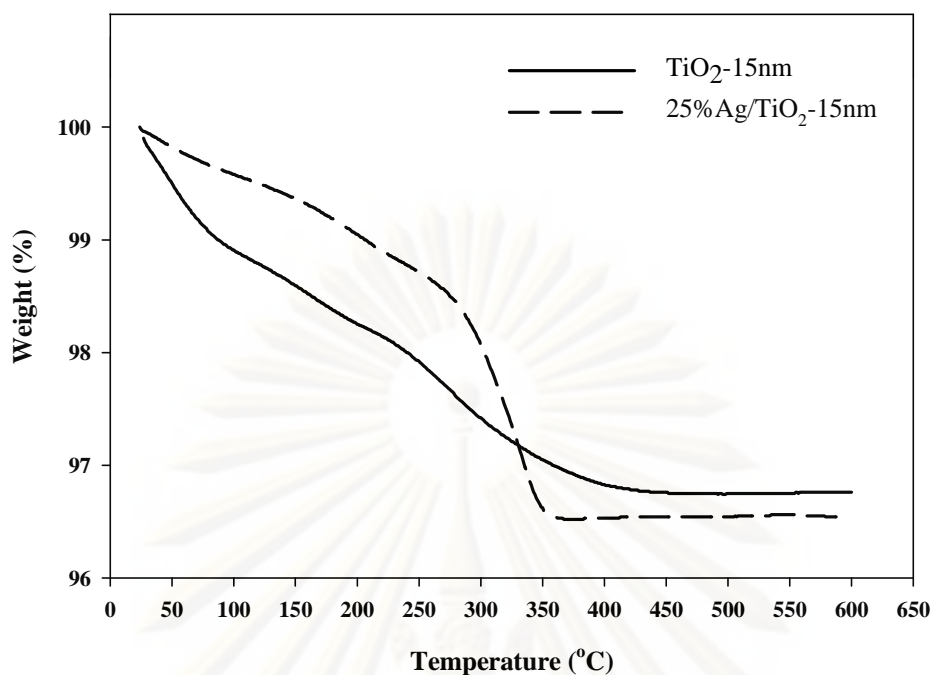
Figure 4.5 TGA curves of TiO$_2$-15nm and 25%Ag/TiO$_2$-15nm.

Table 4.2 The amount of active sites of metal catalysts supported on TiO$_2$-7nm and TiO$_2$-15nm with different atomic loading.

Sample	Active Site (x 10^{18} atoms/g cat.)			
	TiO$_2$-7nm		TiO$_2$-15nm	
	1 at.% Loading	25 at.% Loading	1 at.% Loading	25 at.% Loading
Ag/TiO$_2$	10.5	15.5	22.2	52.3
Co/TiO$_2$	nil.	0.8	0.2	16.4
Ni/TiO$_2$	0.1	8.8	1.2	38.0
Pt/TiO$_2$	4.8	n.d.[d]	10.6	n.d.

n.d. = not determined.

calcination, and reduction steps so that higher metal dispersion was obtained [121,128]. Aggregation of TiO_2 nanoparticles may also have influence upon the reduced surface Ti^{3+} sites for smaller crystallite size TiO_2 leading to lower metal dispersion. Cordero et al. [129] suggested that transference of electronic charge density from TiO_2 to activated carbon (AC) resulted in a high degree of dispersion of TiO_2 on the AC surface. The presence of an intimated contact interface could prevent "surface nano-aggregation". By analogy, the presence of Ti^{3+} defective sites on larger crystallite size TiO_2 in the present work would inhibit agglomeration of the metal clusters to form larger particle size; hence higher metal dispersion could be obtained.

Typically, higher amount of metal loading results in higher number of active species dispersed on support surface when the amount of metal loading is within its monolayer dispersion. When the metal loading was more than the monolayer dispersion threshold, the number of the active species was reduced due to agglomeration, resulting in a suppression of catalytic activity [93]. In the present work, an increase of metal loading from 1 at.% to 25 at.% did not cause a decrease of the amount of active sites. Moreover, metal dispersion on the larger crystallite size of TiO_2 was still higher than those on the smaller one for both low and high metal loadings.

The CO conversion over Ag/TiO_2, Co/TiO_2, Ni/TiO_2, and Pt/TiO_2 catalysts with different crystallite size of TiO_2 supports (7 nm and 15 nm) and different amounts of metal loading (1 at.% and 25 at.%) are shown in **Figure 4.6**. The light-off temperature of each catalyst was also given in **Table 4.3**. Complete conversion of CO (100%) was achieved within 350°C for all the catalysts except 1%Ni/TiO_2-7nm, 1%Ni/TiO_2-15nm, and 1%Co/TiO_2-7nm. The low conversion of these catalysts corresponded to their relatively low metal dispersion as determined from pulse chemisorption experiments. For any crystallite size of TiO_2 support with a similar metal loading, the light-off temperature was found to in the order: Pt < Ag < Co < Ni indicating that the noble metal catalysts were much more effective in CO oxidation than the non-noble ones [130]. The lowest light-off temperature was obtained using 1%Pt/TiO_2 on the TiO_2-15nm support at below 50°C. Compared to the 1%Pt/TiO_2
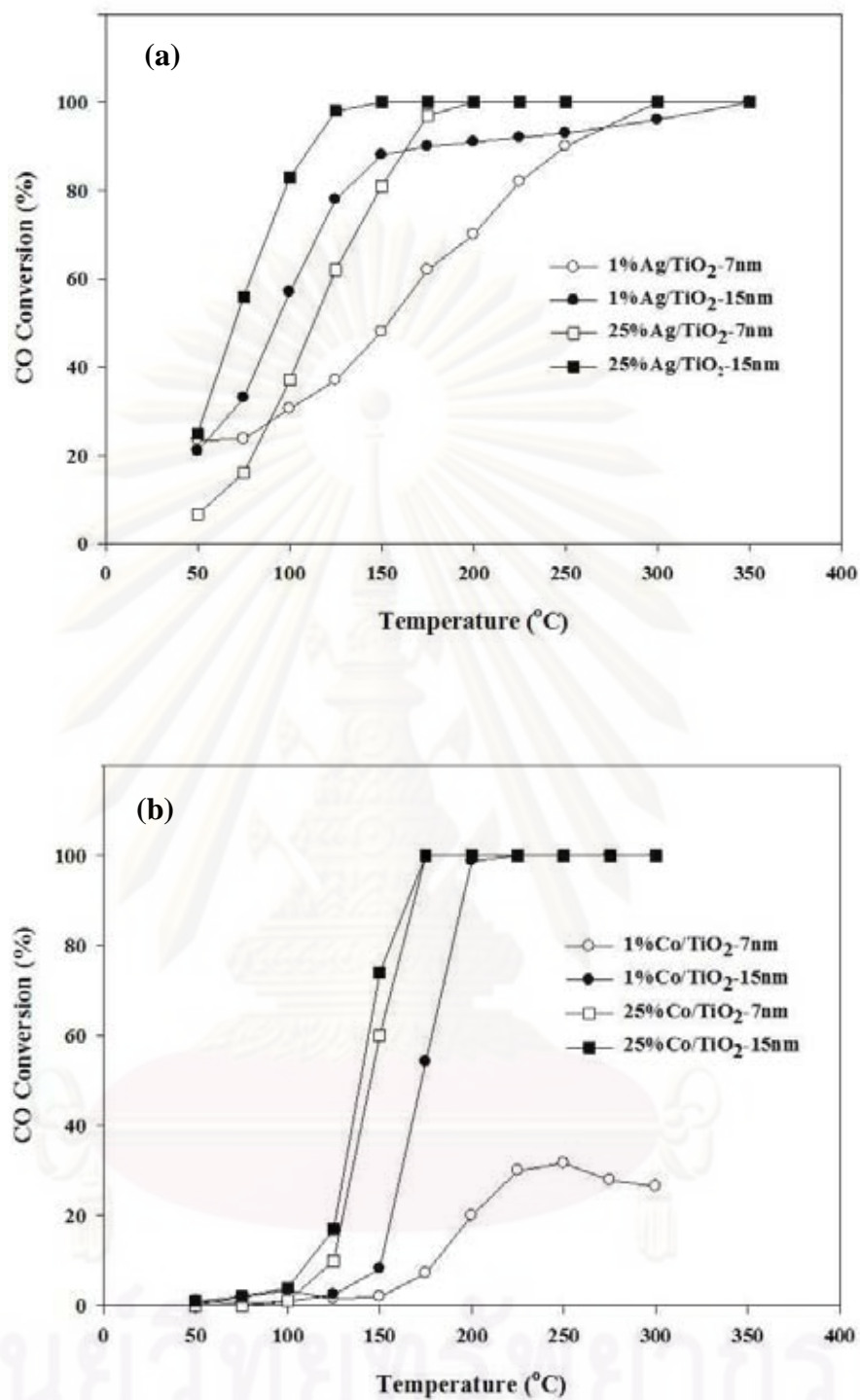
Figure 4.6 CO conversion over the metal catalysts with different crystallite size of TiO$_2$ supports and different amounts of metal loading (a) Ag/TiO$_2$ (b) Co/TiO$_2$ (c) Ni/TiO$_2$ (d) Pt/TiO$_2$.
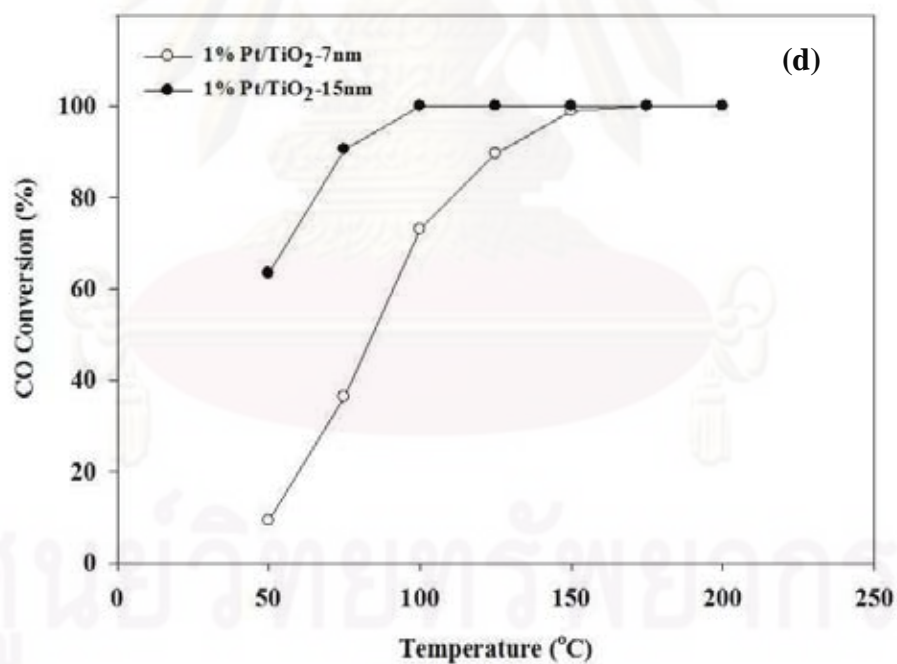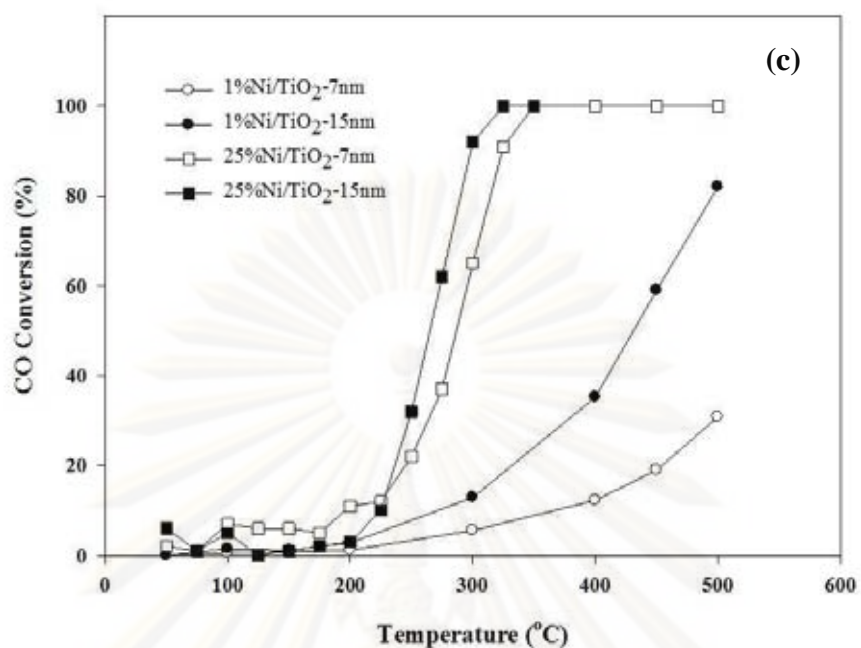
Figure 4.6 CO conversion over the metal catalysts with different crystallite size of TiO$_2$ supports and different amounts of metal loading (a) Ag/TiO$_2$ (b) Co/TiO$_2$ (c) Ni/TiO$_2$ (d) Pt/TiO$_2$ (cont.).

Table 4.3 The light-off temperature of metal catalysts supported on TiO_2-7nm and

TiO_2-15nm with different atomic loading.

Sample	Light off Temperature (^oC)			
	TiO_2-7nm		TiO_2-15nm	
	1 at.% Loading	25 at.% Loading	1 at.% Loading	25 at.% Loading
Ag/TiO_2	152	110	92	70
Co/TiO_2	> 300	145	173	140
Ni/TiO_2	> 500	255	430	220
Pt/TiO_2	84	n.d.[a]	< 50	n.d.

n.d. = not determined

prepared by impregnation method on P-25 TiO_2 as reported by Bamwenda et al.
[131], their light-off temperature under reaction condition of WHSV $\approx$ 20,400 cm^3 h^{-1}
g^{-1} was found to be higher than our case (light-off temperature $\approx$ 66°C).

For any metal type, the light-off temperature of the catalysts with 25 at.% was
lower than those with 1 at.%. Similar trend has been observed by Frey et al. [12] for
Ag/TiO_2 catalyst with different Ag loadings prepared by co-precipitation of Ag- and
TiO-oxalates, in which a large difference of the light-off temperature for 2%Ag/TiO_2
(light-off temperature $\approx$ 220°C) and 10%Ag/TiO_2 (light-off temperature $\approx$ 60°C) was
observed under 1:1 CO/O_2 condition. The number of converted CO molecules per unit
area of the catalytically active metal phase of Ag/TiO_2 catalyst was calculated and the
results are given in **Table 4.4.** The data revealed that there was no significant
difference in terms of specific activity for CO oxidation of Ag/TiO_2 catalysts on TiO_2-
7nm and TiO_2-15nm supports, confirming structure insensitive characteristic of the
CO oxidation reaction. The TEM images and particle size distribution of
25%Ag/TiO_2-7nm catalysts before and after CO oxidation are shown in **Figure 4.7**.
The Ag particle size distribution was not altered after CO oxidation. The catalyst
stability during CO oxidation was also investigated. **Figure 4.8** shows the stability of
25 at.% Ag/TiO_2 catalysts for CO oxidation at 200^oC. The CO conversion was stable

at around 90-95% over 24 h time-on-stream for both 25%Ag/TiO$_2$-7nm and 25%Ag/TiO$_2$-15nm.

Table 4.4 The number of converted CO molecules per unit area of the catalytically active metal phase for Ag/TiO$_2$ catalyst supported on TiO$_2$-7nm and TiO$_2$-15nm at 75 °C with different atomic loading.

Sample	Converted CO molecules / unit area of Ag metal (x 10^{20} molecules/m^2)			
	1 at.% Loading		25 at.% Loading	
	TiO$_2$-7nm	TiO$_2$-15nm	TiO$_2$-7nm	TiO$_2$-15nm
Ag/TiO$_2$	11.6	7.6	5.3	5.5
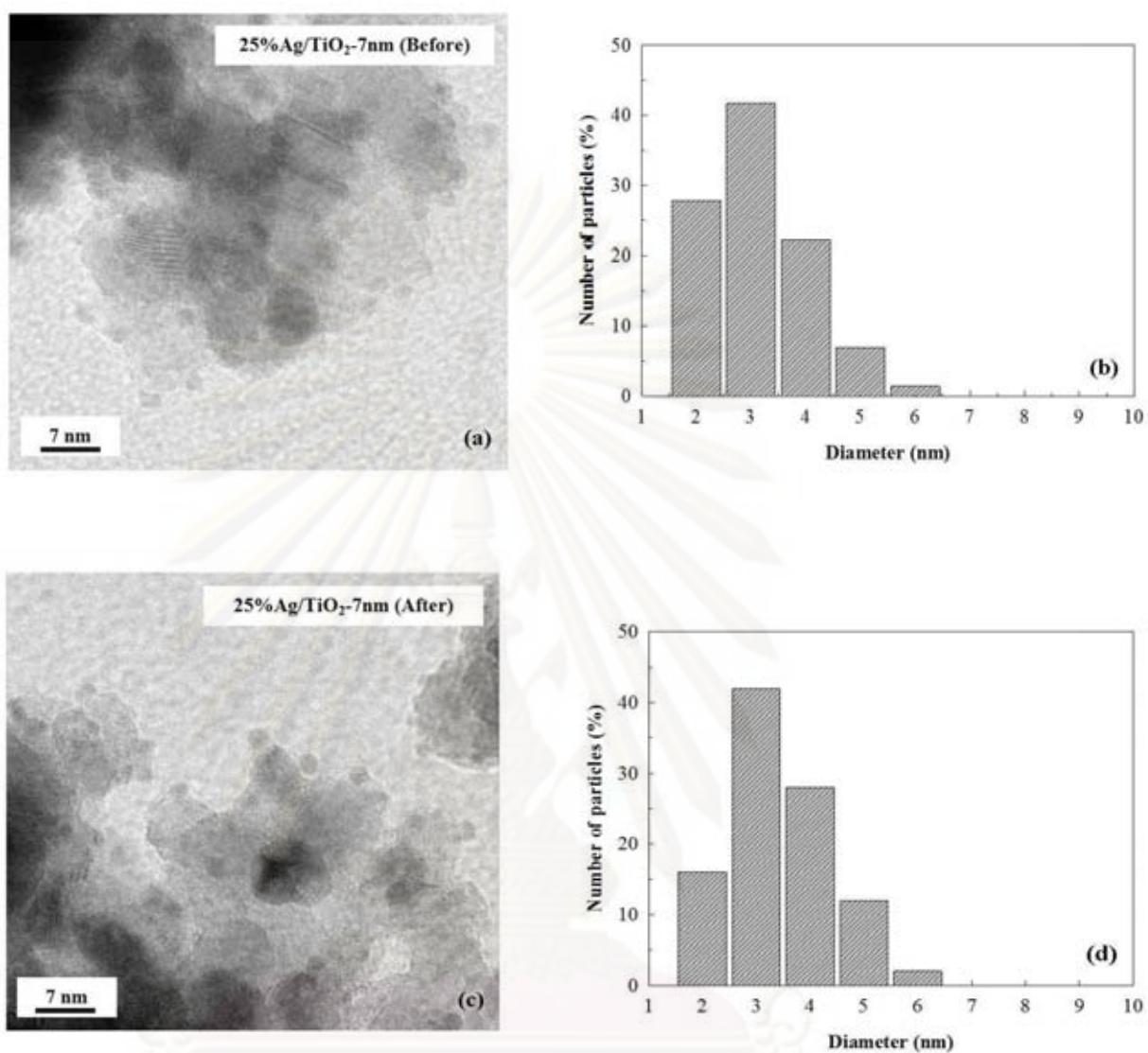
Figure 4.7 TEM images (a,c) and Ag particle size distribution (b,d) of 25%Ag/TiO$_2$-

7nm catalysts before and after CO oxidation.
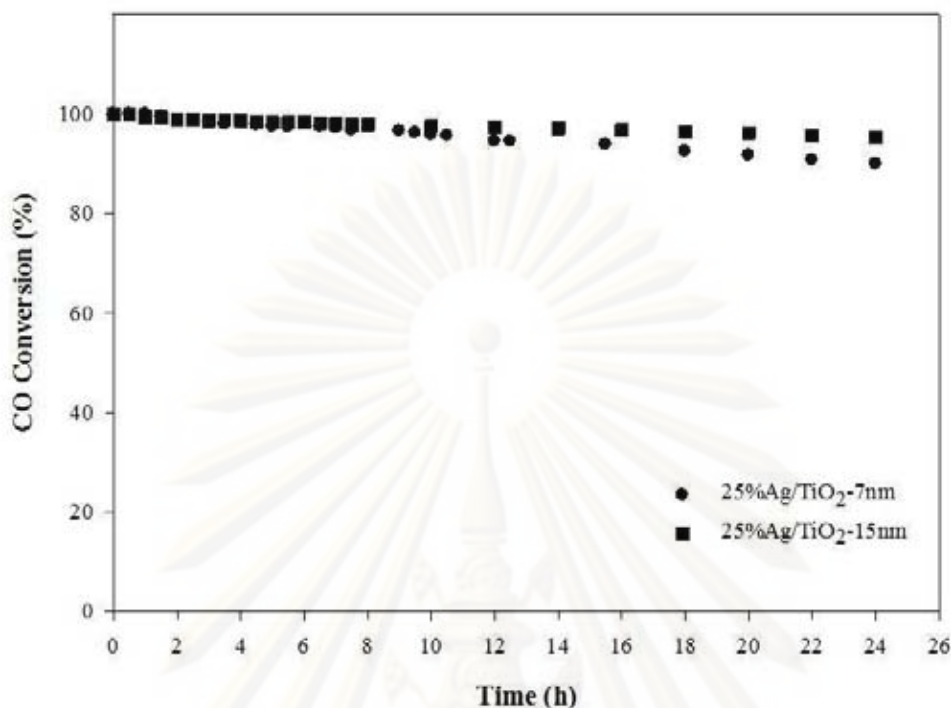
Figure 4.8 Stability of the 25%Ag/TiO$_2$ catalysts with different crystallite sizes of TiO$_2$ supports for CO oxidation at 200 °C.

4.2 Effect of different dopant elements on the activity of Ag/TiO$_2$ in CO oxidation

The modification of TiO$_2$ nanoparticles by doping with trace element was studied in this work. There are three elements were chosen, namely, Al, P, and Si. The dopant element was added together with titania precursor during the synthesis by solvothermal method. The catalyst Ag/TiO$_2$ samples were prepared by incipient wetness impregnation with AgNO$_3$ aqueous solution. The effect of different dopants on catalytic activity of Ag/TiO$_2$ catalyst was investigated in this section.

4.2.1 Effect of different dopants on the properties of Ag/TiO$_2$ catalyst

The XRD patterns of Ag catalyst supported on TiO$_2$ and modified-TiO$_2$ are shown in **Figure 4.9**. It can be seen that all the samples showed the diffraction peaks at around 25°, 38°, 48°, 54°, 55°, 63°, 71°, and 75° 2θ. These peaks were assigned to
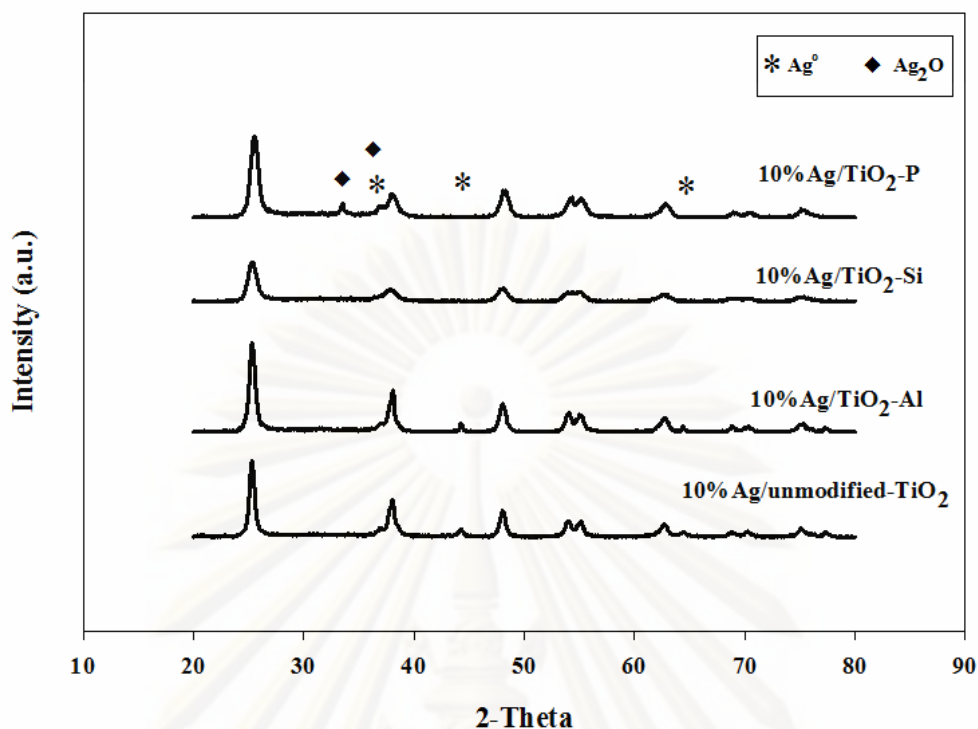
Figure 4.9 XRD patterns of 10%Ag catalysts supported on Al-, Si-, P-modified TiO_2 and unmodified-TiO_2.

the anatase phase. The catalyst modified with P, Si, and Al showed a broad peak that seems to shift to higher angle. The peak position of anatase (101) and lattice parameters of Ag catalyst supported TiO_2 and modified-TiO_2 are shown in **Table 4.5**. The value of 2-theta shifted to higher angle compared with the catalyst supported unmodified-TiO_2. The increase in 2-theta value led to the decrease of d-spacing in anatase (101) structure according to the Bragg's law. The decrease of d-spacing and the lattice parameters indicated that the dopant ions were incorporated into the lattice of TiO_2. The insertion of Al (0.061 nm), Si (0.042 nm), and P (0.035 nm) ion which has a smaller ionic radius than Ti ion (0.064 nm) into the lattice of TiO_2 resulted in the shift of the diffraction peak toward higher angle [132-134]. **Table 4.6** shows the crystallite size of TiO_2 and modified TiO_2 which calculated from the half-height width of the diffraction peak of XRD pattern using Scherrer equation. The TiO_2 crystallite sizes of all the modified catalyst samples were smaller than the unmodified ones and as a consequence the BET surface areas increased.

Table 4.5 The peak position of anatase and lattice parameters of Ag catalyst supported on unmodified TiO_2 and modified TiO_2 with Al, Si, and P.

Sample	Peak position of anatase (101) (2θ) (degree)	d-spacing (nm)	Lattice parameters (A°) a (=b)	c
10%Ag/unmodified-TiO_2	25.32	3.5174	3.7896	9.4522
10%Ag/TiO_2-Al	25.56	3.4849	3.7526	9.3952
10%Ag/TiO_2-Si	25.36	3.5119	3.7803	9.4906
10%Ag/TiO_2-P	25.52	3.4903	3.7545	9.4714

Table 4.6 Physical properties of Ag catalyst supported on unmodified TiO_2 and modified TiO_2 with Al, Si, and P.

Sample	crystallite size (nm)	BET surface area (m^2/g)
10%Ag/unmodified TiO_2	16.2	52
10%Ag/TiO_2-Al	10.7	74
10%Ag/TiO_2-Si	9.1	86
10%Ag/TiO_2-P	10.1	73

A diffraction peak at $2\theta = 38.1°$, 44.4°, and 64.5° was assigned to metallic Ag and the peak at 32.8° and 38° was assigned to Ag_2O [135]. All of the samples showed both metallic silver and silver oxide except for the 10%Ag/TiO_2-Si, where its diffraction peaks were hardly observed. **Figure 4.10** showed TEM images of 10%Ag catalyst supported on unmodified TiO_2 and modified TiO_2 with Al, Si, and P. The average TiO_2 crystallite size of all Ag catalysts supported on modified TiO_2 was ca. 9-11 nm, while those of Ag catalyst supported on umodified TiO_2 was ca. 12-16 nm. These results confirmed that the crystallite size of modified-TiO_2 support smaller than that unmodified ones that the results from TEM were in good agreement with the XRD results. It can be also seen that the Ag particles size on modified-TiO_2 is
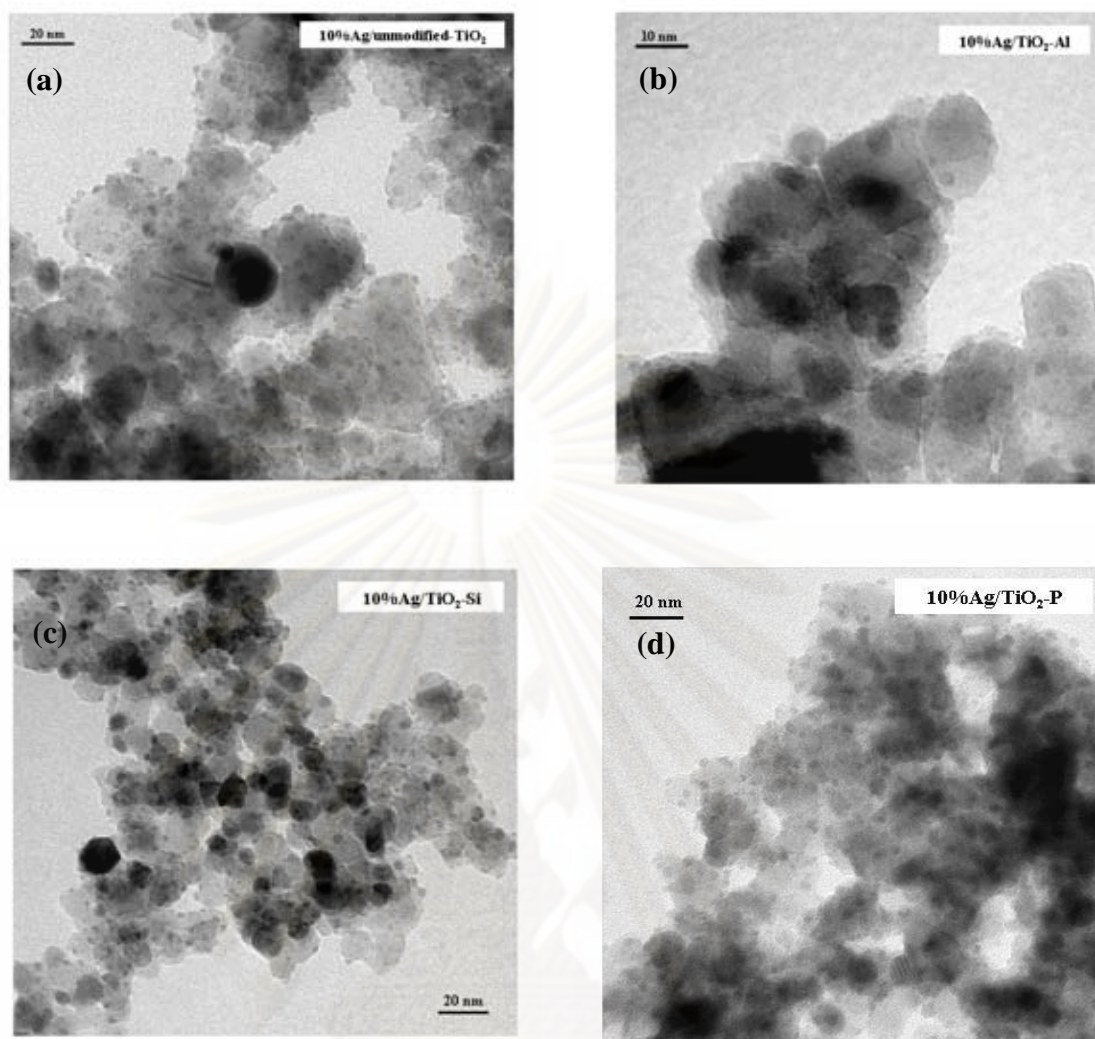
Figure 4.10 TEM images of 10%Ag/unmodified- TiO$_2$ (a), 10%Ag/TiO$_2$-Al (b), 10%Ag/TiO$_2$- Si (c), and 10%Ag/TiO$_2$-P (d).

comparable with the Ag particles size on unmodified TiO$_2$ with the average size in the range of 2-4 nm.

Figure 4.11 shows the FT-IR spectra of modified TiO$_2$ with the different of dopant element in the wave number ranging from 400 to 4000 cm^{-1}. The spectra bands at ca. 1630 and 3400 cm^{-1} were attributed to H-OH bonds of adsorbed water molecules and hydroxyl group of Ti-OH bonds, respectively [136-138]. The incorporation of the element into lattice structure of TiO$_2$ by substitute the Ti ion was revealed by FTIR. The IR spectra band at 1050 and 1075cm^{-1} was assigned to the formation of Ti-O-P [139-141] and Ti-O-Si [142-144] structure, respectively. The IR
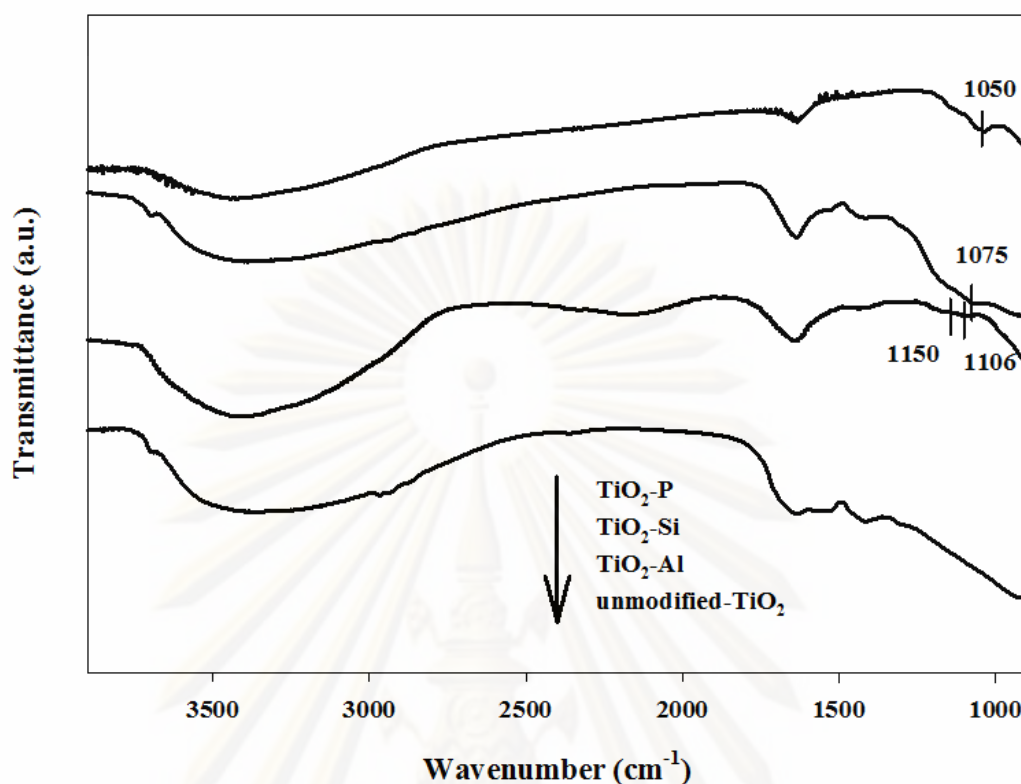
Figure 4.11 FTIR spectra of modified TiO_2 with different of dopant elements.

spectra bands in the 1106-1150 cm^{-1} region were assigned to the Al-O band vibration of intra- and extra framework of TiO_2 anatase [132].

   Table 4.7 showed the XPS results of Ag catalyst supported on TiO_2 and modified- TiO_2 with Al, Si, and P. The binding energy of Ti 2p of all elements-modified TiO_2 shifts slightly towards larger binding energies in comparison with unmodified TiO_2, illustrating the local chemical environment of Ti ions has been significantly influenced by the dopant ions (Al, Si, and P). These results were the evidence for the formation of Ti-O-Al, Ti-O-Si, and Ti-O-P, respectively. The electronegativity of Al, Si, and P is greater than that of Ti, which resulted in the decrease of electron density around Ti atom. As a result, the binding energy of Ti 2p increased [145]. The binding energy of Al 2p was 74.75 eV, indicating a stable oxidation state of Al^{3+} exists in TiO_2 lattice [146]. Meanwhile, The binding energy of Si 2p (102.35 eV) was smaller than SiO_2 (103.2 eV) confirmed that the Ti-O-Si bond

Table 4.7 Binding energies of Ag catalyst supported on unmodified TiO_2 and modified TiO_2 with Al, Si, and P.

Sample	Ti 2p	O 1s	Element 2p: BE	Ag 3d	
				Ag $3d_{5/2}$	Ag $3d_{3/2}$
10%Ag/unmodified-TiO_2	458.75	530.00	-	367.70	373.50
10%Ag/TiO_2-Al	459.15	530.10	Al 2p: 74.75	368.70	374.60
10%Ag/TiO_2-Si	459.15	530.60	Si 2p: 102.35	368.60	374.70
10%Ag/TiO_2-P	459.25	530.60	P 2p: 133.40	368.70	374.60

has been formed in Si-modified TiO_2 samples. The P 2p of P-modified sample shows the binding energy of 133.40 eV which corresponded to P^{5+}. For all element-modified TiO_2, the binding energy of Ag $3d_{5/2}$ and Ag $3d_{3/2}$ centered at ca. 368.7 and 374.7 eV, respectively. However, the slitting between Ag $3d_{5/2}$ and Ag $3d_{3/2}$ of all element-modified TiO_2 was similar to that of the unmodified TiO_2 samples. It has been reported that the slitting between Ag $3d_{5/2}$ and Ag $3d_{3/2}$ was 6.0 eV, indicating a normal state of Ag^0 [147].

4.2.2 Effect of different dopants on the activity of CO oxidation

The CO oxidation activity of Ag catalyst supported on TiO_2 and modified-TiO_2 with Al, Si, and P are shown in **Figure 4.12**. The results showed that the Ag catalyst supported on Si- and Al-modified TiO_2 shows the higher activity in CO oxidation than the catalyst supported on unmodified ones. Both of 10%Ag/TiO_2-Si and 10%Ag/TiO_2-Al catalyst exhibits the lowest light-off temperature at around 65°C, which was much lower than the 10%Ag/unmodified-TiO_2 (light-off temperature $\approx$ 92°C). However, the addition of P into TiO_2 support can not improve the CO oxidation activity of Ag catalyst. Its activity was comparable with that of the 10%Ag/unmodified-TiO_2 and showed the light-off temperature at around 92°C.
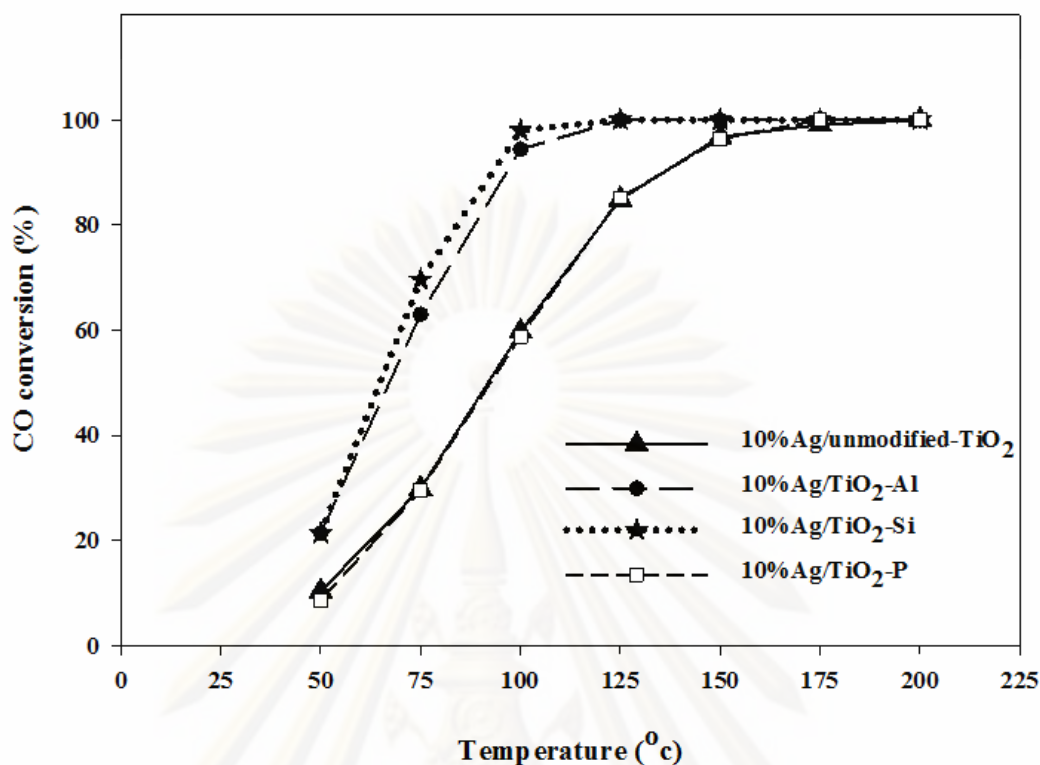
Figure 4.12 CO conversion over 10%Ag catalysts supported on Al-, Si-, P-modified TiO$_2$ and unmodified-TiO$_2$.

The reaction mechanism for catalytic CO oxidation is known to compose of two possible mechanisms (1) the CO molecule and oxygen atom from external source are coadsorbed on metal active site to produce CO$_2$ and (2) the CO molecule is adsorbed on metal catalyst surface to form intermediate complex and then reacted with surface lattice oxygen atom of TiO$_2$ support to generate CO$_2$ [83]. The oxygen from external source in gas phase then dissociates into atomic oxygen and is adsorbed on the oxygen vacancies sites of the TiO$_2$ support. According to the mechanism proposed by Bollinger et al. [29] for CO oxidation over Au/TiO$_2$ catalysts, the adsorption of CO and O$_2$ occurred on two different sites, CO adsorbed on Au and O$_2$ adsorbed on TiO$_2$. Then CO reacted with surface lattice oxygen of TiO$_2$ to form CO$_2$ leading to the formation of surface oxygen vacancies. During the CO oxidation, these oxygen vacancies were filled by chemisorbed oxygen species from gas phase.

As mentioned above, the adsorption and dissociation of oxygen molecules on the catalyst is a major factor that may influence on the CO oxidation activity. The oxygen adsorption and desorption behaviors of the Ag/TiO_2 catalysts were investigated by using O_2-TPD experiments and the results are shown in **Figure 4.13**. According to Masakazu et al. [148], there are three kinds of adsorbed oxygen species on TiO_2 surface. The adsorbed oxygen consists of weakly adsorbed surface oxygen, strongly adsorbed surface oxygen and surface lattice oxygen. The weakly adsorbed oxygen desorption in the range of 100-180°C and ~230°C were assigned to O_2^- and O^- species, respectively [149]. The desorption temperature of strongly adsorbed surface oxygen and surface lattice oxygen were reported in the range of 470-490°C, and 810-870°C, respectively [150, 151]. The results demonstrated that all of modified-TiO_2 supported Ag catalyst produced the larger amount of O^- species than the unmodified ones and there was only one catalyst which produced O_2^- species that was $10\%Ag/TiO_2$-Si. A larger amount and lower temperature of oxygen desorption were a cause of the superior CO oxidation activity of $10\%Ag/TiO_2$-Al and $10\%Ag/TiO_2$-Si catalyst compared with $10\%Ag/unmodified-TiO_2$ catalyst.

However, the catalytic activity of $10\%Ag/TiO_2$-P catalyst was comparable with that of $10\%Ag/unmodified-TiO_2$ catalyst, in spite of larger amount of oxygen adsorption. Ma et al. [152] reported that the high phosphorus content on TiO_2 surface may block the active sites of Au/TiO_2 catalyst and led to low catalytic activity in CO oxidation. Thus, the TiO_2 support having low phosphorus content (molar ratio of P/Ti= 0.01) was prepared. The CO oxidation activity of $10\%Ag/TiO_2$-0.01P and $10\%Ag/TiO_2$-0.03P catalyst was compared, as shown in **Figure. 4.14**. The results demonstrated that the lower content of P in TiO_2 support showed higher activity (light-off temperature $\approx$ 80°C) in CO oxidation compared with $10\%Ag/TiO_2$-0.03P and $10\%Ag/unmodified-TiO_2$ catalyst. The formation of phosphate species on TiO_2 surface of $10\%Ag/TiO_2$-0.03P catalyst was examined by XPS as displayed in **Figure 4.15**. The P 2p spectra of $10\%Ag/TiO_2$-0.03P catalyst showed a shoulder on the high-energy side, and the spectra can be fitted by two peaks located at 133.4 and 135.2 eV, respectively. The binding energy at 133.4 eV was assigned to the monodentate surface complex which phosphate adsorbed to the surface hydroxyl ion with one coordination number. The shoulder peak at high binding energy (135.2 eV) was assigned to
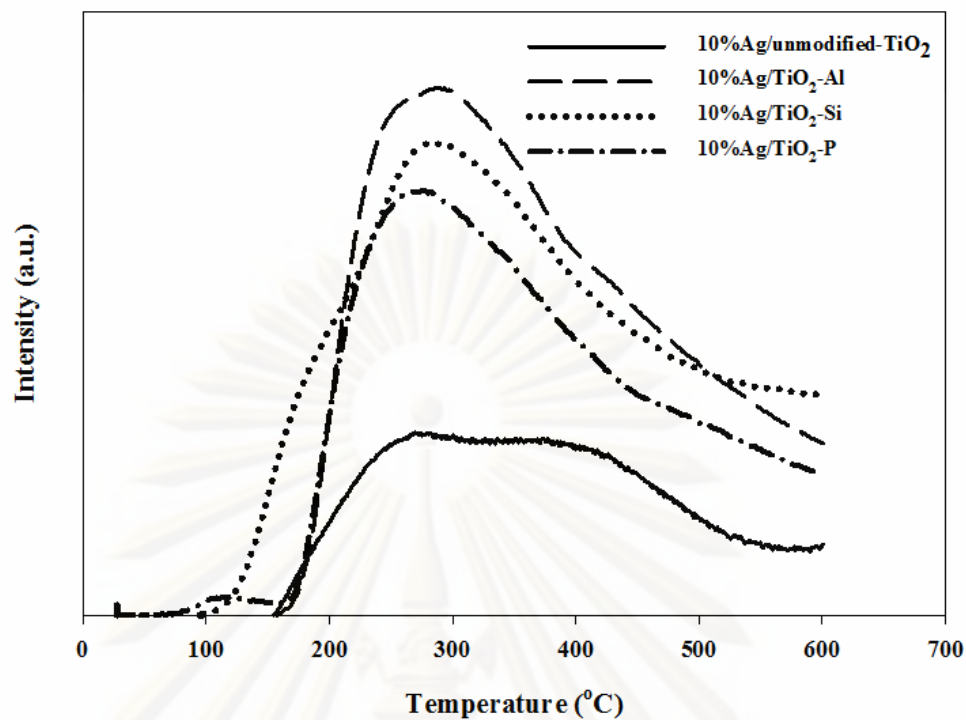
Figure 4.13 O_2-TPD patterns of 10%Ag catalysts supported on Al-, Si-, P-modified TiO_2 and unmodified-TiO_2.
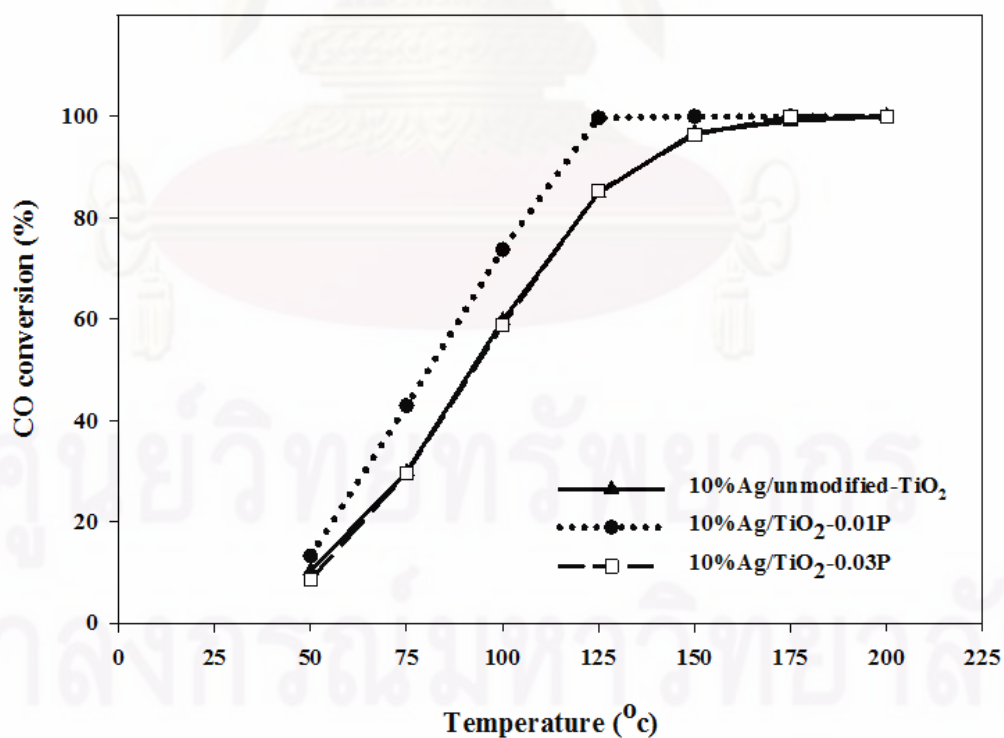
Figure 4.14 CO conversion over 10%Ag catalysts supported on P-modified TiO_2 with different P/Ti molar ratio.
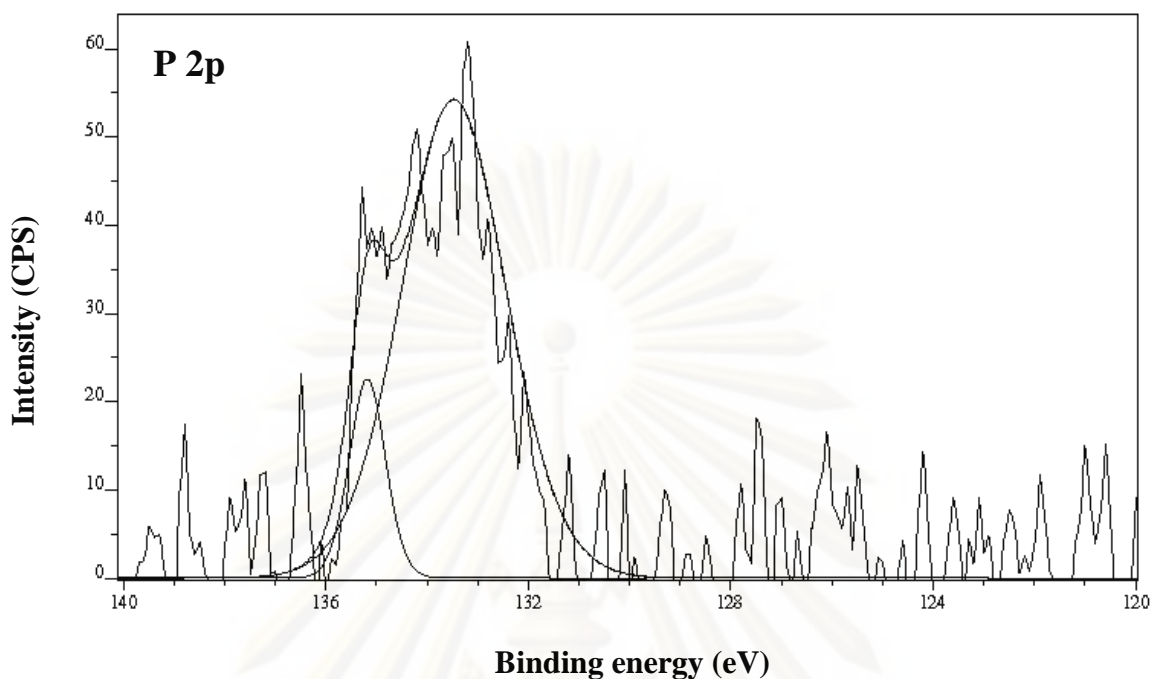
Figure 4.15 The P 2p XPS spectra of 10%Ag/TiO$_2$-P.

bidentate surface complex which phosphate was bound to two surface hydroxyl ions. The existence of the bidentate phosphate species on the TiO$_2$ surface may block the adsorption of CO on the Ag active sites during CO oxidation which cause a decrease in the CO oxidation activity.

4.3 Effect of the Si-doping content in TiO$_2$ support on the activity of Ag/TiO$_2$ in CO oxidation

In this section, Si was doped into TiO$_2$ support with Si/Ti ratios 0.01, 0.05, 0.1, and 0.3. The Si-modified TiO$_2$ was employed as the support for Ag/TiO$_2$ catalysts for CO oxidation reaction. The effect of Si-doping content in TiO$_2$ support synthesized by solvothermal method on the physicochemical properties of TiO$_2$ and the catalytic activities of Ag/TiO$_2$ catalysts in the CO oxidation reaction were investigated.

4.3.1 Effect of Si doping on the properties of TiO$_2$

The XRD patterns of TiO$_2$ and Si-modified TiO$_2$ prepared by the solvothermal method are shown in **Figure 4.16**. All the samples exhibited only pure anatase phase TiO$_2$ without any other phase contamination. The XRD patterns of Si-modified TiO$_2$ showed the major peak of anatase TiO$_2$ at 2θ around 25°. Increasing of Si content can affect the broadening of XRD peak [153]. However, the peak intensity of anatase TiO$_2$ decreased with increasing Si content, indicating that the crystallite size of TiO$_2$ became smaller. The crystallite sizes of TiO$_2$ and Si-modified TiO$_2$ are shown in **Table 4.8**. The crystallite sizes of all Si-modified TiO$_2$ were smaller than the unmodified TiO$_2$.
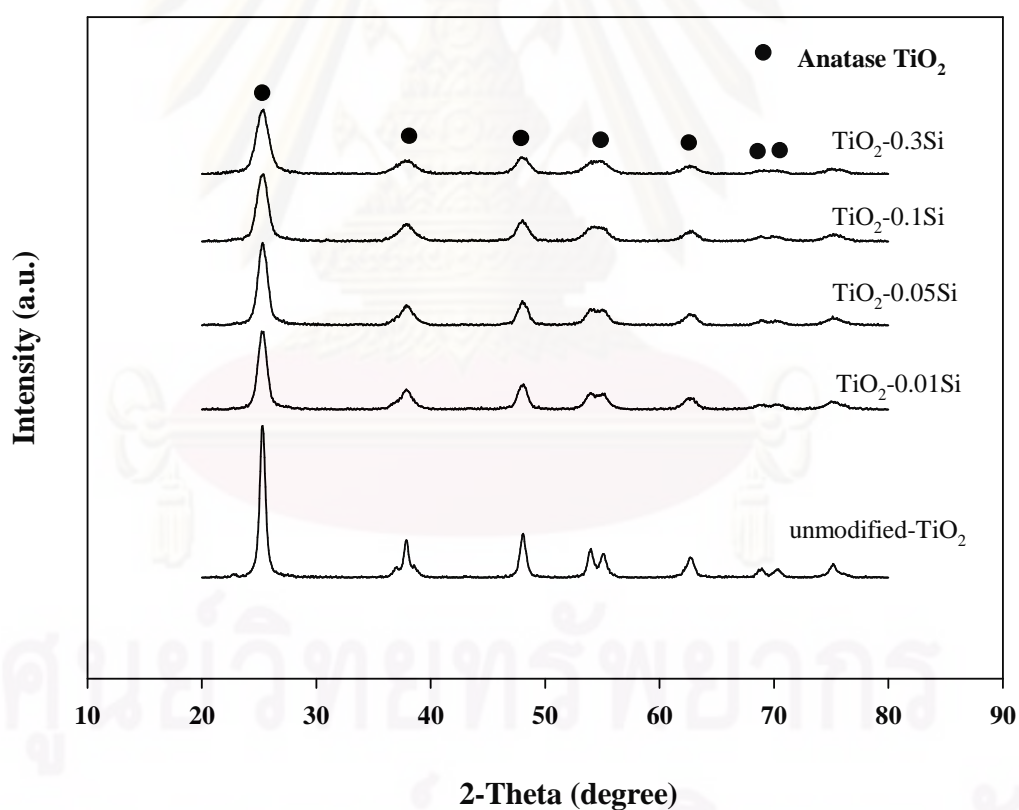
Figure 4.16 XRD patterns of Si-modified TiO$_2$ with different Si/Ti molar ratios.

Table 4.8 Physical properties and amount of active sites of unmodified TiO_2, Si-modified TiO_2 support and 10%Ag/TiO_2-xSi catalysts.

Sample	crystallite size (nm)	BET surface area (m^2/g)	Pore volume (cm^3/g)	Active site of 10%Ag/TiO_2-xSi (x10^{20} atom/g-catalyst)
unmodified TiO_2	15.0	77	0.34	1.27
TiO_2-0.01Si	9.8	103	0.37	2.10
TiO_2-0.05Si	8.5	125	0.32	2.02
TiO_2-0.1Si	7.0	136	0.30	1.98
TiO_2-0.3Si	6.4	96	0.16	2.46

The peak position of anatase (101) and lattice parameters of TiO_2 and Si-modified TiO_2 support are given in **Table 4.9**. The anatase (101) diffraction peaks for all the Si-modified TiO_2 were shifted slightly to a higher angle compared to that of the TiO_2 support, indicating a decrease of the distance between crystal planes which related to the lattice parameters [154]. The decrease of the lattice parameters for the Si-modified TiO_2 compared to the TiO_2 was attributed to an insertion of the smaller ionic radius of Si (0.042 nm) into the lattice of TiO_2 (ionic radius 0.064 nm) [155]. Moreover, the peak intensity of anatase TiO_2 decreased with increasing Si content, indicating that the crystallite size of TiO_2 became smaller.

Table 4.9 The peak position of anatase and lattice parameters of unmodified-TiO_2 and Si-modified TiO_2 support.

Sample	Peak position of anatase (101) (2θ) (degree)	Lattice parameters (A°) a (=b)	c
Unmodified-TiO_2	25.28	3.7934	9.5003
TiO_2-0.01Si	25.52	3.7528	9.5003
TiO_2-0.05Si	25.32	3.7896	9.4523
TiO_2-0.1Si	25.40	3.7766	9.4427
TiO_2-0.3Si	25.40	3.7766	9.4427

Figure 4.17 shows the TEM images of TiO_2 and TiO_2-0.05Si. The particle size distributions were in the range of 12-16 nm and 5-9 nm for the TiO_2 and the TiO_2-0.05Si, respectively. Such results were in good agreement the XRD results in which the crystallite size of TiO_2 supports decreased with Si doping. The existence of Si in the TiO_2 framework may inhibit the TiO_2 moiety to form large crystal [156]. Moreover, the replacement of Ti by Si atom in TiO_2 lattice can also produce Ti-O-Si bond and the lattice shrinkage because the bond length of Si–O bond (1.59 A°) is shorter than that of Ti–O (1.79 A°) [133], as a consequence the crystallite size of TiO_2 is decreased. As also shown in **Table 4.8**, BET surface area of the TiO_2 supports increased with increasing Si content and reached a maximum value of 136 m^2/g for the TiO_2-0.1Si. Further increase of Si/Ti to 0.3 resulted in the decrease of BET surface area. It should be noted that the decrease of the surface area indicated that the SiO_2 particles which come from the excess Si content may be dispersed on the surface of titania and resulted in a strong decrease of the pore volume. Similar results were observed by Jin et al. that the BET surface area of silica-doped TiO_2 prepared by hydrothermal process decreased when the molar ratio of Si/Ti was higher than 0.05 [157].

Figure 4.18 shows the FT-IR spectra of Si-modified TiO_2 with the Si/Ti molar ratio between 0.01-0.3 in the wave number ranging from 400 to 4000 cm^{-1}. The spectra bands at ca. 1630 and 3400 cm^{-1} were attributed to H-OH bonds of adsorbed water molecules and hydroxyl group of Ti-OH bonds, respectively [136-138]. The hydroxyl group at 3400 cm^{-1} of all Si-modified TiO_2 seems to increase compared with the TiO_2 support. These results are in agreement with Chen et al. [158], who reported that the hydroxyl groups of TiO_2 increased after Si-doping in non-humidity system. The IR spectra at ca. 700 and 800 cm^{-1} were attributed to Ti-O-Ti bonds in the TiO_2 lattice [159]. It is noticed that the spectra band in the 400-850 cm^{-1} region became weaker with the increase of Si content, suggesting that the formation of Ti-O-Ti structure was suppressed due to the formation of Ti-O-Si and/or Si-O-Si structure. The presence of Ti-O-Si bond was confirmed by the IR spectra band at ca. 950 cm^{-1} [142-144]. The intensity of Si-O-Si bonds at ca. 1070 cm^{-1} also increased with increasing the Si content. The presence of the amorphous silica could prevent the agglomeration of TiO_2 nanopaticles, leading to a decrease of TiO_2 particle size [160, 161]. The metal active sites of Ag/TiO_2 catalysts were determined by pulse
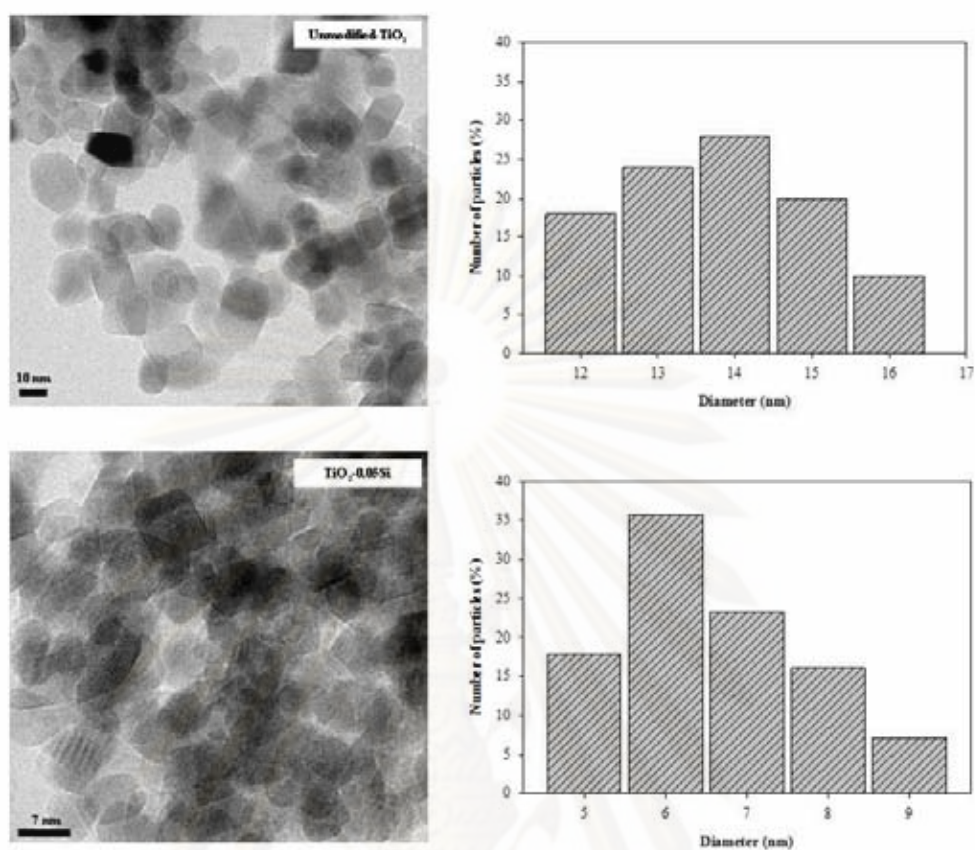
Figure 4.17 TEM images and the size distribution of (a) unmodified-TiO_2 and (b) TiO_2-0.05Si.

chemisorption and are given in **Table 4.8**. It is clearly shown that higher metal dispersion was obtained on the Si-modified TiO_2. The amount of metal active sites on the Si-modified TiO_2 supported catalysts were nearly two times higher than those supported on the unmodified ones. However, the amount of metal active sites on the Si-modified TiO_2 was quite similar especially for those with the Si/Ti ratio 0.01-0.1.
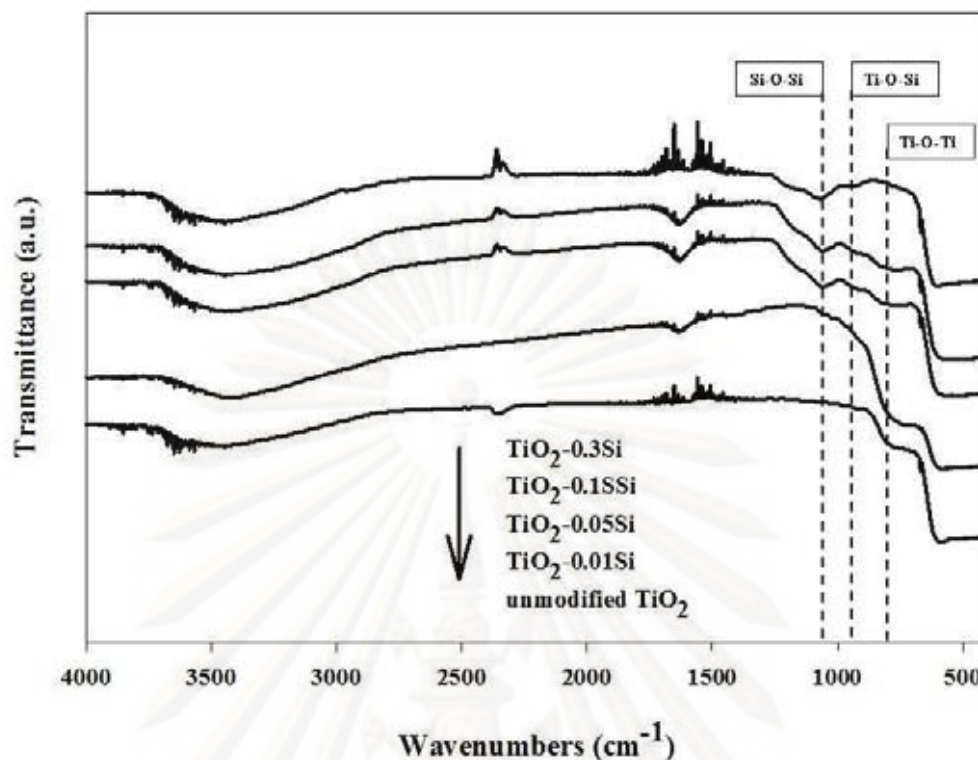
Figure 4.18 FTIR spectra of Si-modified TiO_2 with different Si/Ti molar ratios.

4.3.2 Effect of Si doping on the activity of CO oxidation

The CO conversions as a function of reaction temperature for 10%Ag/TiO_2 with different Si contents in the TiO_2 are shown in **Figure 4.19**. Addition of trace amount of Si in the TiO_2 supports can improve the CO oxidation activity of the TiO_2 supported Ag catalysts. However, there existed an appropriate amount of Si/Ti molar ratio that yielded the higher CO oxidation activity at around 0.05-0.1. At their optimum Si/Ti ratios, the Si-modified TiO_2 supported Ag catalysts showed light-off temperature at 68°C, which were much lower than the corresponding unmodified ones. When the Si contents were higher than their optimum values, the Si-modified TiO_2 supported catalysts exhibited lower CO oxidation activity although these catalysts possessed higher amount of metal active sites as measured by pulse chemisorption. Thus, the modification of TiO_2 with Si atoms not only improved the metal dispersion, but also affected the mechanism of CO oxidation.
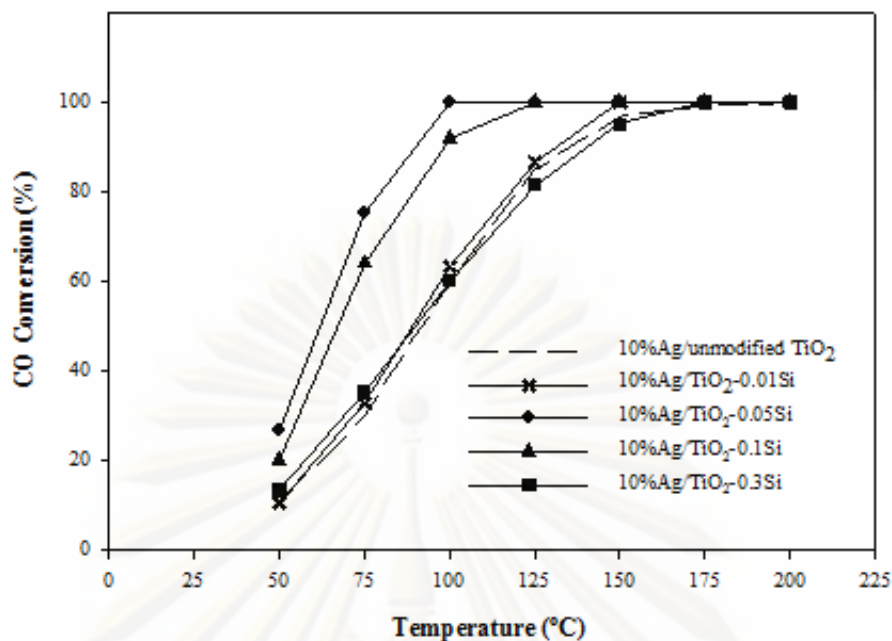
Figure 4.19 CO conversion over 10 at.%Ag catalysts supported on Si-modified TiO_2 with different Si/Ti molar ratios.

According to the reaction mechanism of CO oxidation as described in section 4.2, there were two types of surface oxygen reacted with adsorbed CO molecules, adsorbed oxygen on metal active site and surface lattice oxygen atom of TiO_2 support. The missing of surface lattice oxygen on TiO_2 support was restored by adsorption of oxygen in gas phase. This mechanism occurs more easily on defective surface or basic site surface of metal oxide support [83]. In the present study, the modification of TiO_2 support with trace amount of Si resulted in an increase of the amounts of hydroxyl group and the formation of basic site surface and improved CO oxidation activities. Thus, it is likely that CO oxidation on the Si-modified TiO_2 supported Ag catalysts occurred via such mechanism.

The oxygen adsorption and desorption behaviors of the Ag/TiO_2 catalysts were studied by using O_2-TPD experiments and the results are shown in **Figure 4.20**. The Si-modified TiO_2 supported Ag catalysts with optimum Si/Ti ratios (Si/Ti ≈ 0.05-0.1) exhibited much lower desorption temperature and larger amount of desorbed O_2 compared to the non-modified ones and the ones with excess Si. The results demonstrated that the Si-modified TiO_2 supported Ag catalysts with optimum Si/Ti
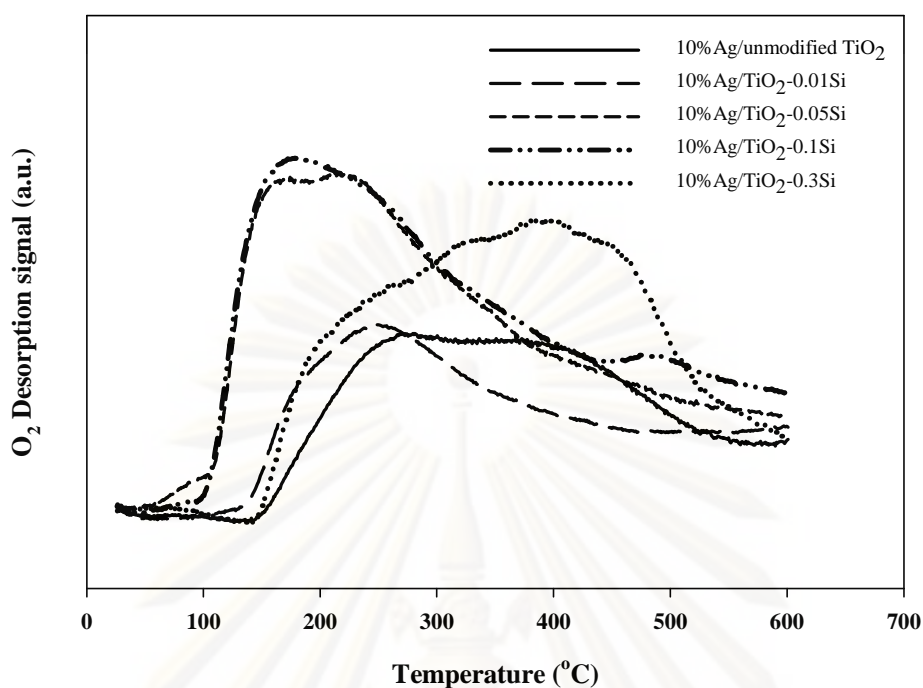
Figure 4.20 O_2-TPD patterns of 10 at.%Ag catalysts supported on Si-modified TiO_2 with different Si/Ti molar ratios.

ratios produced the highest amount of O_2^- (temperature at around 180°C) and O^- species (temperature at around 230°C) whereas the non-modified ones and the ones with excess Si produced O^- species and strongly adsorbed surface oxygen (temperature in the range of 400-450°C). It has been reported that the adsorbed O^- species were the most active species for CO oxidation [118]. In addition, Qu et al. [162] suggested that the strongly adsorbed surface oxygen species blocks the adsorption and diffusion of weakly adsorbed surface oxygen, causing a decrease in the CO oxidation activity of the catalysts.

The results in this work show that oxygen in Ag/TiO_2-0.05Si and Ag/TiO_2-0.1Si catalysts desorbed more easily so that the catalysts exhibited higher CO oxidation activity. It is suggested that the formation of Ti-O-Si bonds produced an appreciable change in the electronic properties of these catalysts. Generally, TiO_2 was classified as a support which exhibits the strong metal-support interaction with precious metals. Bernal et al. [163] reported that the temperatures of oxygen desorption from metal catalyst surface increased when a strong interaction between

the metal particles and support occurred. The addition of Si into TiO_2 lattice to form Ti-O-Si bonds may lead to a decrease of the metal-support interaction and resulted in a decrease of oxygen desorption temperature. In other words, the adsorbed oxygen on the Si-modified TiO_2 with optimum Si/Ti ratios can be dissociated to atomic species which desorbed at lower temperature. Moreover, the presence of Si in TiO_2 could decrease the strength of surface lattice oxygen bonding, resulted in higher mobility of lattice oxygen which has been reported to be beneficial for CO oxidation [151, 164].

On the other hand, an excess Si content in the TiO_2 support (i.e., for Si/Ti=0.3) exhibited the increase of amorphous SiO_2 formation which revealed by Si-O-Si bonds from FTIR results. Qu et al. [165] reported that interaction between Ag and SiO_2 became strongly when the catalyst was pretreated in oxygen at high temperature like a calcination of the catalyst in an oxygen atmosphere. Thus, the formation of SiO_2 in TiO_2 lattice led to a shift of oxygen desorption temperature towards higher temperature and decreased the catalytic activity in CO oxidation.

4.4 The effect of different phosphorus precursors in TiO_2 support on the activity of Ag/TiO_2 in CO oxidation

The influence of different phosphorus precursors on the activity of Ag/TiO_2 in CO oxidation was investigated in this section. During preparation of TiO_2 support by solvothermal method, the precursor of phosphorus was added together with titanium precursor. Different phosphorus precursors, phosphoric acid (H_3PO_4), di-ammonium hydrogen phosphate (($NH_4)_2HPO_4$), triethyl phosphate ($PO_4 (C_2H_5)_3$), and phosphorus pentoxide (P_2O_5) were compared. The silver was supported on the TiO_2 and P-modified TiO_2 using incipient wetness impregnation.

4.4.1 Effect of P doping on the physicochemical properties of Ag/TiO_2 catalysts

The XRD patterns of the unmodified TiO_2 and P-modified TiO_2 supported Ag catalysts prepared with different precursors of phosphorus modifier are shown in

Figure 4.21. All spectra of the catalyst samples showed the major peak of pure anatase (101) phase TiO_2 at 2θ around 25°. Doping of TiO_2 with P led to the broadening of XRD peaks. It can be clearly observed that the XRD reflections of all catalyst supported P-modified TiO_2 were shifted slightly to higher angle compared to that of the TiO_2 support. According to the Bragg's law, the increase in 2θ values indicated the decrease of the distance between crystal planes, which is in close relationship with the lattice parameters. The peak position of anatase (101) and lattice parameters of the catalyst supported TiO_2 and P-modified TiO_2 are given in **Table 4.10**. The decrease of lattice parameters suggests that P ions were incorporated into the lattice of TiO_2 and substitute for lattice Ti ions considering the smaller ionic radius of P ion (0.035 nm) than that of Ti ion (0.064 nm) [134, 155].
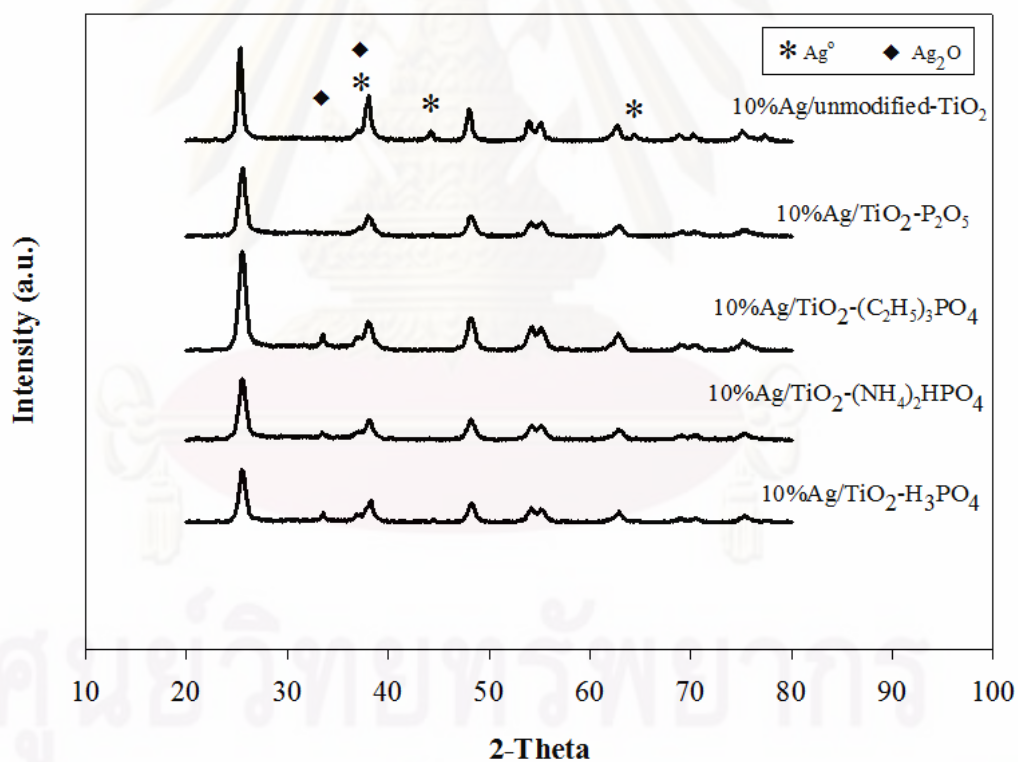
Figure 4.21 XRD patterns of 10 at.%Ag catalysts supported on TiO_2 and P-modified TiO_2 with different phosphorus precursors.

Table 4.10 The peak position of anatase and lattice parameters of 10 at.% Ag catalysts supported on TiO_2 and P-modified TiO_2 with different phosphorus precursors.

Sample	Peak position of anatase (101) (2θ) (degree)	d-spacing (nm)	Lattice parameters (A°)	
			a (=b)	c
10% Ag/unmodified-TiO_2	25.32	3.5174	3.7896	9.4522
10% Ag/TiO_2-H_3PO_4	25.48	3.4957	3.7661	9.3952
10% Ag/TiO_2-$(NH_4)_2HPO_4$	25.56	3.4849	3.7514	9.4142
10% Ag/TiO_2-$(C_2H_5)_3PO_4$	25.52	3.4903	3.7545	9.4714
10% Ag/TiO_2-P_2O_5	25.56	3.4849	3.7478	9.4714

For the 10% Ag/unmodified-TiO_2, diffraction peaks corresponding to metallic Ag appeared at 2θ = 38.1°, 44.4°, and 64.5° and the peaks at 32.8° and 38° were assigned to Ag_2O [135]. The intensities of the XRD characteristic peaks of metallic Ag for the P-modified TiO_2 samples became weak, whereas the peaks of Ag_2O became strong except those of 10% Ag/TiO_2-P_2O in which the peaks corresponding to any Ag species were not clearly seen. The low intensity of metallic Ag peaks for the P-modified TiO_2 may be ascribed to the smaller Ag particles and/or the oxidation of some of the metallic Ag to Ag_2O.

Table 4.11 summarizes the crystallite size of the unmodified and the P-modified TiO_2 supported Ag catalysts, which was calculated from the Scherrer equation. The crystallite sizes of all the P-modified TiO_2 were found to be smaller than the unmodified one, and as a consequence the BET surface areas increased. The existence of phosphorus in the TiO_2 framework may inhibit the growth of anatase TiO_2 crystals [166]. There was little impact of phosphorous precursor on the crystallite size and BET surface area of P-modified TiO_2. All the P-modified TiO_2 had an average crystallite size of ~10 nm and BET surface area of 75 m^2/g.

Table 4.11 Physical properties and amount of active sites of 10 at%Ag catalyst supported on TiO_2 and P-modified TiO_2 with different phosphorus precursors

Catalyst	crystallite size (nm)	BET surface (m^2/g)	Active site ($\times 10^{20}$ atom-Ag/g-cat.)
10%Ag/unmodified-TiO_2	16.2	52	1.27
10%Ag/TiO_2-H_3PO_4	11.2	75	3.57
10%Ag/TiO_2-$(NH_4)_2HPO_4$	10.5	76	3.76
10%Ag/TiO_2-$(C_2H_5)_3PO_4$	10.1	74	3.64
10%Ag/TiO_2-P_2O_5	10.4	75	3.89

The XRD results were found to be in good agreement with those observed from the TEM micrographs **(Figure 4.22).** The average crystallite sizes of unmodified-TiO_2 support decreased from ~15 to ~11 nm when the TiO_2 support was modified with phosphorus. The particle sizes of Ag/Ag_2O on the P-modified TiO_2 supports were determined to be ca. 2.3 nm which were smaller than those dispersed on the unmodified-TiO_2 (ca. 3 nm). The higher metal dispersion on the P-modified TiO_2 supported Ag catalysts was confirmed by the chemisorption results (see also **Table 4.11**). The amount of metal active sites on the P-modified TiO_2 supported Ag catalysts was nearly three times higher than the unmodified ones. However, the amount of metal active sites on the P-modified TiO_2 supported Ag catalysts prepared from different phosphorous precursors were found to be essentially similar in the range of 3.57-3.89 x 10^{20} atoms Ag/g cat.

The FT-IR spectra of unmodified and P-modified TiO_2 are shown in **Figure 4.23**. The spectra bands at ca. 1600 cm^{-1} and 3200 cm^{-1} were attributed to the surface-absorbed water and hydroxyl group, respectively [167, 168]. The IR spectra bands at ca. 400-800 cm^{-1} were attributed to Ti-O-Ti bond. The bands in this range became weak when the TiO_2 support was modified with phosphorus while the bands corresponding to Ti-O-P appeared at ca. 1100 cm^{-1}[139-141]. It is likely that the formation of Ti-O-Ti was suppressed by the formation of Ti-O-P. The incorporation of phosphorus into TiO_2 support could inhibit the agglomeration of TiO_2 crystal,
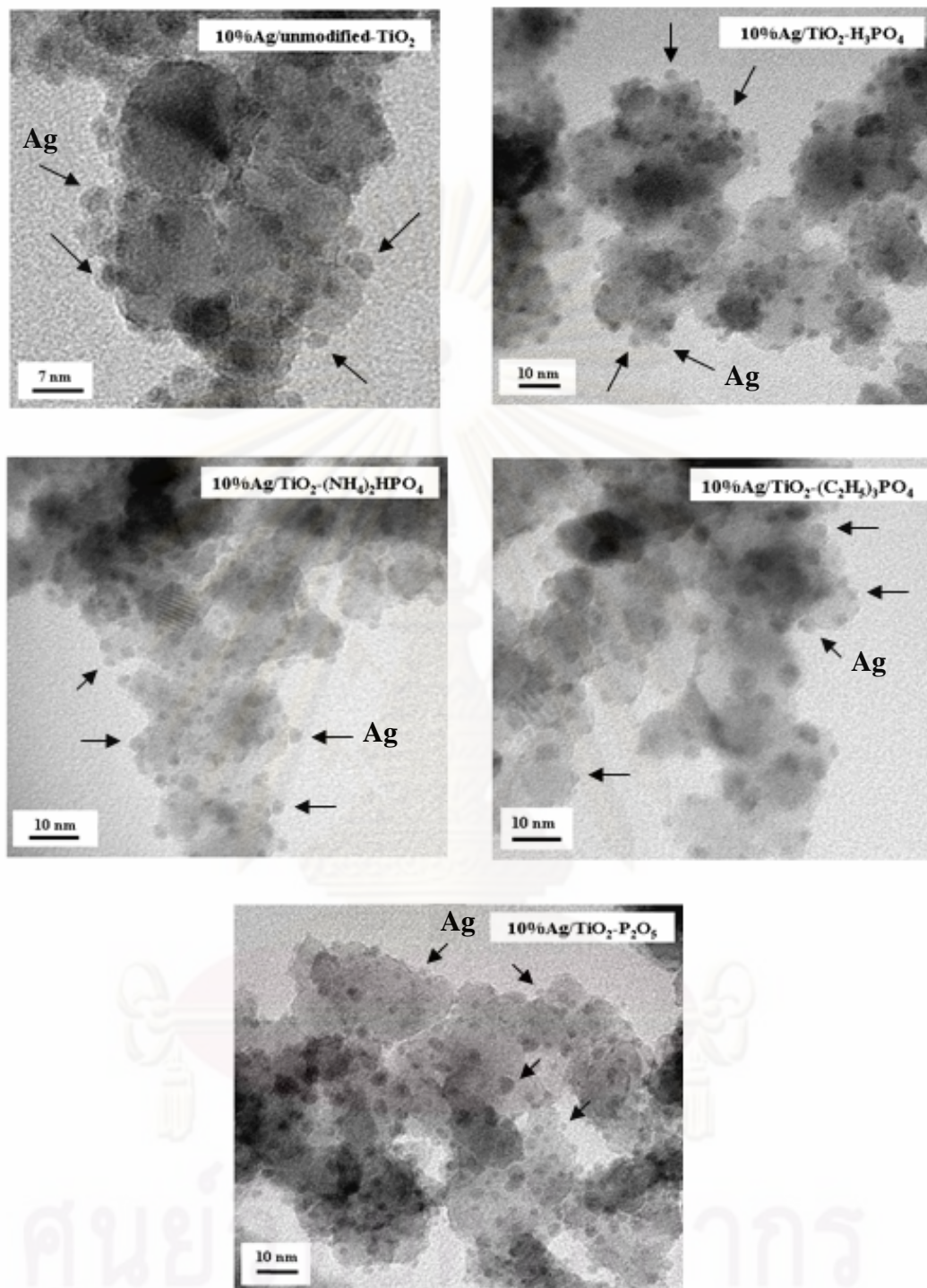
Figure 4.22 TEM images of 10 at.%Ag catalysts supported on TiO_2 and P-modified TiO_2 with different phosphorus precursors.
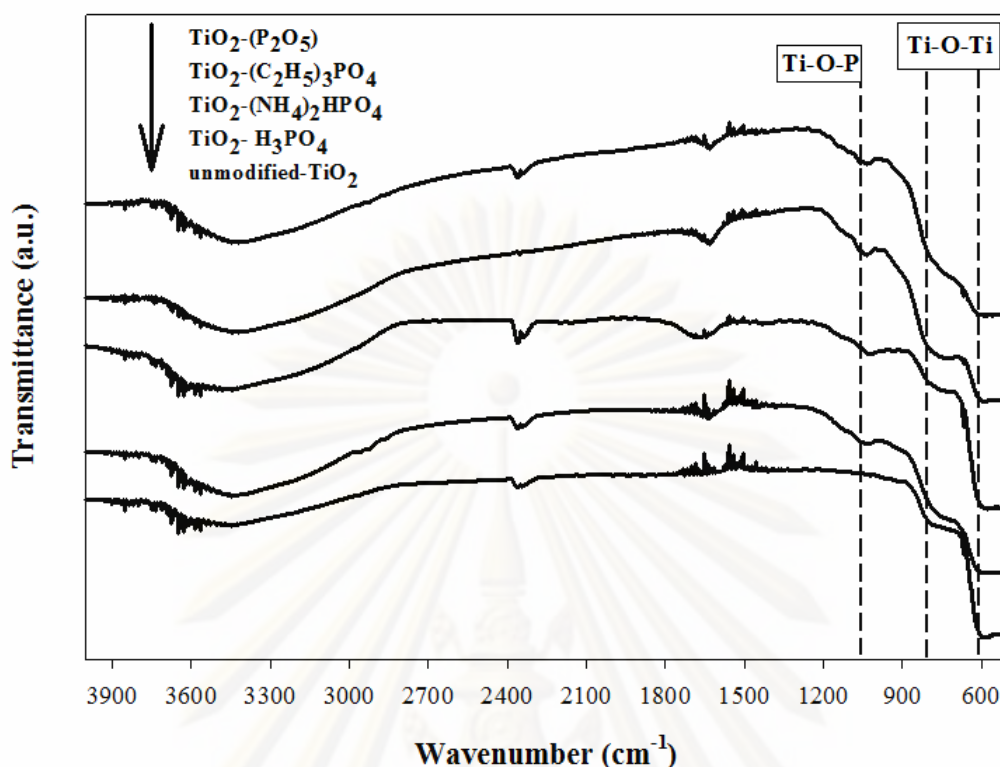
Figure 4.23 FTIR spectra of TiO_2 and P-modified TiO_2 with different phosphorus precursors.

leading to a decrease of TiO_2 crystallite size. The FT-IR results support the characterization by XRD and TEM in which smaller TiO_2 crystallite size was obtained after P-doping.

The oxidation state of element in the sample catalyst was examined by XPS and summarized in **Table 4.12**. The binding energies of Ti 2p, O 1s, Ag 3d, and P 2p were not significantly different among the various catalysts. The Ti 2p peaks consisting of Ti $2p_{3/2}$ and Ti $2p_{1/2}$, with a separation around 5.3 eV, were assigned to the Ti $^{4+}$ in pure anatase TiO_2 [169, 170]. The binding energy of O 1s in all the samples was at ca. 530.0 eV, which was assigned to the Ti-O-Ti lattice oxygen of TiO_2 [171]. The P 2p of all the P-modified TiO_2 shows only one peak in the range of 133.8-134.4 eV, indicating that the oxidation state of phosphorus in TiO_2 was P^{5+}. The absence of P 2p spectra at 129 eV suggested that Ti^{4+} in the lattice of TiO_2 was replaced by P^{5+} [172]. For all the samples, the binding energies of Ag $3d_{5/2}$ and Ag $3d_{3/2}$ were centered at ca. 368 and 374 eV, respectively. According to the literature

[147], the binding energy of Ag $3d_{5/2}$ at 368.2 eV and the slitting between Ag $3d_{5/2}$ and Ag $3d_{3/2}$ 6.0 eV indicates a normal state of Ag^0.

Table 4.12 Binding energies of 10 at.%Ag catalysts supported on TiO_2 and P-modified TiO_2 with different phosphorus precursors.

Sample	Ti 2p		O 1s	Ag 3d		P 2p
	Ti $2p_{3/2}$	Ti $2p_{1/2}$		Ag $3d_{5/2}$	Ag $3d_{3/2}$	
10%Ag/unmodified-TiO_2	458.75	464.55	530.0	367.70	373.50	-
10%Ag/TiO_2-H_3PO_4	459.85	465.65	531.1	369.30	375.00	133.4
10%Ag/TiO_2-$(NH_4)_2HPO_4$	459.35	465.15	530.70	368.70	374.60	133.80
10%Ag/TiO_2-$(C_2H_5)_3PO_4$	459.25	464.85	530.60	368.70	374.60	133.40
10%Ag/TiO_2-P_2O_5	458.45	465.05	530.8	368.90	374.90	134.00

4.4.2 Effect of P doping on the activity of CO oxidation

Figure 4.24 shows the CO conversion as a function of reaction temperature of the unmodified TiO_2 and P-modified TiO_2 supported Ag catalysts prepared with different types of phosphorus precursor. The results show that the type of phosphorus precursor affected to CO oxidation activity of the TiO_2 supported Ag catalysts. The P-modified TiO_2 supported Ag catalysts using the phosphorus precursor in the form of phosphate showed comparable (for 10%Ag/TiO_2-$(NH_4)_2HPO_4$ and 10%Ag/TiO_2-$(C_2H_5)_3PO_4$) or lower activity (10%Ag/TiO_2-H_3PO_4) compared to the 10%Ag/unmodified-TiO_2 (light off temperature ca. 92-97°C). On contrary, the catalyst prepared with the phosphorus precursor in the form of oxide (10%Ag/TiO_2-P_2O_5) showed higher activity than the unmodified-TiO_2 supported catalyst (light-off temperature ~80 °C).
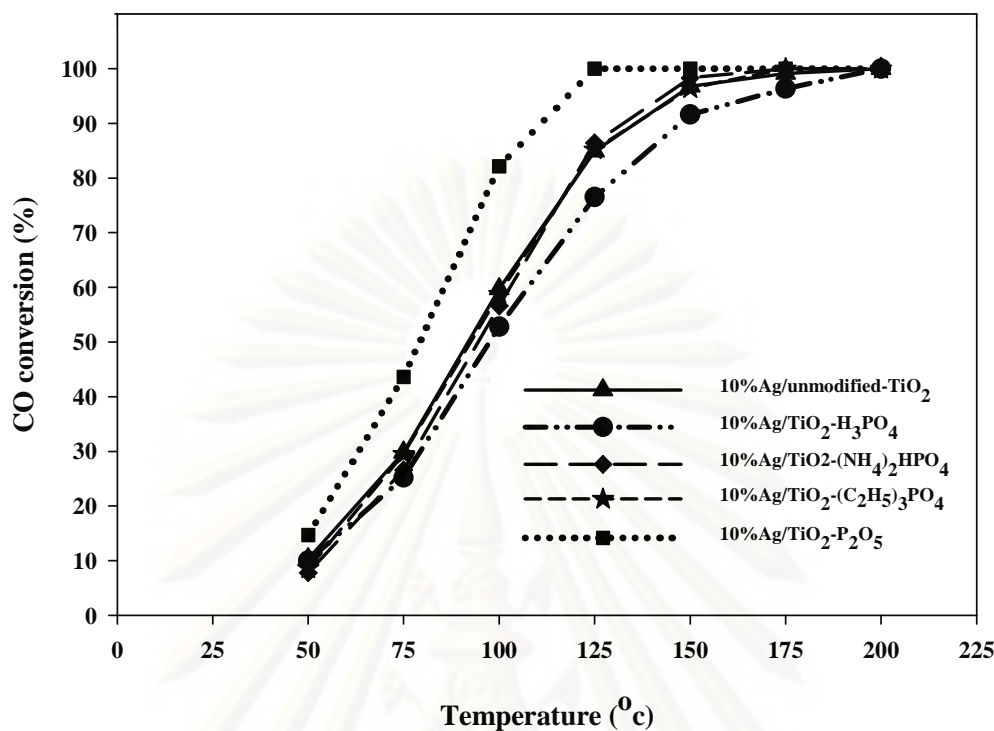
Figure 4.24 CO conversion over 10 at.%Ag catalysts supported on TiO_2 and P-modified TiO_2 with different phosphorus precursors.

Since the physical properties of the P-modified TiO_2 supported Ag catalysts prepared from different phosphorous precursor were quite similar (i.e. in terms of BET surface area, crystallite size, and metal dispersion), the catalytic behaviors were correlated with the O_2 adsorption-desorption behavior on the catalyst surface. **Figure 4.25** shows the O_2-TPD patterns of the unmodified and P-modified TiO_2 supported Ag catalysts with different phosphorus precursors. The Ag catalyst modified with phosphorus exhibited lower desorption temperature and larger amount of desorbed O_2 compared to the unmodified ones. The 10%Ag/unmodified-TiO_2 catalyst shows the lowest amount of adsorbed O_2, with desorption temperature at ca. 300°C. The desorption temperature of 10%Ag/TiO_2-$(C_2H_5)_3PO_4$ and 10%Ag/TiO_2-P_2O_5 catalyst appeared at lower temperature in comparison with the 10%Ag/unmodified-TiO_2. The desorption peak appeared in the range of 250 to 265°C was assigned to O^- species [149]. For the 10%Ag/TiO_2-$(NH_4)_2HPO_4$ and 10%Ag/TiO_2-H_3PO_4, a small shoulder
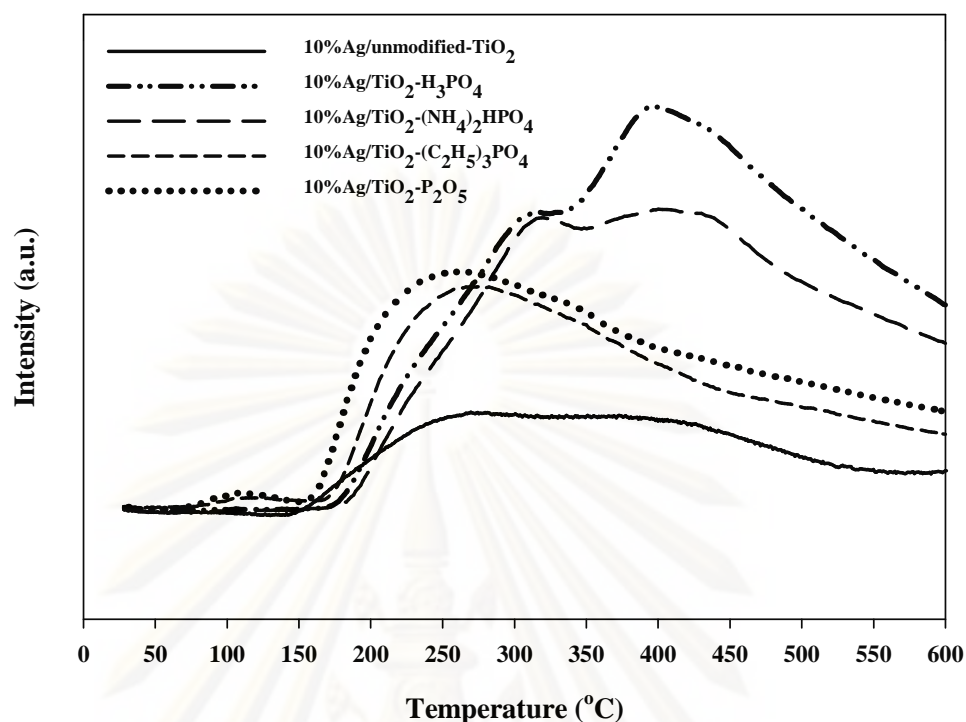
Figure 4.25 O_2-TPD patterns of 10 at.%Ag catalysts supported on TiO_2 and P-modified TiO_2 with different phosphorus precursors.

of O_2 desorption peak at around 250-265°C and large desorption peaks at higher temperature in the range of 300-320°C and 400-430°C were obsereved.

The strongly adsorbed surface oxygen species blocks the adsorption and diffusion of weakly adsorbed surface oxygen, causing a decrease in the CO oxidation activity [162]. It is clearly seen from the O_2-TPD results that the 10%Ag/TiO$_2$-(NH$_4$)$_2$HPO$_4$ and 10%Ag/TiO$_2$-H$_3$PO$_4$ exhibited higher amount of strongly adsorbed oxygen than the other catalysts, thus lower CO oxidation activities were obtained. The desorption profiles of 10%Ag/TiO$_2$-(C$_2$H$_5$)$_3$PO$_4$, however, was quite similar to the 10%Ag/TiO$_2$-P$_2$O$_5$, although the catalytic activities in CO oxidation were different.

Based on the XPS analysis (**Figure 4.26**), the phosphate species on the P-modified TiO_2 surface were identified. The P 2p spectra of 10%Ag/TiO$_2$-(C$_2$H$_5$)$_3$PO$_4$

were slightly different from that of 10%Ag/TiO$_2$-P$_2$O$_5$ in which a shoulder at binding energy 135.2 eV appeared in addition to the major peak at 133.4 eV. The P 2p spectra at a binding energy at 133.4 eV was assigned to the monodentate surface complex, which phosphate adsorbed to the surface hydroxyl ion with one coordination number. The shoulder peak at higher binding energy (135.2 eV) was assigned to the bidentate surface complex which phosphate was bound to two surface hydroxyl ions. The bidentate adsorption is very difficult to remove by a washing step during the preparation of P-modified TiO$_2$ [171, 173]. In other words, the 10%Ag/TiO$_2$-(C$_2$H$_5$)$_3$PO$_4$ produced bidentate of phosphate species on the surface of TiO$_2$ that could result in the blocking of active sites and lower activity in CO oxidation.
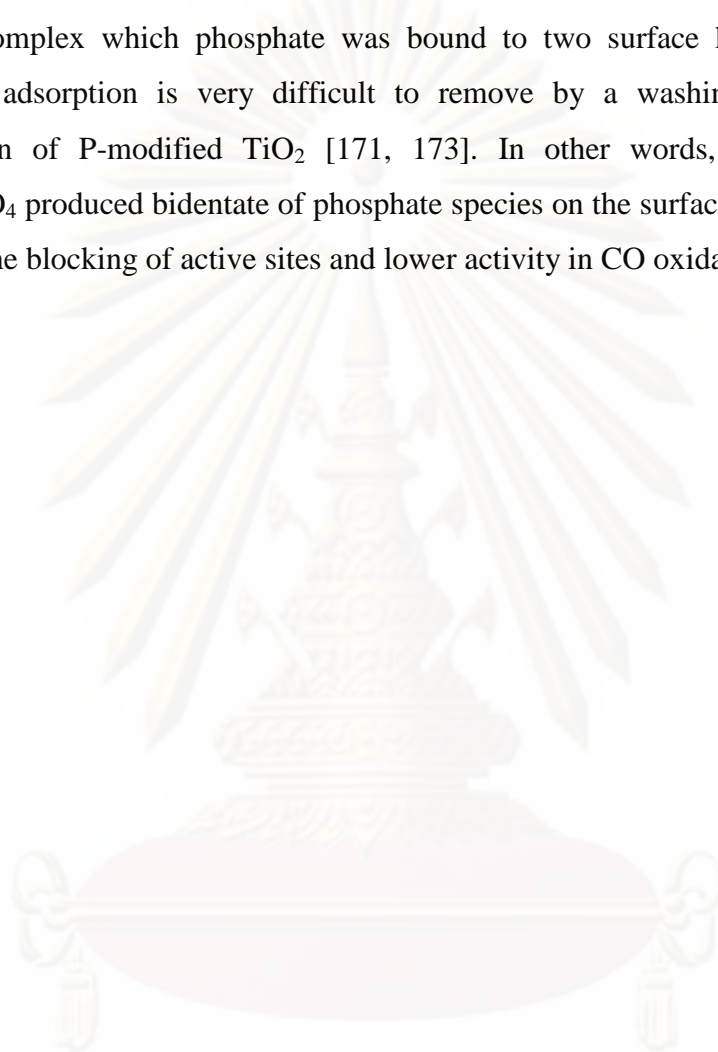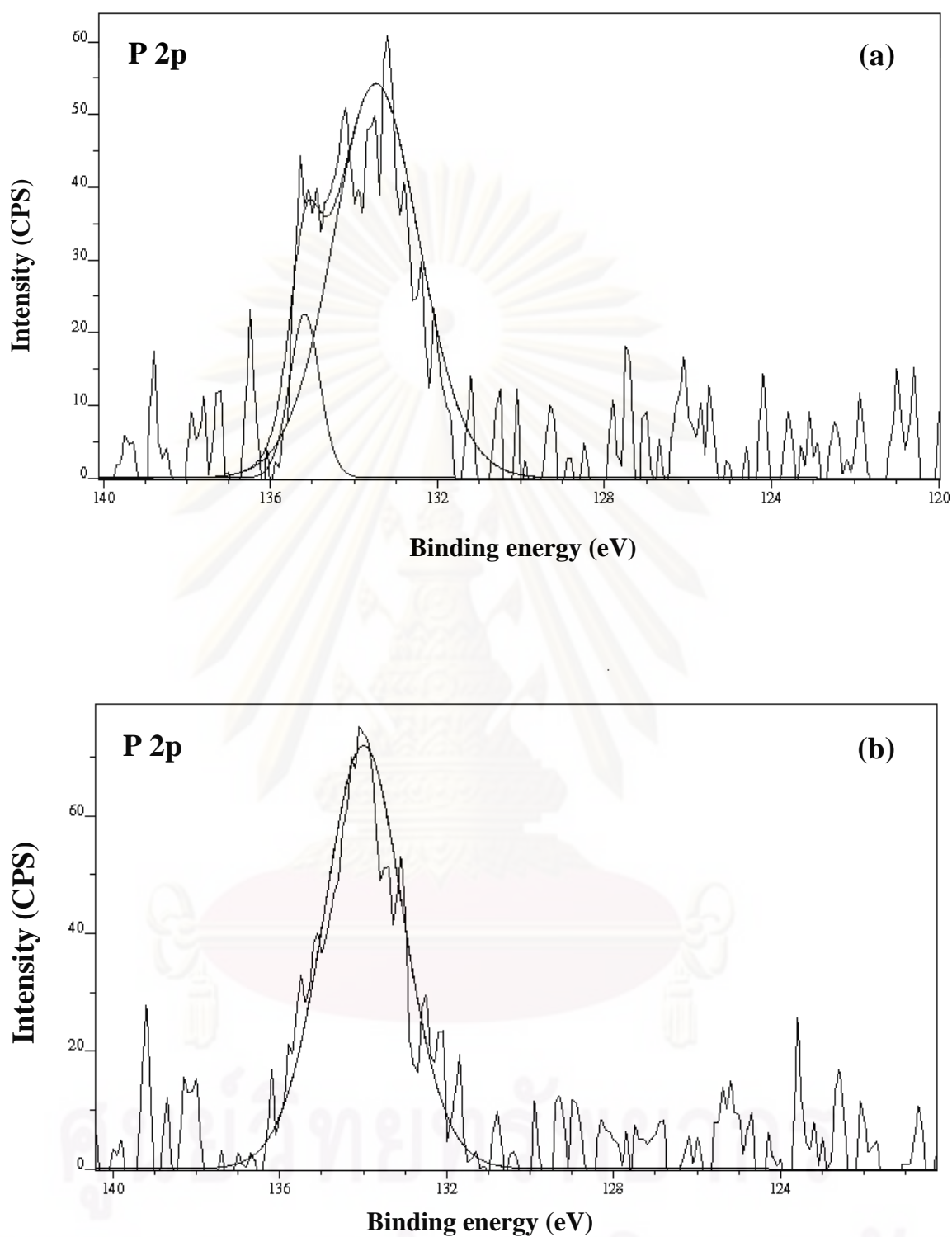
Figure 4.26 The P 2p XPS spectra of (a) 10%Ag/TiO$_2$-(C$_2$H$_5$)$_3$PO$_4$ and (b)

10%Ag/TiO$_2$-P$_2$O$_5$ catalyst.

CHAPTER V
CONCLUSIONS AND RECOMMENDATIONS

This research has investigated the effect of support modification on the catalytic activity in CO oxidation. The method for surface modification of TiO_2 support that was used in this study was the creation of surface defects and the modification with trace element. The parameters which may affect the CO oxidation activity were investigated, such as the amount of surface defect, the type of element dopant, the amount of dopant element and the type of precursor of dopant element. The recommendation for further study is also given in the end of this chapter.

5.1 Conclusions

5.1.1 The use of larger crystallite size TiO_2 (15 nm) which possessed higher amount of Ti^{3+} defective sites as supports for preparation of TiO_2-supported four different transition metals (Ag, Co, Ni, and Pt) resulted in higher metal dispersion and CO oxidation activities compared to the one with smaller crystallite size (7 nm).

5.1.2 The presence of higher amount of Ti^{3+} on the larger crystallite size TiO_2 could play role in stabilization of small metal particles during impregnation, calcination, and reduction steps so that higher metal dispersion was obtained.

5.1.3 All the dopant (i.e., Al, Si, and P) elements used for modification of TiO_2 were inserted into TiO_2 support by substitution at Ti atom in the lattice and showed a different behavior of adsorption and desorption of oxygen species.

5.1.4 The Si-modified TiO_2 exhibited the highest catalytic performance of Ag/TiO_2 catalysts in the CO oxidation when molar ratio of element /Ti was 0.03.

5.1.5 The presence of trace amount of Si atoms in the TiO_2 supports with Si/Ti = 0.05-0.1 has resulted in an improved catalytic performance of Ag/TiO_2 catalysts in the CO oxidation.

5.1.6 The excess Si content (i.e., Si/Ti=0.3) resulted in higher oxygen desorption temperature and no improvement of the catalyst activity, due probably to the formation of amorphous SiO_2.

5.1.7 The modification of the TiO_2 supports with different phosphorus precursors altered the catalytic behaviors of Ag/TiO_2 catalysts in the CO oxidation. The P-modified TiO_2 supported Ag catalysts using the phosphorus precursor in the form of phosphate produced the strongly adsorbed oxygen species and/or the bidentate of phosphate species on the TiO_2 supports, which resulted in no improvement in the CO oxidation activity.

5.1.8 The use of phosphorus precursor in the form of oxide enhanced the CO oxidation activity of Ag/TiO_2 catalysts due to the promotion of weakly adsorbed oxygen species.

5.2 Recommendations

5.2.1   In order to explain why the increase of suface defect on TiO2 support can not improve the amount of active site, the further work is need to investigate.

5.2.2   The other metal catalyst such as Cu, Pt, etc., should be used to study the effect of dopant element to confirm the results of Ag/TiO2 in this work.

5.2.3   The other precursor of dopant element such as Si, Al, etc., should be used to study the effect of dopant precursor to confirm the results of phosphorus precursor in this work.

5.2.4   The behavior of adsorption and desorption of oxygen species of the modification with P_2O_5 and $(C_2H_5)_3PO_4$ shows the similar profile but different in CO oxidation activity. The further work is needed to investigate this point.

REFERENCES

[1] Matos, J., Laine, J. and Herrmann, J. M. Effect of the Type of Activated Carbons on the Photocatalytic Degradation of Aqueous Organic Pollutants by UV-Irradiated Titania. *Journal of Catalysis* 200, 1 (2001): 10-20.

[2] Hoffmann, M. R., Martin, S. T., Choi, W. and Bahnemann, D. W. Environmental applications of semiconductor photocatalysis. *Chemical Reviews* 95, 1 (1995): 69-96.

[3] Malato, S., Blanco, J., Richter, C. and Maldonado, M. I. Optimization of pre-industrial solar photocatalytic mineralization of commercial pesticides: Application to pesticide container recycling. *Applied Catalysis B: Environmental* 25, 1 (2000): 31-38.

[4] Mills, A. and Morris, S. Photomineralization of 4-chlorophenol sensitized by titanium dioxide: a study of the initial kinetics of carbon dioxide photogeneration. *Journal of Photochemistry and Photobiology A: Chemistry* 71, 1 (1993): 75-83.

[5] Ding, Z., Lu, G. Q. and Greenfield, P. F. Role of the Crystallite Phase of TiO_2 in Heterogeneous Photocatalysis for Phenol Oxidation in Water. *The Journal of Physical Chemistry B* 104, 19 (2000): 4815-4820.

[6] S.J. Tauster, S.C. Fung and R.L. Garten Strong metal-support interactions. Group 8 noble metals supported on titanium dioxide. *Journal of the American Chemical Society* 100, (1978): 170-175.

[7] Haller, G. L., Resasco, D. E., D.D. Eley, H. P. and Paul, B. W. Metal-Support Interaction: Group VIII Metals and Reducible Oxides. *Advances in Catalysis* 36, (1989): 173-235.

[8] Vannice, M. A. and Sen, B. Metal-support effects on the intramolecular selectivity of crotonaldehyde hydrogenation over platinum. *Journal of Catalysis* 115, 1 (1989): 65-78.

[9] Claus, P. et al. Hydrogenation of crotonaldehyde on Pt/TiO$_2$ catalysts: Influence of the phase composition of titania on activity and intramolecular selectivity. *Applied Catalysis A: General* 165, 1-2 (1997): 429-441.

[10] Murrell, L. L., Yates, D. J. C., Seiyama, T. and Tanabe, K. Strong Metal-Support Interactions with Ultradispersed Rhodium. *Studies in Surface Science and Catalysis* 7, (1981): 1470-1471.

[11] Haruta, M. and Date, M. Advances in the catalysis of Au nanoparticles. *Applied Catalysis A: General* 222, 1-2 (2001): 427-437.

[12] Frey, K., Iablokov, V., Melaet, G., Guczi, L. and Kruse, N. CO Oxidation Activity of Ag/TiO$_2$ Catalysts Prepared via Oxalate Co-precipitation. *Catalysis Letters* 124, 1 (2008): 74-79.

[13] Rieck, J. S. and Bell, A. T. Studies of the interactions of H$_2$ and CO with silica- and lanthana-supported palladium. *Journal of Catalysis* 96, 1 (1985): 88-105.

[14] Ko, E. I. and Wagner, N. J. Evidence of metal–support interaction for an Ni/TiO$_2$–SiO$_2$ catalyst. *Journal of the Chemical Society, Chemical Communications articles*, (1984): 1274-1275.

[15] Karvinen, S. The effects of trace elements on the crystal properties of TiO$_2$ *Solid State Sciences* 5, 5 (2003): 811-819.

[16] Fujishima, A., Hashimoto, K. and Watanabe, T. *TiO$_2$ Photocatalysis: Fundamentals and Applications.* pp. 46-64. Tokyo: Bkc Inc., 1999.

[17] Bokhimi, X. and Zanella, R. Crystallite Size and Morphology of the Phases in Au/TiO$_2$ and Au/Ce-TiO$_2$ Catalysts. *The Journal of Physical Chemistry C* 111, 6 (2007): 2525-2532.

[18] Zhang, X., Wang, H. and Xu, B. Q. Remarkable nanosize effect of zirconia in Au/ZrO$_2$ catalyst for CO oxidation. *The Journal of Physical Chemistry B* 109, 19 (2005): 9678-9683.

[19] Sirikajorn, T., Mekasuwandumrong, O., Praserthdam, P., Goodwin, J. and Panpranot, J. Effect of Support Crystallite Size on Catalytic Activity and Deactivation of Nanocrystalline ZnAl$_2$O$_4$-Supported Pd Catalysts in Liquid-Phase Hydrogenation. *Catalysis Letters* 126, 3 (2008): 313-318.

[20] Adams, R. Millennium says global TiO$_2$ demand fell by 5% in 2005. *Focus on Pigments* 2005, 12 (2005): 1-2.

[21] Kumazawa, N., Rafiqul Islam, M. and Takeuchi, M. Photoresponse of a titanium dioxide chemical sensor. *Journal of Electroanalytical Chemistry* 472, 2 (1999): 137-141.

[22] Savage, N. O., Akbar, S. A. and Dutta, P. K. Titanium dioxide based high temperature carbon monoxide selective sensor. *Sensors and Actuators B: Chemical* 72, 3 (2001): 239-248.

[23] Savage, N. et al. Composite n-p semiconducting titanium oxides as gas sensors. *Sensors and Actuators B: Chemical* 79, 1 (2001): 17-27.

[24] Hadjiivanov, K. I. and Klissurski, D. G. Surface chemistry of titania (anatase) and titania-supported catalysts. *Chemical Society Reviews* 25, (1996): 61-69.

[25] Armor, J. N. Environmental catalysis. *Applied Catalysis B: Environmental* 1, 4 (1992): 221-256.

[26] Weber, R., Sakurai, T. and Hagenmaier, H. Low temperature decomposition of PCDD/PCDF, chlorobenzenes and PAHs by TiO_2-based V_2O_5-WO_3 catalysts. *Applied Catalysis B: Environmental* 20, 4 (1999): 249-256.

[27] Boccuzzi, F. et al. Gold, silver and copper catalysts supported on TiO_2 for pure hydrogen production. *Catalysis Today* 75, 1-4 (2002): 169-175.

[28] Li, J., Jacobs, G., Das, T. and Davis, B. H. Fischer-Tropsch synthesis: effect of water on the catalytic properties of a ruthenium promoted Co/TiO_2 catalyst. *Applied Catalysis A: General* 233, 1-2 (2002): 255-262.

[29] Bollinger, M. A. and Vannice, M. A. A kinetic and DRIFTS study of low-temperature carbon monoxide oxidation over Au--TiO_2 catalysts. *Applied Catalysis B: Environmental* 8, 4 (1996): 417-443.

[30] Kim, H., Won Park, D., Chul Woo, H. and Shik Chung, J. Reduction of SO_2 by CO to elemental sulfur over Co_3O_4-TiO_2 catalysts. *Applied Catalysis B: Environmental* 19, 3-4 (1998): 233-243.

[31] Despres, J., Koebel, M., Krocher, O., Elsener, M. and Wokaun, A. Storage of NO_2 on BaO/TiO_2 and the influence of NO. *Applied Catalysis B: Environmental* 43, 4 (2003): 389-395.

[32] Melemeni, M., Stamatakis, D., Xekoukoulotakis, N. P., Mantzavinos, D. and Kalogerakis, N. Disinfection of municipal wastewatwe by TiO_2 photocatalysis with UV-A, visible and solar irradiation and BDD electrolysis. *Global NEST Journal* 11, 3 (2009): 357-363.

[33] Carp, O., Huisman, C. L. and Reller, A. Photoinduced reactivity of titanium dioxide. *Progress in Solid State Chemistry* 32, 1-2 (2004): 33-177.

[34] Diebold, U. et al. Intrinsic defects on a $TiO_2(110)(1x1)$ surface and their reaction with oxygen: a scanning tunneling microscopy study. *Surface Science* 411, 1-2 (1998): 137-153.

[35] Thompson, T. and Yates, J. TiO2-based Photocatalysis: Surface Defects, Oxygen and Charge Transfer. *Topics in Catalysis* 35, 3 (2005): 197-210.

[36] Henderson, M. A. A surface perspective on self-diffusion in rutile TiO_2. *Surface Science* 419, 2-3 (1999): 174-187.

[37] Li, M. et al. Oxygen-induced restructuring of the $TiO_2(110)$ surface: a comprehensive study. *Surface Science* 437, 1-2 (1999): 173-190.

[38] Onishi, H. and Iwasawa, Y. Dynamic Visualization of a Metal-Oxide-Surface/Gas-Phase Reaction: Time-Resolved Observation by Scanning Tunneling Microscopy at 800 K. *Physical Review Letters* 76, 5 (1996): 791.

[39] Henderson, M. A. Mechanism for the bulk-assisted reoxidation of ion sputtered TiO_2 surfaces: diffusion of oxygen to the surface or titanium to the bulk? *Surface Science* 343, 1-2 (1995): L1156-L1160.

[40] Li, M., Hebenstreit, W., Diebold, U., Henderson, M. A. and Jennison, D. R. Oxygen-induced restructuring of rutile $TiO_2(110)$: formation mechanism, atomic models, and influence on surface chemistry. *Faraday Discuss* 114, (1999): 245-258.

[41] Li, M. et al. The Influence of the Bulk Reduction State on the Surface Structure and Morphology of Rutile $TiO_2(110)$ Single Crystals. *The Journal of Physical Chemistry B* 104, 20 (2000): 4944-4950.

[42] Phillips, L. G. and Barbano, D. M. The Influence of Fat Substitutes Based on Protein and Titanium Dioxide on the Sensory Properties of Lowfat Milk. *Journal of Dairy Science* 80, (1997): 2726.

[43] Fujishima, A. Electrochemical Photolysis of Water at a Semiconductor Electrode. *Nature* 238, (1972): 37-38.

[44] Fujishima, A. Discovery and applications of photocatalysis: Creating a comfortable future by making use of light energy *Japan Nanonet Bulletin* 44, (2005): 1-3.

[45] Mills, A. and Le Hunte, S. An overview of semiconductor photocatalysis. *Journal of Photochemistry and Photobiology A: Chemistry* 108, 1 (1997): 1-35.

[46] Madhusudan Reddy, K., Gopal Reddy, C. V. and Manorama, S. V. Preparation, Characterization, and Spectral Studies on Nanocrystalline Anatase TiO_2. *Journal of Solid State Chemistry* 158, 2 (2001): 180-186.

[47] Tang, H., Prasad, K., Sanjines, R. and Levy, F. TiO_2 anatase thin films as gas sensors. *Sensors and Actuators B: Chemical* 26, 1-3 (1995): 71-75.

[48] Xu, Y., Yao, K., Zhou, X. and Cao, Q. Platinum-titania oxygen sensors and their sensing mechanisms. *Sensors and Actuators B: Chemical* 14, 1-3 (1993): 492-494.

[49] Calatayud, M., Markovits, A., Menetrey, M., Mguig, B. and Minot, C. Adsorption on perfect and reduced surfaces of metal oxides. *Catalysis Today* 85, 2-4 (2003): 125-143.

[50] Barteau, M. A. Organic Reactions at Well-Defined Oxide Surfaces. *Chemical Reviews* 96, 4 (1996): 1413-1430.

[51] Kirner, U. et al. Low and high temperature TiO_2 oxygen sensors. *Sensors and Actuators B: Chemical* 1, 1-6 (1990): 103-107.

[52] Diebold, U. The surface science of titanium dioxide. *Surface Science Reports* 48, 5-8 (2003): 53-229.

[53] Busca, G., Lietti, L., Ramis, G. and Berti, F. Chemical and mechanistic aspects of the selective catalytic reduction of NOx by ammonia over oxide catalysts: A review. *Applied Catalysis B: Environmental* 18, 1-2 (1998): 1-36.

[54] Trung, T., Cho, W.-J. and Ha, C.-S. Preparation of TiO_2 nanoparticles in glycerol-containing solutions. *Materials Letters* 57, 18 (2003): 2746-2750.

[55] Sugimoto, T., Zhou, X. and Muramatsu, A. Synthesis of Uniform Anatase TiO_2 Nanoparticles by Gel-Sol Method: 1. Solution Chemistry of $Ti(OH)_{n(4-n)}^{+}$ Complexes. *Journal of Colloid and Interface Science* 252, 2 (2002): 339-346.

[56] Arnal, P., Corriu, R. J. P., Leclercq, D., Mutin, P. H. and Vioux, A. A Solution Chemistry Study of Nonhydrolytic Sol-Gel Routes to Titania. *Chemistry of Materials* 9, 3 (1997): 694-698.

[57] Kim, C.-S., Moon, B. K., Park, J.-H., Tae Chung, S. and Son, S.-M. Synthesis of nanocrystalline TiO_2 in toluene by a solvothermal route. *Journal of Crystal Growth* 254, 3-4 (2003): 405-410.

[58] Kim, C.-S., Moon, B. K., Park, J.-H., Choi, B.-C. and Seo, H.-J. Solvothermal synthesis of nanocrystalline TiO_2 in toluene with surfactant. *Journal of Crystal Growth* 257, 3-4 (2003): 309-315.

[59] Nian, J.-N. and Teng, H. Hydrothermal Synthesis of Single-Crystalline Anatase TiO_2 Nanorods with Nanotubes as the Precursor. *The Journal of Physical Chemistry B* 110, 9 (2006): 4193-4198.

[60] Kolen'ko, Y. V., Churagulov, B. R., Kunst, M., Mazerolles, L. and Colbeau-Justin, C. Photocatalytic properties of titania powders prepared by hydrothermal method. *Applied Catalysis B: Environmental* 54, 1 (2004): 51-58.

[61] Kim, D. H., Hong, H. S., Kim, S. J., Song, J. S. and Lee, K. S. Photocatalytic behaviors and structural characterization of nanocrystalline Fe-doped TiO_2

synthesized by mechanical alloying. *Journal of Alloys and Compounds* 375, 1-2 (2004): 259-264.

[62] Guimaraes, J. L., Abbate, M., Betim, S. B. and Alves, M. C. M. Preparation and characterization of TiO$_2$ and V$_2$O$_5$ nanoparticles produced by ball-milling. *Journal of Alloys and Compounds* 352, 1-2 (2003): 16-20.

[63] Kamei, M. and Mitsuhashi, T. Hydrophobic drawings on hydrophilic surfaces of single crystalline titanium dioxide: surface wettability control by mechanochemical treatment. *Surface Science* 463, 1 (2000): L609-L612.

[64] Oh, S.-M. and Ishigaki, T. Preparation of pure rutile and anatase TiO$_2$ nanopowders using RF thermal plasma. *Thin Solid Films* 457, 1 (2004): 186-191.

[65] Bischoff, B. L. and Anderson, M. A. Peptization properties in the sol-gel preparation of porous anatase (TiO$_2$). *Chemistry Material* 7, (1995): 1772-1778.

[66] Ding, X.-Z., Qi, Z.-Z. and He, Y.-Z. Effect of hydrolysis water on the preparation of nano-crystalline titania powders via a sol-gel process. *Journal of Materials Science Letters* 14, 1 (1995): 21-22.

[67] Vorkapic, D. and Matsoukas, T. Effect of temperature and alcohols in the preparation of titania nanoparticles from alkoxides. *Journal of the American Ceramic Society* 81, (1998): 2815-2820.

[68] Wang, C., Deng, Z.-X., Zhang, G., Fan, S. and Li, Y. Synthesis of nanocrystalline TiO$_2$ in alcohols. *Powder Technology* 125, 1 (2002): 39-44.

[69] Chen, S.-J. et al. Preparation and characterization of nanocrystalline zinc oxide by a novel solvothermal oxidation route. *Journal of Crystal Growth* 252, 1-3 (2003): 184-189.

[70] Liu, J. et al. Surfactant-aided solvothermal synthesis of dinickel phosphide nanocrystallites using red phosphorus as starting materials. *Journal of Crystal Growth* 252, 1-3 (2003): 297-301.

[71] Kang, M. Synthesis of Fe/TiO$_2$ photocatalyst with nanometer size by solvothermal method and the effect of H$_2$O addition on structural stability and photodecomposition of methanol. *Journal of Molecular Catalysis A: Chemical* 197, 1-2 (2003): 173-183.

[72] Samano, E., Kim, J. and Koel, B. Investigation of CO Oxidation Transient Kinetics on an Oxygen Pre-covered Au(211) Stepped Surface. *Catalysis Letters* 128, 3 (2009): 263-267.

[73] Hagen., J. *Industrial Catalysis-A Practical Approach.* pp. 174. New York: Wiley-VCH, 1999.

[74] Zecchina, A. et al. IR studies of CO and NO adsorbed on well characterized oxide single microcrystals. *Catalysis Today* 27, 3-4 (1996): 403-435.

[75] Konova, P., Naydenov, A., Tabakova, T. and Mehandjiev, D. Deactivation of nanosize gold supported on zirconia in CO oxidation. *Catalysis Communications* 5, 9 (2004): 537-542.

[76] Boccuzzi, F., Chiorino, A., Tsubota, S. and Haruta, M. FTIR Study of Carbon Monoxide Oxidation and Scrambling at Room Temperature over Gold Supported on ZnO and TiO$_2$. *The Journal of Physical Chemistry* 100, 9 (1996): 3625-3631.

[77] Fahmi, A. and Minot, C. A theoretical study of CO adsorption on TiO$_2$. *Journal of Organometallic Chemistry* 478, 1-2 (1994): 67-73.

[78] Markovits, A., Fahmi, A. and Minot, C. A theoretical study of CO$_2$ adsorption on TiO$_2$. *Journal of Molecular Structure: THEOCHEM* 371, (1996): 219-235.

[79] Lin, H.-F., Lin, H.-M. and Hsu, S.-L. Molecular simulation for gas adsorption at TiO$_2$ (rutile and anatase) surface. *Nanostructured Materials* 12, 1-4 (1999): 357-360.

[80] Iizuka, Y. et al. Adsorption of CO on gold supported on TiO$_2$. *Catalysis Today* 36, 1 (1997): 115-123.

[81] Dutta, P. K. et al. Interaction of Carbon Monoxide with Anatase Surfaces at High Temperatures: Optimization of a Carbon Monoxide Sensor. *The Journal of Physical Chemistry B* 103, 21 (1999): 4412-4422.

[82] Comini, E., Guidi, V., Frigeri, C., Ricc, I. and Sberveglieri, G. CO sensing properties of titanium and iron oxide nanosized thin films. *Sensors and Actuators B: Chemical* 77, 1-2 (2001): 16-21.

[83] Mguig, B., Calatayud, M. and Minot, C. CO oxidation over anatase TiO$_2$-(001). *Journal of Molecular Structure: THEOCHEM* 709, 1-3 (2004): 73-78.

[84] Over, H. et al. Atomic-Scale Structure and Catalytic Reactivity of the RuO$_2$(110) Surface. *Science* 287, 5457 (2000): 1474-1476.

[85] Hendriksen, B. L. M. and Frenken, J. W. M. CO Oxidation on Pt(110): Scanning Tunneling Microscopy Inside a High-Pressure Flow Reactor. *Physical Review Letters* 89, 4 (2002): 046101.

[86] Bond, G. C. and Thompson, D. T. Catalysis by Gold. *Catalysis Reviews: Science and Engineering* 41, 3 (1999): 319-388.

[87] Martin, C. et al. Surface reactivity and morphology of vanadia-titania catalysts. *Surface Science* 251-252, 1 (1991): 825-830.

[88] Haruta, M. Nanoparticulate gold catalysts for low-temperature CO oxidation. *Journal of New Materials for Electrochemical Systems* 7, 3 (2004): 163-172.

[89] Okumura, M., Masuyama, N., Konishi, E., Ichikawa, S. and Akita, T. CO oxidation below room temperature over Ir/TiO$_2$ catalyst prepared by deposition precipitation method. *Journal of Catalysis* 208, 2 (2002): 485-489.

[90] Kang, M., W Song, M. and Lee, C. H. Catalytic carbon monoxide oxidation over CoOx/CeO$_2$ composite catalysts *Applied Catalysis A: General* 251, (2003): 143-156.

[91] Zheng, X., Zhang, X., Wang, S., Wang, X. and Wu, S. Effect of Addition of Base on Ceria and Reactivity of CuO/CeO$_2$ Catalysts for Low-Temperature CO Oxidation. *Journal of Natural Gas Chemistry* 16, 2 (2007): 179-185.

[92] Zheng, X., Zhang, X., Wang, X., Wang, S. and Wu, S. Preparation and characterization of CuO/CeO$_2$ catalysts and their applications in low-temperature CO oxidation. *Applied Catalysis A: General* 295, 2 (2005): 142-149.

[93] Huang, J. et al. Synthesis and characterization of CuO/TiO$_2$ catalysts for low-temperature CO oxidation. *Catalysis Communications* 7, 12 (2006): 1029-1034.

[94] Zheng, X. C. et al. The preparation and catalytic behavior of copper-cerium oxide catalysts for low-temperature carbon monoxide oxidation. *Applied Catalysis A: General* 283, 1-2 (2005): 217-223.

[95] Tu, C.-H., Wang, A.-Q., Zheng, M.-Y., Wang, X.-D. and Zhang, T. Factors influencing the catalytic activity of SBA-15-supported copper nanoparticles in CO oxidation. *Applied Catalysis A: General* 297, 1 (2006): 40-47.

[96] Tauster, S. J., Fung, S. C. and Garten, R. L. Strong metal-support interactions. Group 8 noble metals supported on titanium dioxide. *Journal of the American Chemical Society* 100, 1 (1978): 170-175.

[97] Burch, R. and Flambard, A. R. Support effects in nickel catalysts. *Journal of Catalysis* 85, 1 (1984): 16-24.

[98] Dow, W. P. and Huang, T. J. Effects of Oxygen Vacancy of Yttria-Stabilized Zirconia Support on Carbon Monoxide Oxidation over Copper Catalyst. *Journal of Catalysis* 147, 1 (1994): 322-332.

[99] Tsai, D.-H. and Huang, T.-J. Activity behavior of samaria-doped ceria-supported copper oxide catalyst and effect of heat treatments of support on carbon monoxide oxidation. *Applied Catalysis A: General* 223, 1-2 (2002): 1-9.

[100] Wang, J. B., Lee, H.-K. and Huang, T.-J. Synergistic Catalysis of Carbon Dioxide Hydrogenation into Methanol by Yttria-Doped Ceria/γ-Alumina-Supported Copper Oxide Catalysts: Effect of Support and Dopant. *Catalysis Letters* 83, 1 (2002): 79-86.

[101] Henrich, V. E. and Kurtz, R. L. Surface electronic structure of TiO_2: Atomic geometry, ligand coordination, and the effect of adsorbed hydrogen. *Physical Review B* 23, 12 (1981): 6280.

[102] Mezhenny, S. et al. STM studies of defect production on the TiO_2(1 1 0)-(1x1) and TiO_2(1 1 0)-(1x2) surfaces induced by UV irradiation. *Chemical Physics Letters* 369, 1-2 (2003): 152-158.

[103] Pan, J. M., Maschhoff, B. L., Diebold, U. and Madey, T. E. (1992) Ttile., 38th National Symposium of the American Vacuum Society. AVS, Seattle, Washington (USA).

[104] Nakamura, I. et al. Role of oxygen vacancy in the plasma-treated TiO_2 photocatalyst with visible light activity for NO removal. *Journal of Molecular Catalysis A: Chemical* 161, 1-2 (2000): 205-212.

[105] Zhang, Z. and Henrich, V. E. Electronic interactions in the vanadium/TiO_2(110) and vanadia/TiO_2(110) model catalyst systems. *Surface Science* 277, 3 (1992): 263-272.

[106] Bourgeois, S., Jomard, F. and Perdereau, M. Use of isotopic labelling in a SIMS study of the hydroxylation of TiO_2(100) surfaces. *Surface Science* 279, 3 (1992): 349-354.

[107] Pan, J.-M. and Madey, T. E. (1993) Ttile., 39th National Symposium of the American Vacuum Society. AVS, Chicago, Illinois (USA).

[108] Payakgul, W., Mekasuwandumrong, O., Pavarajarn, V. and Praserthdam, P. Effects of reaction medium on the synthesis of TiO_2 nanocrystals by thermal decomposition of titanium (IV) n-butoxide. *Ceramics International* 31, 3 (2005): 391-397.

[109] Sirisuk, A., Klansorn, E. and Praserthdam, P. Effects of reaction medium and crystallite size on Ti^{3+} surface defects in titanium dioxide nanoparticles prepared by solvothermal method. *Catalysis Communications* 9, 9 (2008): 1810-1814.

[110] Wallace, W. T., Min, B. K. and Goodman, D. W. The stabilization of supported gold clusters by surface defects. *Journal of Molecular Catalysis A: Chemical* 228, 1-2 (2005): 3-10.

[111] Suriye, K., Praserthdam, P. and Jongsomjit, B. Impact of Ti^{3+} Present in Titania on Characteristics and Catalytic Properties of the Co/TiO_2 Catalyst. *Industrial & Engineering Chemistry Research* 44, 17 (2005): 6599-6604.

[112] Burch, R. and Flambard, A. R. Strong metal-support interactions in nickel/titania catalysts: The importance of interfacial phenomena. *Journal of Catalysis* 78, 2 (1982): 389-405.

[113] Ruckenstein, E. and Li, Z. F. Surface modification and functionalization through the self-assembled monolayer and graft polymerization. *Advances in Colloid and Interface Science* 113, 1 (2005): 43-63.

[114] Pukánszky, B. and Fekete, E. *Adhesion and Surface Modification.* pp. 109-153. Berlin: Heidelberg, 1999.

[115] Grancharov, S. G. et al. Bio-functionalization of Monodisperse Magnetic Nanoparticles and Their Use as Biomolecular Labels in a Magnetic Tunnel Junction Based Sensor. *The Journal of Physical Chemistry B* 109, 26 (2005): 13030-13035.

[116] Pestryakov, A. N. et al. Influence of modifying additives on electronic state of supported gold. *Journal of Molecular Structure* 642, 1-3 (2002): 129-136.

[117] Tai, Y. et al. Oxidation of carbon monoxide on Au nanoparticles in titania and titania-coated silica aerogels. *Applied Catalysis A: General* 268, 1-2 (2004): 183-187.

[118] Yu, J., Wu, G., Mao, D. and Lu, G. Effect of La_2O_3 on Catalytic Performance of Au/TiO_2 for CO Oxidation. *Acta Physico-Chimica Sinica* 24, 10 (2008): 1751-1755.

[119] Evans, J. W., Wainwright, M. S., Bridgewater, A. J. and Young, D. J. On the determination of copper surface area by reaction with nitrous oxide. *Applied Catalysis* 7, 1 (1983): 75-83.

[120] Weerachawanasak, P. et al. Effect of strong metal-support interaction on the catalytic performance of Pd/TiO_2 in the liquid-phase semihydrogenation of phenylacetylene. *Journal of Catalysis* 262, 2 (2009): 199-205.

[121] Suriye, K., Praserthdam, P. and Jongsomjit, B. Effect of surface sites of TiO_2 support on the formation of cobalt-support compound in Co/TiO_2 catalysts. *Catalysis Communications* 8, 11 (2007): 1772-1780.

[122] Park, D. R., Zhang, J., Ikeue, K., Yamashita, H. and Anpo, M. Photocatalytic oxidation of ethylene to CO_2 and H_2O on ultrafine powdered TiO_2 photocatalysts in the presence of O_2 and H_2O. *Journal of Catalysis* 185, 1 (1999): 114-119.

[123] Watterich, A., Hofstaetter, A., Wuerz, R. and Scharmann, A. Ti^{3+} centres in reduced $ZnWO_4$:Ti single crystals. *Solid State Commun* 100, 7 (1996): 513-518.

[124] Zeng, Y., Zheng, Y., Yu, S., Chen, K. and Zhou, S. An ESR study of the electrocatalytic oxidation of hypophosphite on a nickel electrode. *Electrochemistry Communications* 4, 4 (2002): 293-295.

[125] Kongsuebchart, W. et al. Effect of crystallite size on the surface defect of nano-TiO_2 prepared via solvothermal synthesis. *Journal of Crystal Growth* 297, 1 (2006): 234-238.

[126] Li, M., Tang, P., Hong, Z. and Wang, M. High efficient surface-complex-assisted photodegradation of phenolic compounds in single anatase titania under visible-light. *Colloids and Surfaces A: Physicochemical and Engineering Aspects* 318, 1-3 (2008): 285-290.

[127] Nissinen, T., Leskela, M., Gasik, M. and Lamminen, J. Decomposition of mixed Mn and Co nitrates supported on carbon. *Thermochimica Acta* 427, 1-2 (2005): 155-161.

[128] Kongsuebchart, W., Panpranot, J., Satayaprasert, C. and Praserthdam, P. Effect of TiO_2 crystallite size on the dispersion of Co on nanocrystalline TiO_2. *Reaction Kinetics and Catalysis Letters* 91, 1 (2007): 119-126.

[129] Cordero, T., Chovelon, J.-M., Duchamp, C., Ferronato, C. and Matos, J. Surface nano-aggregation and photocatalytic activity of TiO_2 on H-type activated carbons. *Applied Catalysis B: Environ* 73, (2007): 227-235.

[130] Schryer, D. R. et al. A proposed mechanism for Pt/SnO_x-catalyzed CO oxidation. *Journal of Catalysis* 130, 1 (1991): 314-317.

[131] Bamwenda, G. R., Tsubota, S., Nakamura, T. and Haruta, M. The influence of the preparation methods on the catalytic activity of platinum and gold supported on TiO_2 for CO oxidation. *Catalysis Letters* 44, (1997): 83.

[132] Liu, S., Liu, G. and Feng, Q. Al-doped TiO_2 mesoporous materials: synthesis and photodegradation properties. *Journal of Porous Materials* 17, 2 (2009): 197-206.

[133] Yang, K., Dai, Y. and Huang, B. First-principles calculations for geometrical structures and electronic properties of Si-doped TiO_2. *Chemical Physics Letters* 456, 1-3 (2008): 71-75.

[134] Yu, H.-F. Photocatalytic abilities of gel-derived P-doped TiO_2. *Journal of Physics and Chemistry of Solids* 68, 4 (2007): 600-607.

[135] Nanba, T., Masukawa, S., Uchisawa, J. and Obuchi, A. Effect of support materials on Ag catalysts used for acrylonitrile decomposition. *Journal of Catalysis* 259, 2 (2008): 250-259.

[136] Xu, G., Zheng, Z., Wu, Y. and Feng, N. Effect of silica on the microstructure and photocatalytic properties of titania. *Ceramics International* 35, 1 (2009): 1-5.

[137] Kang, C. et al. Mesoporous SiO_2-Modified Nanocrystalline TiO_2 with High Anatase Thermal Stability and Large Surface Area as Efficient Photocatalyst. *The Journal of Physical Chemistry C* 113, 3 (2008): 1006-1013.

[138] Braconnier, B. et al. Ag- and SiO_2-doped porous TiO_2 with enhanced thermal stability. *Microporous and Mesoporous Materials* 122, 1-3 (2009): 247-254.

[139] Yu, J. C., Yu, J. G., Ho, W. K., Jiang, Z. T. and Zhang, L. Z. Effects of F-Doping on the Photocatalytic Activity and Microstructures of Nanocrystalline TiO$_2$ Powders. *Chemistry of Materials* 14, 9 (2002): 3808-3816.

[140] Bhaumik, A. and Inagaki, S. Mesoporous Titanium Phosphate Molecular Sieves with Ion-Exchange Capacity. *Journal of the American Chemical Society* 123, 4 (2001): 691-696.

[141] Zhang, X. and Shen, J. Self-Assembled Ultrathin Films: From Layered Nanoarchitectures to Functional Assemblies. *Advanced Materials* 11, 13 (1999): 1139-1143.

[142] Martyanov, I. N., Uma, S., Rodrigues, S. and Klabunde, K. J. Decontamination of Gaseous Acetaldehyde over CoO$_x$-Loaded SiO$_2$ Xerogels under Ambient, Dark Conditions. *Langmuir* 21, 6 (2005): 2273-2280.

[143] Nur, H. Modification of titanium surface species of titania by attachment of silica nanoparticles. *Materials Science and Engineering: B* 133, 1-3 (2006): 49-54.

[144] Ren, J., Li, Z., Liu, S., Xing, Y. and Xie, K. Silica-titania mixed oxides: Si-O-Ti connectivity, coordination of titanium, and surface acidic properties. *Catalysis Letters* 124, 3-4 (2008): 185-194.

[145] Yan, X., He, J., G. Evans, D., Duan, X. and Zhu, Y. Preparation, characterization and photocatalytic activity of Si-doped and rare earth-doped TiO$_2$ from mesoporous precursors. *Applied Catalysis B: Environmental* 55, 4 (2005): 243-252.

[146] Liu, S., Liu, G. and Feng, Q. Al-doped TiO$_2$ mesoporous materials: synthesis and photodegradation properties. *Journal of Porous Materials* 17, 2 (2010): 197-206.

[147] Wang, H., Niu, J., Long, X. and He, Y. Sonophotocatalytic degradation of methyl orange by nano-sized Ag/TiO$_2$ particles in aqueous solutions. *Ultrasonics Sonochemistry* 15, 4 (2008): 386-392.

[148] Iwamoto, M., Yoda, Y., Yamazoe, N. and Seiyama, T. Study of metal oxide catalysts by temperature programmed desorption. 4. Oxygen adsorption on various metal oxides. *The Journal of Physical Chemistry* 82, 24 (1978): 2564-2570.

[149] Chon, H. and Pajares, J. Hall effect studies of oxygen chemisorption on zinc oxide. *Journal of Catalysis* 14, 3 (1969): 257-260.

[150] Li, R., Ma, J., Xu, J., Zhou, X. and Su, Z. Studies on the Surface Oxygen Species and the Catalytic Activity for CO Oxidation of La$_{1-x}$Sr$_x$Co$_{1-x}$Mn$_x$O$_3$, a Perovskite-Type Oxides Catalyst. *Reaction Kinetics and Catalysis Letters* 70, 2 (2000): 363-370.

[151] Luo, L., Shao, G. and Duan, Z. Catalytic Oxidation Properties and Characterization of LaSrCo$_{0.9}$B'$_{0.1}$O$_4$ (B'= Mn, Fe, Ni, Cu) Mixed Oxides. *Turkish Journal of Chemistry* 29, (2005): 597-605.

[152] Ma, Z., Brown, S., Overbury, S. H. and Dai, S. Au/PO$_4^{3-}$/TiO$_2$ and PO$_4^{3-}$/Au/TiO$_2$ catalysts for CO oxidation: Effect of synthesis details on catalytic performance. *Applied Catalysis A: General* 327, 2 (2007): 226-237.

[153] Djerdj, I. and Tonejc, A. M. Structural investigations of nanocrystalline TiO$_2$ samples. *Journal of Alloys and Compounds* 413, 1-2 (2006): 159-174.

[154] Gao, B., Lim, T. M., Subagio, D. P. and Lim, T.-T. Zr-doped TiO2 for enhanced photocatalytic degradation of bisphenol A. *Applied Catalysis A: General* 375, 1 (2010): 107-115.

[155] Yang, H. et al. Synthesis of WO$_3$/TiO$_2$ nanocomposites via sol-gel method. *Journal of Alloys and Compounds* 398, 1-2 (2005): 200-202.

[156] Jung, K. Y., Park, S. B., Matsuoka, M. and Anpo, M. In-situ investigations of the photoluminescence properties of SiO_2/TiO_2 binary and Boron-SiO_2/TiO_2 ternary oxides prepared by the sol-gel method and their photocatalytic reactivity for the oxidative decomposition of trichloroethylene. *INTERNATIONAL JOURNAL OF PHOTOENERGY* 5, (2003): 31-36.

[157] Jin, R., Wu, Z., Liu, Y., Jiang, B. and Wang, H. Photocatalytic reduction of NO with NH_3 using Si-doped TiO_2 prepared by hydrothermal method. *Journal of Hazardous Materials* 161, 1 (2009): 42-48.

[158] Chen, Q., Jiang, D., Shi, W., Wu, D. and Xu, Y. Visible-light-activated Ce-Si co-doped TiO_2 photocatalyst. *Applied Surface Science* 255, 18 (2009): 7918-7924.

[159] Liqiang, J. et al. Effects of Sn dopant on the photoinduced charge property and photocatalytic activity of TiO_2 nanoparticles. *Applied Catalysis B: Environmental* 62, 3-4 (2006): 282-291.

[160] Kim, Y., Kim, E., Whang, C. and Lee, W. Microstructure and Photocatalytic Property of SiO_2-TiO_2 Under Various Process Condition. *Journal of Sol-Gel Science and Technology* 33, (2005): 87-91.

[161] Lee, I. et al. The relationship between photo-catalytic performance and optical property over Si-incorporated TiO_2. *Journal of Industrial and Engineering Chemistry* 14, 6 (2008): 869-873.

[162] Zhenping, Q., Mojie, C., Chuan, S. and Xinhe, B. Influence of Pretreatment on the Interaction of Oxygen with Silver and the Catalytic Activity of Ag/SiO_2 Catalysts for CO Selective Oxidation in H_2. *Journal of Natural Gas Chemistry* 14, 1 (2005): 4-12.

[163] Bernal, S. et al. Some recent results on metal/support interaction effects in NM/CeO$_2$ (NM: noble metal) catalysts. *Catalysis Today* 50, 2 (1999): 175-206.

[164] Rui, L. et al. Catalytic Activity and Characterization of Oxygen Mobility on Pt/Ce$_{0.75}$Zr$_{0.25}$O$_2$ Catalyst by Isotopic Exchange with ^{18}O. *Chinese Journal of Catalysis* 27, 2 (2006): 109-114.

[165] Qu, Z., Cheng, M., Dong, X. and Bao, X. CO selective oxidation in H$_2$-rich gas over Ag nanoparticles--effect of oxygen treatment temperature on the activity of silver particles mechanically mixed with SiO$_2$. *Catalysis Today* 93-95, (2004): 247-255.

[166] Fan, X. et al. Role of phosphorus in synthesis of phosphated mesoporous TiO$_2$ photocatalytic materials by EISA method. *Applied Surface Science* 254, 16 (2008): 5191-5198.

[167] Zhu, J. et al. Nanocrystalline anatase TiO$_2$ photocatalysts prepared via a facile low temperature nonhydrolytic sol-gel reaction of TiCl$_4$ and benzyl alcohol. *Applied Catalysis B: Environmental* 76, 1-2 (2007): 82-91.

[168] Nagaveni, K., Hegde, M. S., Ravishankar, N., Subbanna, G. N. and Madras, G. Synthesis and Structure of Nanocrystalline TiO$_2$ with Lower Band Gap Showing High Photocatalytic Activity. *Langmuir* 20, 7 (2004): 2900-2907.

[169] Silversmit, G., De Doncker, G. and De Gryse, R. A Mineral TiO$_2$(001) Anatase Crystal Examined by XPS. *Surface Science Spectra* 9, 1 (2002): 21-29.

[170] Maiti, C. K., Samanta, S. K., Dalapati, G. K., Nandi, S. K. and Chatterjee, S. Electrical characterization of TiO$_2$ gate oxides on strained-Si. *Microelectronic Engineering* 72, 1-4 (2004): 253-256.

[171] Zhao, D. et al. Surface Modification of TiO_2 by Phosphate: Effect on Photocatalytic Activity and Mechanism Implication. *The Journal of Physical Chemistry C* 112, 15 (2008): 5993-6001.

[172] Shi, Q., Yang, D., Jiang, Z. and Li, J. Visible-light photocatalytic regeneration of NADH using P-doped TiO_2 nanoparticles. *Journal of Molecular Catalysis B: Enzymatic* 43, 1-4 (2006): 44-48.

[173] Shin, E. W. et al. Phosphate Adsorption on Aluminum-Impregnated Mesoporous Silicates: Surface Structure and Behavior of Adsorbents. *Environmental Science & Technology* 38, 3 (2003): 912-917.

APPENDICES

APPENDIX A

CALCULATION FOR CATALYST PREPARATION

A.1 Calculation for the preparation of support modification

Example calculation for the preparation of TiO_2-0.03Si (molar ratio of Si/Ti = 0.03)

Data for calculation: Mw. of tetraethylorthosilicate (TEOS) = 208.33 g/mole

Mw. of titanium (IV) n-butoxide (TNB) = 340.36 g/mole

Based on 25 g of TNB *(Titanium precursor for solvothermal synthesis, Ti[O(CH₂)₃CH₃]₄)*

The composition of the modified support will be as follows:

Si = 0.03 mole

Ti = 1 mole

For 25 g of TNB = $25 / 340.36$ = 0.0734 mole of Ti

Si required = 0.03×0.0734 = 2.2×10^{-3} mole

Si 2.2×10^{-3} mole was prepared from TEOS, so

Weight of TEOS required = *mole of Si required $\times$ MW of TEOS*

= $2.2 \times 10^{-3} \times 208.33$

= 0.46 g

A.2 Calculation for the preparation of metal loading catalyst (atomic %)

Example calculation for the preparation of 10% Ag/TiO$_2$

Data for calculation: Mw. of TiO$_2$ = 79.88 g/mole

Mw. of AgNO$_3$ = 169.8 g/mole

Atomic weight of Ag = 107.8682 g/mole

Based on 100 mole of catalyst used

The composition of the catalyst will be as follows:

Ag = 10 mole

TiO$_2$ = 100-10 = 90 mole

For 1 g of TiO$_2$ (1/79.88 mole)

Ag required = $(1/79.88) \times (10/90)$ = 1.39x10^{-3} mole

= 0.15 g

Ag 0.15 g was prepared from $AgNO_3$

$AgNO_3$ required = $\dfrac{MW \ of \ AgNO_3 \ \times silver \ required}{Atomic \ weigth \ of \ Ag}$

$= (169.8/107.8682) \times 0.15$ = 0.236 g

APPENDIX B
CALCULATION FOR CRYSTALLITE SIZE

B.1 The calculation of crystallite size by Debye-Scherrer equation

The crystallite size was calculated from the half-height width of the diffraction peak of XRD pattern using the Debye-Scherrer equation.

From Scherrer equation:

$$D = \frac{K\lambda}{\beta \cos\theta}$$ (C.1)

Where D = Crystallite size, Å

K = Crystallite–shape factor (= 0.9)

λ = X-ray wavelength (= 1.5418 Å for CuK$_\alpha$)

θ = Observed peak angle, degree

β = X-ray diffraction broadening, radian

The X-ray diffraction broadening (β) is the pure width of power diffraction free from all broadening due to the experimental equipment. α-Alumina is used as a standard sample to observe the instrumental broadening since its crystallite size is larger than 2000 Å. The X-ray diffraction broadening (β) can be obtained by using Warren's formula.

From Warren's formula:

$$\beta = \sqrt{B_M^2 - B_S^2}$$

(C.2)

Where B_M = the measure peak width in radians at half peak height.

B_S = the corresponding width of the standard material.

B.2 The calculation of lattice parameter of TiO₂ nanoparticles

B.2.1 From the XRD patterns, it was compared the position of anatase peak with the standard XRD in order to indentify the plane of crystal (hkl).

B.2.2 Calculated d spacing from Bragg's law;

$$n\lambda = 2d \sin \theta$$

$$d = \frac{n\lambda}{2 \sin \theta}$$

Where; λ = the wavelength of Co Kα radiation (1.5418 $\overset{o}{A}$)

d = the distance of the crystal plane (d-spacing)

θ = the angle of diffraction peak

B.2.3 Calculated d spacing from the tetraganal

$$d_{hkl} = \frac{a_0}{\sqrt{h^2 + k^2 + \left(\dfrac{l}{c}\right)^2}}$$

B.2.4 Solved the above equations to determine the lattice parameters (a_0 and c)

APPENDIX C

CALCULATION FOR PULSE CHEMISORPTION

Pulse chemisorption was employed to determine the metal active sites on the catalyst. There are three methods were used in this work:

(1) CO pulse chemisorption for Pt/TiO_2

(2) H_2 pulse chemisorpion for Ni/TiO_2 and Co/TiO_2 catalysts

(3) N_2O pulse chemisorption for Ag/TiO_2

The reaction stoichiometry of each metal as shown below:

$$CO: Pt \quad = \; 1 : 1$$
$$H_2: Ni \quad = \; 1 : 2$$
$$H_2: Co \quad = \; 1 : 2$$
$$N_2O: Ag \; = \; 1 : 2$$

C.1 Calculation of the metal active site from CO chemisorption

Let the weight of catalyst used	=	W	g
Integral area of CO peak after adsorption	=	A	unit
Integral area of 86 µl of standard CO peak	=	B	unit
Amounts of CO adsorbed on catalyst	=	B-A	unit
Volume of CO adsorbed on catalyst	=	$86 \times [(B-A)/B]$	µl
Volume of 1 mole of CO at 30°C	=	24.86	µl
Mole of CO adsorbed on catalyst	$= [(B-A)/B] \times [86/24.86]$		µmole

Molecule of CO adsorbed on catalysts

$$= [(B-A)/B] \times [86/24.86] \times [6.02 \times 10^{23}] \text{ molecule}$$

Molecule of CO adsorbed per g-cat.

$$= [(B-A)/B] \times [2.08 \times 10^{24}] \times [1/W] \text{ molecule/g-cat.}$$

Amount of metal active site

$$= \textit{Molecule of CO adsorbed per g} - \textit{cat.} \; \times \; 1 \text{ atom per g-cat.}$$

C.2 Calculation of the metal active site from H_2 chemisorption

Let the weight of catalyst used	=	W	g
Integral area of H_2 peak after adsorption	=	A	unit
Integral area of 132 µl of standard H_2 peak	=	B	unit
Amounts of H_2 adsorbed on catalyst	=	B-A	unit
Volume of 1 mole of H_2 at 30°C	=	24.86	µl
Mole of H_2 adsorbed on catalyst		$= [(B-A)/B] \times [132/24.86]$	µmole

Molecule of H_2 adsorbed on catalysts

$$= [(B-A)/B] \times [132/24.86] \times [6.02 \times 10^{23}] \text{ molecule}$$

Molecule of H_2 adsorbed per g-cat.

$$= [(B-A)/B] \times [3.19 \times 10^{24}] \times [1/W] \text{ molecule/g-cat.}$$

Amount of metal active site

$$= \textit{Molecule of } H_2 \textit{ adsorbed per g} - \textit{cat.} \times 2 \text{ atom per g-cat.}$$

C.3 Calculation of the metal active site from N_2O chemisorption

| Let the weight of catalyst used | = | W | g |

Integral area of N_2O remain after decomposition = A unit

Integral area of 100 μl of standard N_2O peak = B unit

Amounts of N_2O decomposition on catalyst = B-A unit

Volume of N_2O decomposition on catalyst = $100 \times [(B-A)/B]$ μl

Volume of 1 mole of N_2O at 30°C = 24.86 μl

Mole of N_2O decomposition on catalyst = $[(B-A)/B] \times [100/24.86]$ μmole

Molecule of N_2O decomposition on catalyst

$$= [(B-A)/B] \times [100/24.86] \times [6.02 \times 10^{23}] \text{ molecule}$$

Molecule of N_2O decomposition per g-cat

$$= [(B-A)/B] \times [2.42 \times 10^{24}] \times [1/W] \text{ molecule/g-cat.}$$

Amount of metal active site

$$= \textit{Molecule of } N_2O \textit{ adsorbed per g} - \textit{cat.} \times 2 \text{ atom per g-cat.}$$

APPENDIX D
CONDITION OF GAS CHROMATROGRAPHY

D.1 The condition of Gas Chromatography (GC) analysis for CO oxidation reaction

A Shimadzu GC-8ATP gas chromatograph model was used to analyze the feed and effluent gases from reactor. An operating conditions used in this experiment are given in table D.1.

Table D.1 GC analysis condition of CO oxidation reaction.

| Gas Chromatograph	SHIMADZU GC-8ATP
Detector type	TCD
Packed column	Molecular sieve 5A
Carrier gas	He (UHP)
Flow rate of carrier gas	45 ml/min
Injector temperature	100°C
Column temperature	70°C
Detector temperature	100°C
Current	80 mA
Analyzed gas	O_2, N_2, CO

D.2 The condition of Gas Chromatography (GC) analysis for N_2O chemisorption

A Shimadzu GC-8A gas chromatograph model was used to analyze the nitrous oxide gases from reactor. An operating conditions used in this experiment are given in table D.2.

Table D.2 GC analysis condition N_2O chemisorption

Gas Chromatograph	SHIMADZU GC-8ATP
Detector type	TCD
Packed column	Porapak N
Carrier gas	He (UHP)
Flow rate of carrier gas	30 ml/min
Injector temperature	150°C
Column temperature	130°C
Detector temperature	150°C
Current	60 mA
Analyzed gas	N_2O

APPENDIX E

CALIBRATION CURVE
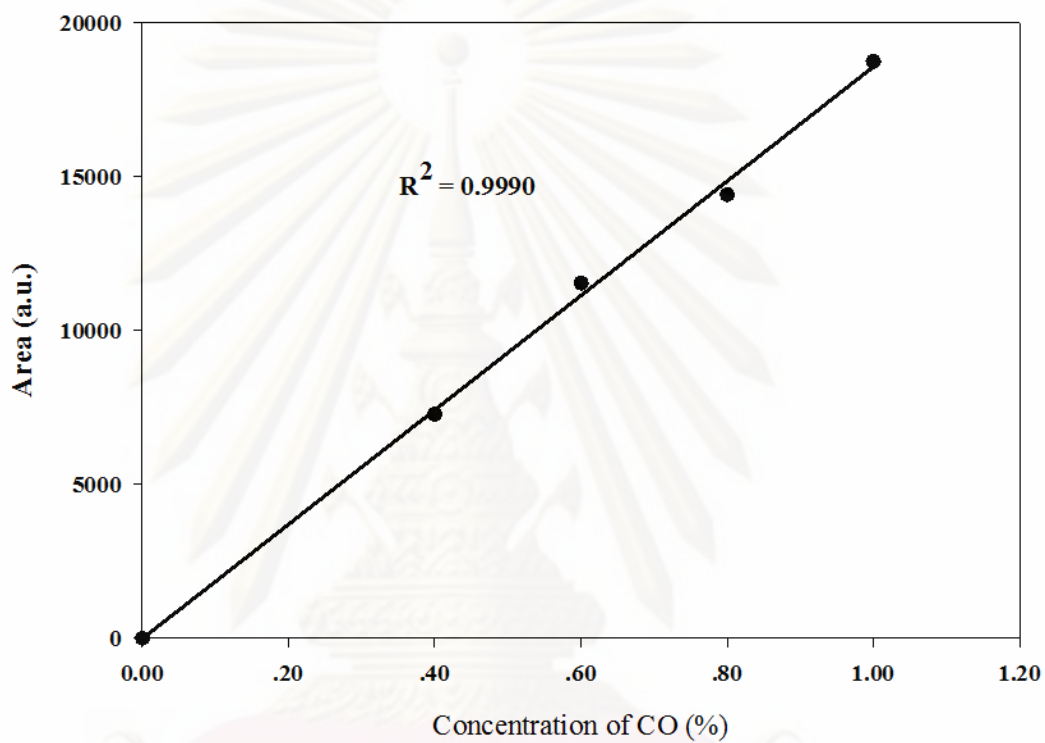
Figure E.1 The calibration curve of CO for CO oxidation reaction

VITAE

Mrs. Nattaya Comsup was born in Bangkok, Thailand, on February 13, 1972. She received the Bachelor's Degree in Chemical engineering from Kasetsart University in April 1998 and Master's Degree in Chemical engineering from Chulalongkorn University in July, 2003. She entered the doctor of Engineering program in Chemical Engineering at Chulalongkorn University.

List of publications

1. Nattaya Comsup, Joongjai Panpranot, and Piyasan Praserthdam, Effect of TiO_2 Crystallite Size on the Activity of CO Oxidation, *Catalysis Letters*, (2009), 133, 76-83.

2. Nattaya Comsup, Joongjai Panpranot, and Piyasan Praserthdam, The influence of Si-modified TiO_2 on the activity of Ag/TiO_2 in CO oxidation, *Journal of Industrial and Engineering Chemistry*, (Accepted).

3. Nattaya Comsup, Joongjai Panpranot, and Piyasan Praserthdam, The effect of phosphorous precursor on the CO oxidation activity of P-modified TiO_2 supported Ag catalysts, *Catalysis Communication*, (Submitted).